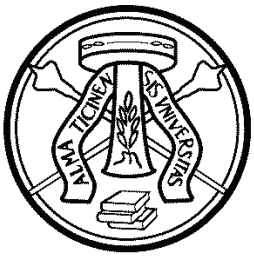

UNIVERSITÀ
DI PAVIA

PhD IN BIOMEDICAL SCIENCES
DEPARTMENT OF BRAIN AND BEHAVIORAL SCIENCES
UNIT OF NEUROPHYSIOLOGY

Genetic and molecular mechanisms of Aicardi-Goutières Syndrome in *RNASEH2* mutated patients

PhD Tutor: Dr. Cristina Cereda

PhD dissertation of
Jessica Garau

a.a. 2019-2020

Abstract

Aicardi-Goutières Syndrome (AGS) is a rare encephalopathy with autosomal recessive and dominant inheritance and onset in the first year of life. The disease has been discovered in 1984 and it is characterised by developmental arrest, basal ganglia calcifications, chronic cerebrospinal fluid (CSF) lymphocytosis, raised levels of interferon-α in CSF and, sometimes, positive interferon signature. Since 2000, 7 genes have been related to the pathogenesis of this disease: *TREX1, RNASEH2A, RNASEH2B, RNASEH2C, SAMHD1, ADAR1* and *IFIH1*. Mutations in the first six genes lead to an accumulation of undigested endogenous nucleic acids that consequently determines the activation of an abnormal innate immune response, which is usually triggered by viral nucleic acids. *IFIH1* mutations lead to the same result but with a different mechanism. This gene encodes a protein (MDA5) that acts as a cytoplasmic sensor of the nucleic acids and, when mutated, this sensor binds more "avidly" to the cytoplasmic RNA causing an excessive activation of the type I interferon response.

More then a half of the AGS cases reported worldwide carries mutations in one of three genes that encodes the three subunits of the RNase H2 enzyme. RNase H2A is the catalytic subunit whereas RNase H2B and RNase H2C represent the two auxiliary subunits necessary to stabilise and form an enzymatically active heterotrimer. This complex represents the major source of ribonuclease activity in mammals and has the ability to remove single ribonucleotides misincorporated in genomic DNA and to degrade the RNA strand of RNA:DNA hybrids. A loss of function of RNase H2, caused by mutations in one of the three subunits, may lead to the accumulation of RNA:DNA hybrids.

RNA:DNA hybrids are physiologically involved in many physiological processes such as transcription, DNA and mtDNA replication, immunoglobulin class switching recombination, but an abnormal accumulation of these species may be sensed by immunological pathways, such as TLR9 and cGAS-STING pathways, triggering a pathological production of type I IFN which is typical of AGS.

First aim of this project was to characterize the Italian cohort of patients affected by AGS from a genetic and clinical point of view. Furthermore, we also decided to evaluate the interferon signature of some of our AGS patients, in order to identify a possible correlation between mutations and interferon score results. We found 5 novel mutations and a possible correlation between mutations in *RNASET2* gene and AGS, but, more interestingly, our results highlighted differences in the phenotype of patients carrying the most common mutation: p.A177T in *RNASEH2B* gene. Indeed, patients with this mutation may present with a mild or a classic severe phenotype, although the pathological mechanisms underlining the clinical variability is still not known. Therefore, another objective of this

project was to perform a transcriptomic analysis and a DNA methylation profiling of these two subgroups of patients.

Mild patients presented a lower transcript deregulation than severe patients who showed a downregulation of mRNAs involved in GABA receptor activity and in the DNA and RNA helicase activity. Among the downregulated transcripts in both subtypes of patients, we observed AC009950.1, which is predicted to be the antisense of *SP110*. SP110 is linked to STAT1, transcription activator that mediates cellular responses to IFNs and to DDX58 (DExD/H-Box Helicases), RNA helicases involved in viral double-stranded RNA recognition and the regulation of immune response.

Regarding DNA methylation, we can observe a general hypermethylation in both subtypes of patients and we discovered a widespread shared epigenetic background between mild and severe patients. All patients show a strong hypomethylation of interferon regulated genes such as *IFI44L, IFITM1* and *MX1* and all these genes are more hypomethylated in severe patients, probably highlighting a deeper involvement of the immune system. We discovered that pathways of differentially methylated genes in mild patients follow those found in both subtypes of patients, probably highlighting that a common pathological mechanism underlies both phenotypes. Remarkably, different methylation patterns are observed in severe patients and they comprehend leukocyte cell adhesion, lymphocyte differentiation, regulation of viral life cycle, regulation of NF-kB activity and regulation of interleukin release, suggesting that further mechanisms contribute to the deterioration of their clinical conditions.

We then continue our project focusing on *RNASEH2B* and *RNASEH2A* mutated LCLs in order to study the molecular mechanism underlying AGS in these patients. An abnormal RNA:DNA hybrids accumulation and colocalization of these hybrids with endolysosomes of *RNASEH2B* LCLs was found compared to control LCLs. *RNASEH2B* LCLs also showed an increased expression of MYD88 and IRF7, which are involved in the downstream signaling of TLR9, and an induction of two ISGs, IFIT1 and IFI44. This activation has not been observed in *RNASEH2A* mutated LCLs. Recent studies demonstrated that antimalarial drugs, such as hydroxychloroquine (HCQ), can inhibit immunological pathways activation and they are already used to treat other autoimmune diseases such as Systemic Lupus Erythematosus and Rheumatoid Arthritis. Therefore, our last aim was to understand if HCQ is able to modulate the innate immune system activation also in AGS patients. After the HCQ treatment, the RNA:DNA hybrids content of *RNASEH2B* LCLs decreased and the colocalization between endolysosomes and RNA:DNA hybrids previously seen in LCLs mutated in *RNASEH2B* was no longer present. In parallel to this, the expression level of both the ISGs that we have studied, IFIT1 and IFI44, decreased significantly only in *RNASEH2B* LCLs, suggesting that the drug could actively interfere with their immune response. As expected, after the treatment with HCQ, we also found out

a statistically significant increase of LC3 protein level, confirming its ability to block the autophagic process and leading to the accumulation of the autophagic factors. Therefore, HCQ seems able to reduce RNA:DNA hybrids content and to stop IFN-α activation and release, possibly representing an efficient therapeutic approach in patients that present an overexpression of ISGs, as observed in *RNASEH2B* LCLs.

In summary, we characterized for the first time the Italian cohort of AGS patients from a genetic and a clinical point of view, highlighting the fundamental importance of an integrated approach in the diagnosis of this rare disease. Furthermore, the transcriptomic and DNA methylation experiments contributed to a deeper understanding of the pathological mechanisms underlying AGS severity in *RNASEH2B* mutated patients. Both of them allowed us to identify a dysregulation of IFN-induced genes, underlining once again the importance of the immune system activation in the pathogenesis of this disease. We also identified some biological pathways that are specifically impaired in severe patients and that will address further researches in the AGS field. At last, in our project we demonstrated that HCQ may represent an efficient therapeutic approach in patients that present an overexpression of ISGs, as observed in *RNASEH2B* LCLs, opening new scenarios in a personalized medicine approach in AGS.

Summary

1. Introduction

1.1. Aicardi-Goutières Syndrome

Aicardi-Goutières Syndrome (AGS) is an early-onset rare genetic disorder with both recessive and dominant inheritance characterised by developmental arrest, basal ganglia calcifications, chronic cerebrospinal fluid (CSF) lymphocytosis and raised levels of interferon-α in CSF (1,2). The disease has been firstly discovered in 1984 when Jean Aicardi and Françoise Goutières described 8 infants, from 5 different families, whose symptoms were characterised by chronic CSF lymphocytosis, basal ganglia calcifications and leukodystrophy (3). The clinical pictures of 1these children resembled those of some congenital infections, although they had always resulted negative to the TORCH complex analysis (Toxoplasma, Other, Rubella, Cytomegalovirus, Herpes simplex). In addition to these classic features, patients also showed other symptoms such as chilblains, bilateral spasticity, ocular jerks, acquired progressive microcephaly, dystonia, progressive brain atrophy and deep white matter hypodensities. Taking all these characteristics together, the authors supposed a possible genetic condition with autosomal recessive inheritance and after the identification of other similar cases, the disorder was listed under the eponym "Aicardi-Goutières syndrome" (4).

The first gene associated to Aicardi-Goutières syndrome was discovered in 2000, when researchers identified a locus for the disorder on chromosome 3p21 (where *TREX1* gene is located) by a genome-wide linkage analysis of 23 children with AGS (5). Later, more studies allowed the discovery of other 6 genes involved in AGS pathogenesis: *RNASEH2A, RNASEH2B, RNASEH2C, SAMHD1, ADAR1* and *IFIH1*. All these genes are involved in nucleic acids metabolism and sensing and alteration in these processes may determine an inappropriate innate immune response, triggering an increased secretion of interferon-α (IFN-α) (6). All genes present an autosomal recessive pattern of inheritance with the exception of *TREX1* and *ADAR1*, which have both autosomal recessive and autosomal dominant inheritance, and of *IFIH1*, that only has autosomal dominant inheritance (2). Today, AGS is considered a rare, genetically determined encephalopathy with autosomal recessive and dominant inheritance and onset in the first year of life. In some cases, AGS may present a less severe clinical course, a later onset and a variability of the overall picture even within single families (7) and across genotypes (2).

1.1.1 Neurological signs

The first phase of the disease is typically associated with peculiar neurological symptoms. AGS children usually develop lethargy resulting in poor interaction and feeding, truncal hypotonia,

irritability, limb dystonia, poor head control and distal spasticity, in a context of developmental delay (8,9). Patients also present with pyramidal and extrapyramidal signs, such as dystonic postures and movements, persistence of archaic reflexes and microcephaly (6). Neurodevelopmental regression, neonatal acute encephalopathy, seizures and deafness are also among common neurological symptoms of this syndrome (8,10).

A peculiar sign of the Aicardi-Goutières Syndrome is represented by the so-called "startle reactions". Normally they are a physiological response to an unexpected stimulus (11), but AGS patients present these abnormal startle reactions in response even to mild sensory stimuli (6). This phenomenon usually has a non-epileptic origin, but in certain cases the differentiation from epilepsy was difficult to define (9).

1.1.2 Extraneurological signs

Extraneurological symptoms are commonly found in AGS patients. The skin is affected by chilblains (Figure 1), which can be located on the hands, feet and ears and are found in the 31.2% of patients (2). Besides chilblains, also epidermal necrosis with intraepidermal bulla and papules formation can be associated to AGS (12).

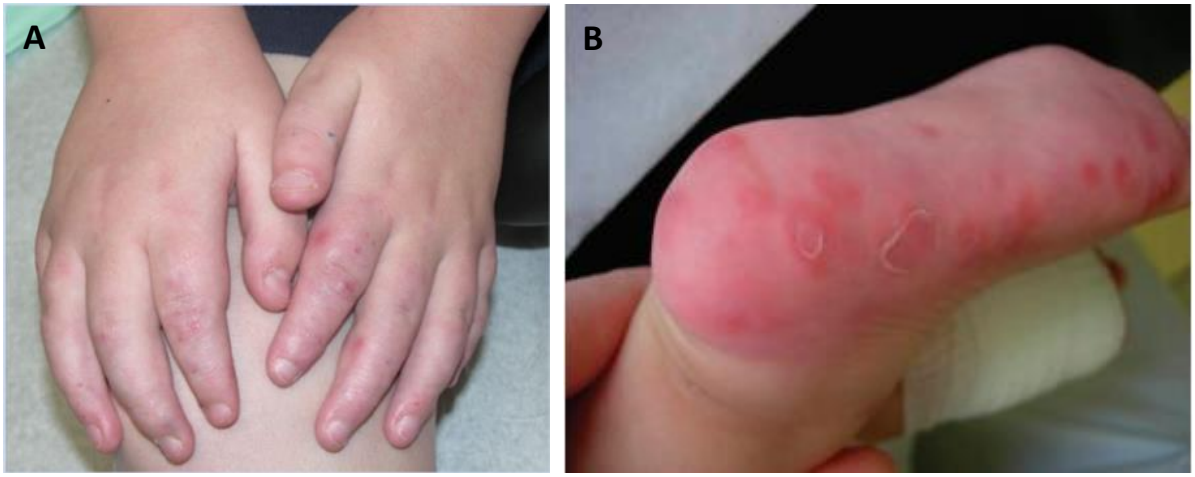

Figure 1. (A) Clinical photograph of hand and fingers presenting erythematous and violaceous papules consistent with perniosis (chilblains) (13). (B) Infiltrated papules on the erythematous and swollen soles (14).

Second most common extraneurological feature is represented by glaucoma, which is usually identified during the first six months of life and it is recorded in 6.3% of children affected by AGS (2). Other extraneurological signs are: hypothyroidism (3.9% of patients), hypertrophic cardiomyopathy (3.3%), inflammatory gastrointestinal problems, insulin-dependent diabetes mellitus, raised levels of autoantibodies, polygammaglobulinaemia, demyelinating peripheral

neuropathy, micropenis, transitory antidiuretic hormone deficiency, hepatosplenomegaly, raised transaminases, transitory thrombocytopenia and haemolytic anaemia (2,6,9,15).

1.1.3 Neuroimaging findings

There are three main neuroradiological features in AGS and they are represented by: cerebral calcifications, cerebral atrophy and white matter abnormalities (6).

Computed Tomography (CT) and, sometimes, Magnetic Resonance Imaging (MRI) are the two techniques used to evaluate the presence, localization, and severity of brain calcification. This feature is identified in 90.9% of AGS patients and, in the majority of children (75.5%), they are limited to classical localizations such as thalami, deep white matter and lentiform nuclei. Severe calcifications, defined as involving multiple locations beyond the classical ones, were observed in 24.6% of AGS patients and few of them also reported striatal necrosis (Figure 2).

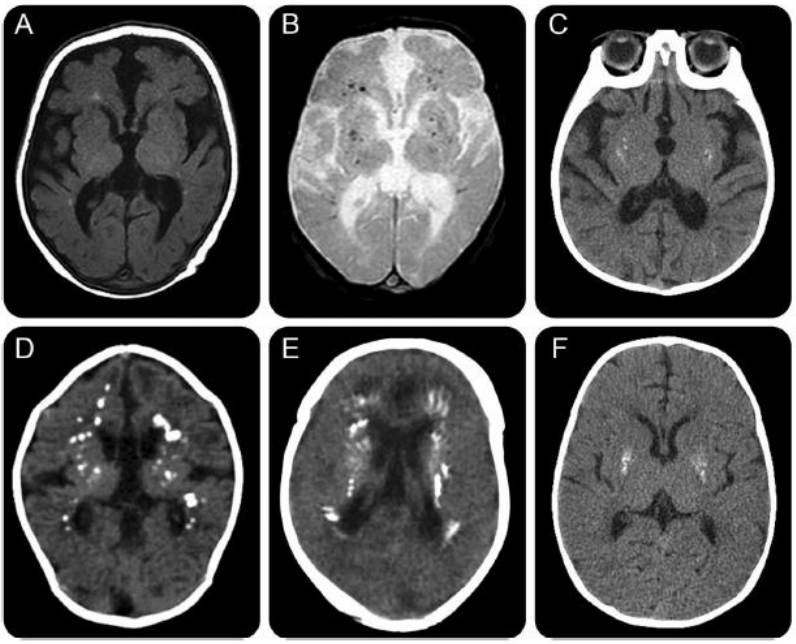

Figure 2. Calcium deposits could be visualized on axial T1-weighted (A) and T2-weighted gradient-echo images (B). (C) Spot-like calcifications located in the lentiform nuclei and left posterior white matter. (D) Severe confluent calcifications. (E) Linear pattern. (F) Calcifications limited to the putamina in a patient with ADAR1 mutations (16).

The presence, localization, and severity of cerebral atrophy are usually evaluated by magnetic resonance images. This neuroradiological finding is observed in 91.8% of AGS patients and cases with bilateral striatal necrosis also presented basal ganglia atrophy. Brain atrophy becomes worse in 35.7% of children, but few cases with cerebral atrophy improvement are described too and it was associated with progressed myelination.

At last, white matter abnormalities are identified by MRI and they are found in 99.8% of children affected by this syndrome. The leukoencephalopathy usually shows three patterns of involvement: frontotemporal predominance (50.9%), diffuse involvement (41.7%) and periventricular predominance (7.4%). These white matter abnormalities got worse in 23.2% of patients and half of patients also shows white matter rarefaction (16).

Beside these three main features, there are also other neuroradiological findings that are less commonly identified in AGS patients such as: vascular lesions, pontocerebellar hypoplasia, brainstem signal abnormalities, hypogenesis of the corpus callosum and cerebellar atrophy (16,17,18).

1.1.4 Cerebrospinal fluid

The analysis of the cerebrospinal fluid (CSF) of AGS patients is of fundamental importance for the diagnosis of this syndrome. The main findings in patients CSF are represented by a chronic lymphocytosis (>5–100 cells/mm^3) and high levels of interferon-α (>2 UI/ml) in the absence of signs that may reconduct to an active inflammatory process (6). Both features are more evident during the first stages of the disease and they are negatively correlated with age (2) since they start to reach normal levels between the 3 and 4 years of age (9,19). Interestingly, increased levels of interferon-α can also be found in patients' plasma, but this increase is usually less marked and less constant than the one identified in the CSF, so it does not have the same diagnostic value (4). Moreover, the interferon activity in patients' serum is lower than the activity identified in the CSF (2).

Other researchers suggested that another cytokine may be important for AGS diagnosis: CXCL10 (20). This cytokine presents considerably raised levels in patients' CSF and could represent an additional marker of the syndrome. It acts as a chemoattractant for activated lymphocytes, possibly explaining the chronic lymphocytosis found in the CSF of AGS patients (6). Moreover, the same researchers observed a lack of IL-6 and CXCL8 increased levels, supporting once again that the inflammatory status reported in AGS patients is not linked and is different from a viral disease (20).

Moreover, other CSF markers of AGS have been identified by Blau and colleagues in 2003. They first described raised levels of pterins and reduced levels of folates in patients' CSF. In particular, the concentration of neopterin and biopterin was extremely high and it was combined with lowered 5-methyltetrahydrofolate levels in the CSF (21). Remarkably, the levels of pterins (mainly neopterin) in the CSF of AGS children are negatively correlated with age (2). Neopterin is a nonspecific marker of the T-helper cell–related immune response and, in clinical practice, an increased concentration of neopterin in CSF represents a useful marker of inflammation in acute and chronic disorders of the central nervous system (22,23).

1.1.5 Interferon signature

More recently, Rice and colleagues introduced the analysis of the so-called “interferon signature” in peripheral blood of AGS patients (24). The type I interferons are thought to play an important role in the pathogenesis of autoimmune diseases, such as systemic lupus erythematosus (SLE) and some patients with AGS may also develop an early onset form of SLE (25,26). Patients affected by SLE present a dysregulated expression of type I interferon-stimulated genes (ISGs) in peripheral blood, which represent the so-called interferon signature (27).

Since AGS patients show increased levels of IFN-α both in CSF and peripheral blood, Rice and colleagues decided to assess interferon-related biomarkers in a large cohort of AGS patients (24).

In their work, Rice and colleagues demonstrated that in the peripheral blood of AGS patients the transcription levels of some ISGs are increased for a long period of time. The ISGs considered for the interferon signature of AGS patients are *IFI27, IFI44, IFIT1, ISG15, RSAD2* and *SIGLEC1* and can be induced by both type I interferon (α, β, ε, κ, ω) and type II interferon (γ) (Rice et al., 2013). The expression of the 6 genes is measured by quantitative Real-Time PCR and normalized on the two housekeeping genes *HPRT1* and *18S*. A threshold that defines the positivity or negativity of the interferon signature is defined by analysing healthy controls and above this threshold the "signature" is considered positive.

Interestingly, patients mutated in the *RNASEH2B* gene very frequently present a negative interferon score (31%). On the other hand, patients with mutation in *TREX1, RNASEH2A, RNASEH2C*, *SAMHD1, ADAR1* and *IFIH1* show positive scores in almost all cases. This results lead to the conclusion that a negative score does not exclude the diagnosis of AGS (2,24).

1.2 Interferon-α and type I interferonopathies

Three types of interferon have been described in literature: type I IFN (IFN-α, IFN-β, IFN-ω, IFN-ε, IFN-κ), type II IFN (IFN-γ) and type III IFN (IFN-λ). They all present an antiviral activity although their efficacy varies according to the type (28). The type I IFN has been discovered and described for the first time more than 50 years ago by Isaacs and Lindenmann, who described the interferon as a soluble factor able to inhibit the influenza virus growth (29). Besides this antiviral action, IFNs also exert their activity in a variety of processes such as cellular growth, differentiation and metabolism, immune function, and cancer development (30,31,32).

There are different species of type I interferon which are encoded by 17 distinct genes located in human chromosome 9p. 13 out of these 17 species of type I IFN are represented by distinct subtypes of IFN-α whereas the remaining 4 species are represented by IFNs β/ε/κ/ω (33). Almost all subtypes of cells can produce type I IFNs even if the cellular source of these cytokines may vary according to

the type of viral infections which is occurring in the body (34). More specifically, plasmacytoid dendritic cells play an important role in the production and release of IFN-α and they also represent the main source of serum interferon (35).

IFNs act through the binding to the heterodimeric IFNα/β receptor 1 (IFNAR1) which is located on cellular membranes. These cytokines start a signalling cascade that, in the end, determines the expression of interferon-stimulated genes (ISGs) and IFNs, establishing a self-sustaining loop (Figure 3) (36,37).

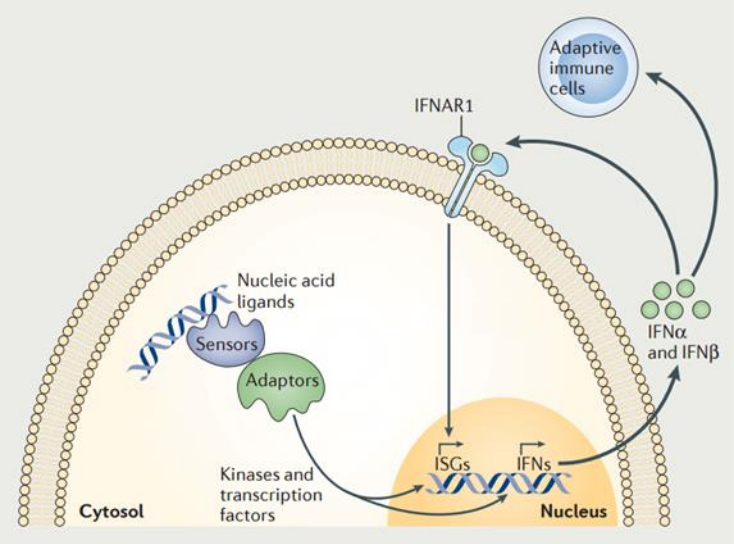

Figure 3. Mechanism of type I interferon exposure (adapted from 36)

In mammalian cells, the immune response against viral infection which involves the release of IFN-α, needs the activation of different types of receptors and sensors, such as Toll-like receptors, RIG-I-like receptors and cGAS. The activation of these pathways ends with the release of antiviral cytokines, such as type I IFNs, which modulate the innate and adaptive immune response (36).

AGS patients usually show higher levels of IFN-α in CSF rather than in plasma, demonstrating an intrathecal synthesis of this cytokine. Remarkably, IFN-α is also produced by astrocytes and microglia (38,39), with probably the aim to protect the brain against viral infections, but when produced in high levels, such as in AGS, it may have deleterious effects (40).

Disorders characterized by a constitutive overexpression of type I IFN that may be related to the pathogenesis of the disease, are now defined as "type I interferonopathy" (36). At the moment, this group of disorders are mainly characterized by neurological and dermatological manifestations.

The first disease that has been associated to this context was SLE, whereas AGS was the first monogenic disease to be associated with a type I IFN upregulation. In SLE IFN-α levels are connected to disease activity and may be used as a biomarker of the disease activity (41). Moreover, patients

who present increased levels of IFN-α in serum have a significantly higher prevalence of cutaneous manifestations and a trend toward renal disease (42).

Besides SLE and AGS, there are other disorders belonging to the group of the type I interferonopathies. Among these the spondyloenchondromatosis (SPENCD) can be found, which is caused by mutations in ACP5 gene, it is characterized by high interferon signature (43) and an increased risk of developing SLE (36). Other interferonopathies are represented by familial chilblain lupus caused by mutations in *TREX1* and *SAMHD1* (genes also related to AGS), STING-associated vasculopathy with onset in infancy (SAVI) which is caused by mutations in STING gene and the Singleton-Merten syndrome determined by mutation in *IFIH1* (one of the genes related to AGS) (36).

1.3 Genetics

AGS is a rare genetic disease characterized mainly by a recessive pattern of inheritance, even if a dominant inheritance has been highlighted for some genes. Up to now, mutations in 7 genes have been related to AGS (Table 1). Remarkably, all the genes involved in AGS pathogenesis are involved in nucleic acids sensing and metabolism (2) triggering an abnormal innate immune response (Figure 4).

Gene	Locus	Pattern of inheritance
TREX1 (AGS1)	3p21	AR, AD
RNASEH2A (AGS2)	19p13	AR
RNASEH2B (AGS3)	13q14	AR
RNASEH2C (AGS4)	11q13	AR
SAMHD1 (AGS5)	20q11	AR
ADAR1 (AGS6)	1q21	AR, AD
IFIH1 (AGS7)	2q24	AD

Table 1. AGS-related genes names, location on chromosomes and pattern of inheritance. AR: autosomal recessive, AD: autosomal dominant.

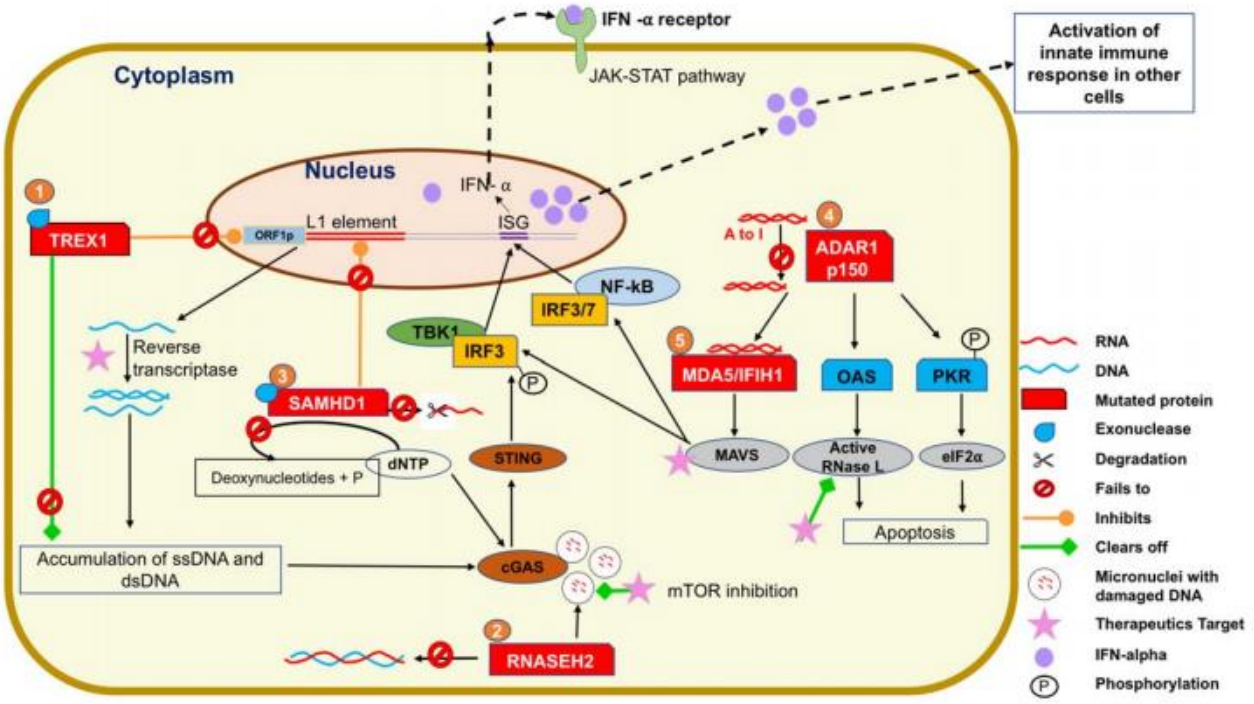

Figure 4. Genes involved in AGS pathogenesis and mechanisms of activation of innate immune signaling pathways (44).

Recently, five patients mutated in *RNASET2* showing a phenotype resembling AGS have been described in literature (45), suggesting that this gene may represent the eighth AGS-related gene.

1.3.1 *TREX1* (*AGS1*)

TREX1 has been the first gene to be associated to AGS. A locus heterogeneity on chromosome 3p21 in AGS patients has been identified in 2000 (46), whereas a link between mutations in *TREX1* gene and AGS has been demonstrated 6 years later by Crow and colleagues (47). *TREX1* is located on the short arm of chromosome 3 (3p21) (Figure 5) and it encodes for the main 3'→ 5' DNA exonuclease found in mammalian cells (also known as DNAse III) (48). It binds very strongly and exerts its action on single strand DNA (ssDNA) removing mismatched 3' terminal deoxyribonucleotides at a DNA strand break (49). Mutations in this enzyme may determine an accumulation of intracellular DNA which is able to trigger an inflammatory immune response (47). More recent studies has also highlighted that TREX1 is not only a DNA exonuclease, but it can also considered a exoribonuclease since mutations in this gene may lead to an accumulation of RNA as well (50).

Mutations in this gene has also been described in a variety of autoimmune diseases such as SLE (51), familial chilblain lupus (FCL) (52) and retinal vasculopathy with cerebral leukodystrophy (RVCL) (53).

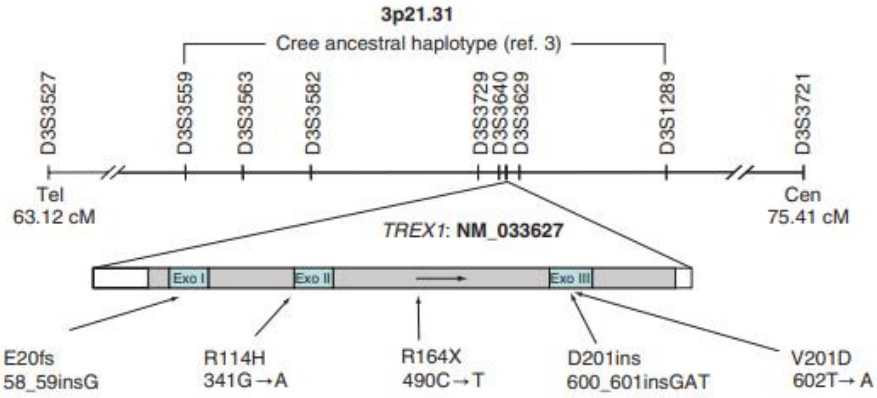

Figure 5. Schematic of the AGS1 critical interval on chromosome 3p21.31 and *TREX1* gene depicting the location of identified mutations (47).

1.3.2 *RNASEH2B* (*AGS2*), *RNASEH2C* (*AGS3*) and *RNASEH2A* (*AGS4*)

During 2006, a second AGS locus has been identified at chromosome 13q14–21 (54) and, few months later, Crow and colleagues described three new genes associated to AGS (55). The three AGS-related genes described were: *RNASEH2B* (*AGS2*) which is located on the long arm of chromosome 13 (13q14); *RNASEH2C* (*AGS3*) placed on the long arm of chromosome 11 (11q13) and *RNASEH2A* (*AGS4*) located on the short arm of chromosome 19 (19p13) (55).

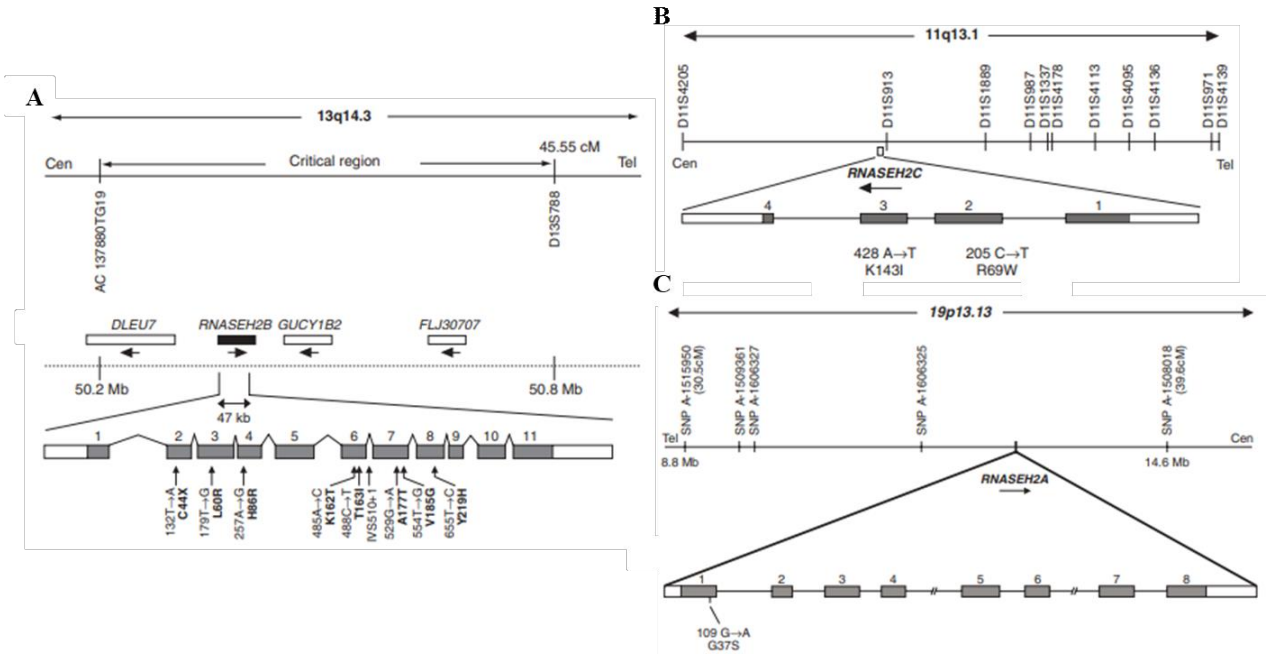

Figure 6. (A) *RNASEH2B*, (B) *RNASEH2C* and (C) *RNASEH2A* genes, genomic locations, gene structure and relevant mutations (55).

These genes encode for the three subunits of RNase H2, an enzyme involved in the removal of ribonucleotides misincorporated in genomic DNA and in cleavage of the RNA portion of RNA:DNA hybrids (56).

RNASEH2B gene encodes a 308–amino acid protein which is found in the majority of human tissues. RNase H2B functions were unknown at that time, but researchers found a strong homology between human RNase H2B and *S. cerevisiae* Rnh2Bp which represents one of the three subunits of the yeast RNase H2 enzyme (Figure 7). This lead to the hypothesis that RNase H2B in human may have the same functions of Rnh2Bp in the yeast, suggesting that also the other two subunits, RNase H2A and RNase H2C could be mutated in AGS (55).

RNASEH2C gene encodes a 164–amino acid protein and it is the human ortholog of Rnh2Cp of *S. Cerevisiae.* Mutations in this gene have been described as AGS-causing.

Due to the similarities between human *RNASEH2B* and *RNASEH2C* and yeast Rnh2Bp and Rnh2Cp, Crow and colleagues decided to analyse also the enzymatic subunit of RNase H2 enzyme: RNase H2A. *RNASEH2A* became the fourth gene to be related to AGS and, therefore, it is also known as *AGS4* (55).

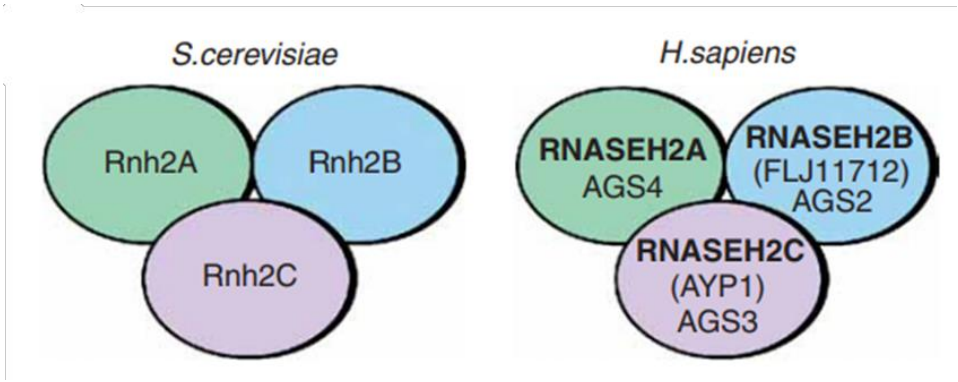

Figure 7. Schematic representation of the proposed human RNase H2 complex and its *S. cerevisiae* counterpart (55).

1.3.3 *SAMHD1* (*AGS5*)

The fifth gene related to AGS was discovered in 2009 by Rice and colleagues and it is represented by *SAMHD1* (*AGS5*). *SAMHD1* is located at the long arm of chromosome 20 (20q11) and encodes a 626 amino-acid protein (57). Sterile alpha motif and histidine-aspartate domain containing protein 1 (SAMHD1) encodes a triphosphohydrolase that determines the conversion of deoxyribonucleoside triphosphate to deoxyribonucleoside and triphosphate (58). It is composed of three regions: N-terminus (residues 1–109), a deoxyribonucleoside triphosphate triphosphohydrolase (dNTPase) catalytic core domain (residues 110–599), and the C-terminus (residues 600–626) (Figure 8).

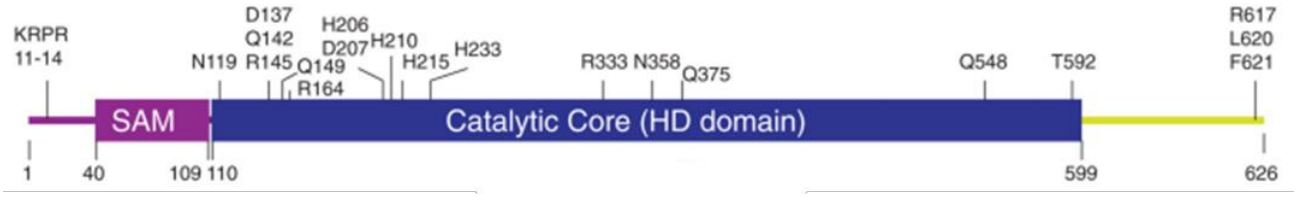

Figure 8. A schematic representation of SAMHD1 three domains: the N-terminus (purple), catalytic core (blue) and the C-terminus (yellow).

It interacts with both ssDNA and ssRNA, binding with a higher affinity ssRNA. The enzyme is mainly known for its ability to restrict HIV-1 infection by preventing efficient completion of reverse transcription (59) and it also contributes to the stability of the genome by controlling the replication of mutagenic retroelements (60). Inactive SAMHD1 exists in a monomeric and a dimeric form, whereas in the presence of dGTP SAMHD1 forms tetramers which represent its active form (61). Its activations is a complex process that requires different steps. The activation process starts with the binding of a dGTP to the A1 site of a monomer inducing dimerization. This step is followed by the occupancy of the A2 site located in each monomer by a dNTP which determines the creation of the active tetramer (Figure 9) (62).

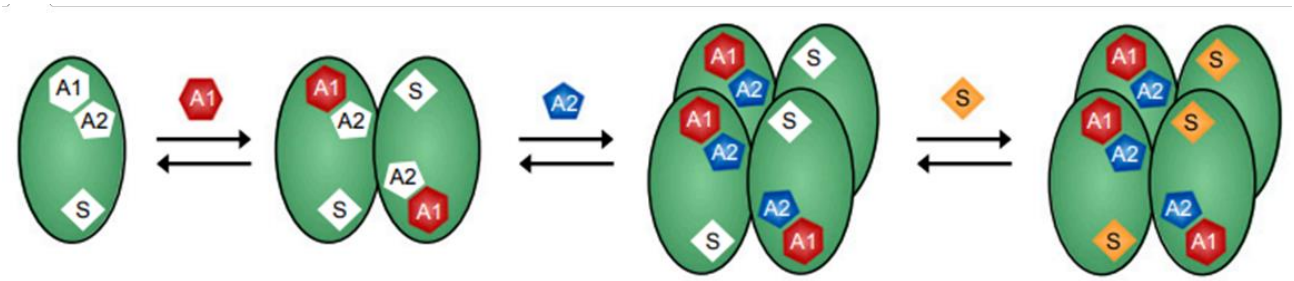

Figure 9. Model for ordered essential activation and oligomerization by GTP activators and dNTP coactivator/substrates involving the formation of a long-lived activated tetramer (62).

Once the enzyme is in its active form, it regulates and controls the dNTP pool of immune cells, by cleaving dNTPs into deoxyribonucleosides and triphosphates (63). Mutations in SAMHD1 determines an accumulation of the enzyme in the cytoplasm, whereas it is normally found in the nucleus (57). Furthermore, mutated SAMHD1 is no more capable of inhibit LINE-1 retrotransposition, leading to the accumulation of LINE-1 nucleic acids in cells and, consequently, to the activation of nucleic acids sensors such as cGAS, RIG-I and TLR3 (64).

1.3.4 *ADAR1* (*AGS6*)

The sixth AGS-related gene was identified in 2009 and it is located at the long arm of chromosome 1 (1q21) (Figure 10) (65). There are different types of ADARs and they catalyse the hydrolytic

deamination of adenosine to inosine in dsRNA (66). ADAR1 and ADAR2 are the only two enzymes with a known catalytic activity in mammals. Two main isoforms of ADAR1 are found in humans: a truncated form which is constitutively expressed (p110) and a full-length form which is inducible by IFN (p150) (67). Both isoforms move from the nucleus to the cytoplasm and viceversa (65).

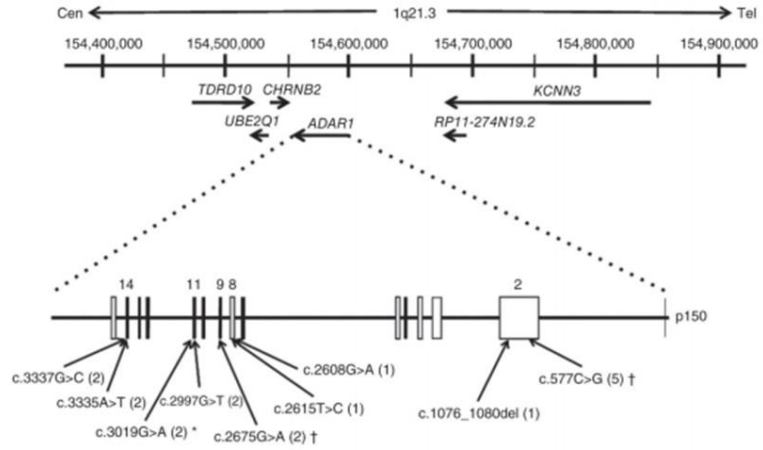

Figure 10. Schematic picture of the human *ADAR1* gene (65).

ADAR1 has a particular structure. It is composed of a C-terminal deaminase catalytic domain, three dsRNA-binding domains (dsRBDs) located in the central portion and one or two N-terminal ZDNA–binding domains. Moreover, the p150 isoform of human ADAR1 presents an additional 295 N-terminal amino acids which contains a nuclear export signal and an extra ZDNA/Z-RNA–binding domain (known as Zα) (Figure 11) (68).

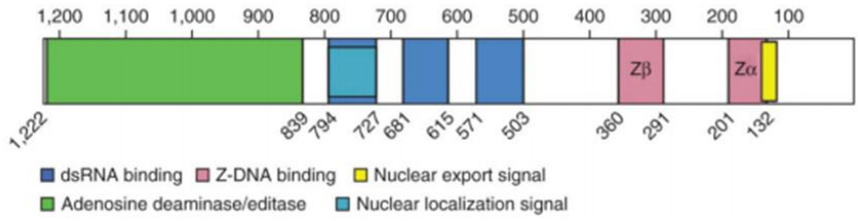

Figure 11. Schematic of the position of protein domains and their amino-acid boundaries in the p150 isoform of ADAR1. The p110 isoform does not include the Zα DNA/RNA-binding domain and nuclear export signal (65).

ADAR1 exerts its action not only on coding sequences, since the majority of its action is on non-coding sequences (69). ADAR1 acts on retrotransposons (Alu elements) playing an essential role in regulating the innate immune response (70) and representing a major contributor to transcriptome diversity (71). Mutations in ADAR1 lead to a reduction of RNA editing, especially when mutations

occur in the IFN-inducible p150 isoform (70). This reduction may determine an increase of immunoreactive dsRNA that may induce the release of type I IFN (72), one of the main signs of AGS.

1.3.5 *IFIH1* (*AGS7*)

The last gene associated to AGS was described for the first time in 2014 by Rice and colleagues (73). *IFIH1* (also known as *AGS7*) maps at the long arm of chromosome 2 (2q24) (Figure 12A) and it is the only AGS-related gene which exclusively presents a dominant pattern of inheritance. Few cases of dominant inheritance have been observed also for *TREX1* and *ADAR1* genes, although they are usually inherited in a recessive pattern (2). *IFIH1* is also known as MDA5 (melanoma differentiation-associated protein 5) and encodes a cytoplasmic helicase capable of inducing an interferon response to viral RNA (74). It is one of the three members of the RIG-I-like receptors (RLRs) and is ubiquitously expressed at low levels (75,76). IFIH1 contains two N terminal caspase activation and recruitment domains (CARDs) which are involved in activating MAVS, a central helicase domain responsible for RNA-binding and RNA-dependent ATP hydrolysis (73), a DExD/H-box RNA helicase domain and a C terminal domain (CTD) representing additional domains involved in RNA binding (Figure 12B) (74).

Mutations in *IFIH1* lead to chronic type I IFN release. There are two possible explanations: the first is that mutated MDA5 signals constitutively in an RNA independent manner (77); the second one suggests that mutations in IFIH1 may alter the interaction between sensor and RNA, determining a spontaneous signal triggered by cellular RNAs (76).

IFIH1 mutations are not only related to AGS, but they are also found in other rare diseases characterised by an abnormal type I IFN production, such as the Singleton-Merten Syndrome (78).

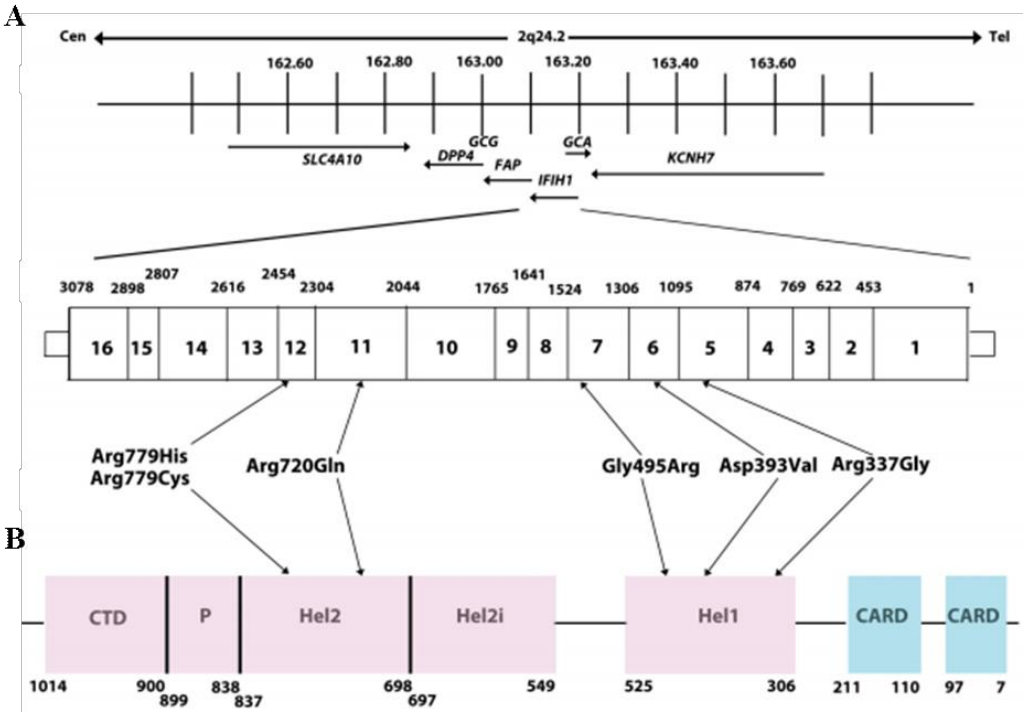

Figure 12. (A) Schematic representation of the human *IFIH1* gene cryptic region. (B) Schematic representation of the position of protein domains and their amino acid boundaries within the IFIH1 1025 amino acid protein (73).

1.3.6 Genotype-phenotype correlations and frequencies of mutations

Mutations in one of the 7 AGS-related genes have not the same frequency among all patients. There are some genes that are found more frequently mutated in the AGS population. Considering the worldwide cohort of AGS patients described by Crow and collaborators in 2015, it is evident that mutations in *RNASEH2B* and *TREX1* are definitely more frequent than mutations in other genes. (Figure 13). Other cohorts of patients have been described in literature. In the one described by Al Mutairi and colleagues the most commonly mutated genes were *RNASEH2B* and *RNASEH2A*, and the most frequent mutation was p.D119G in *RNASEH2B* instead of p.A177T found in the group of patients described by Crow and colleagues (2,79). Therefore, these data highlights that differences among the percentage of mutation in AGS-causing genes may be found according to the ethnicity of the AGS patients.

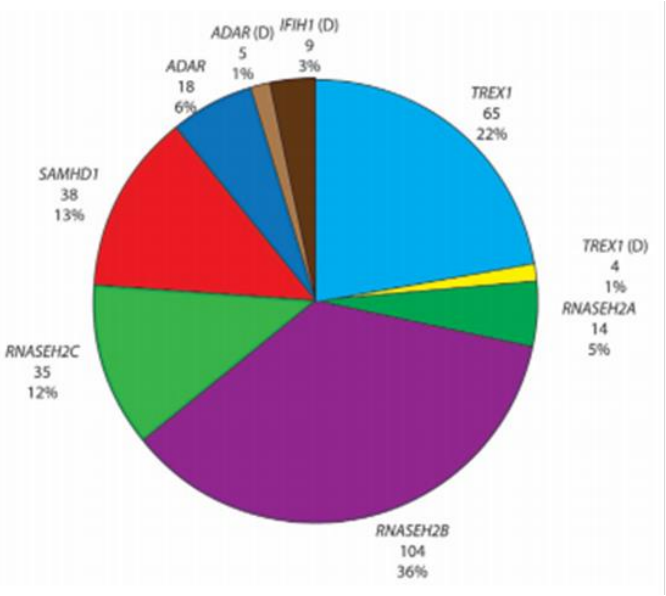

Figure 13. Numbers and percentages of patients affected by Aicardi-Goutières syndrome (AGS) (2).

Although AGS patients with different mutations usually conform to the relatively stereotyped clinical profile, some genotype-phenotype correlations can be found. For example, patients carrying mutations in *ADAR1* gene are more likely to present an acute or sub-acute onset of severe dystonia and to develop features of bilateral striatal necrosis (80). Patients mutated in *RNASEH2B*, *SAMHD1*, *ADAR1* and *IFIH1* are more likely to retain some motor and communication abilities, whereas children with mutations in *TREX1* gene present the highest mortality rate (2). Mutations in *RNASEH2B* gene usually determine later-onset forms of AGS with a longer life expectancy (6) and patients mutated in this gene are more likely to have a negative interferon score (2). Sometimes phenotype differences can be found between siblings carrying the same mutation in the same gene (2).

1.4 Pathogenesis

The detection of nucleic acids of viral origin is the main element of the antiviral immune response. This mechanism is orchestrated by the IFN-α which coordinates the immune response in order to limit the viral replication and to provide a long-term immunity against the virus (81,82).

This interferon response against exogenous nucleic acids is linked to two immunological pathways. The first mechanism involves TLRs which are localized on the cell membrane or in intracellular organelles and, according to their localization, they recognize microbial cell membranes or microbial or viral nucleic acids (83). The second one is represented by RIG-I and MDA5 (also known as IFIH1) helicases which detect nucleic acids inside cell cytoplasm and activate the immune response through the adaptor protein MAVS (84). Although these two mechanisms are important in the defence response against virus, the discrimination between exogenous and endogenous nucleic acids is not

always perfect and a defective removal of endogenous nucleic acids can cause IFN-associated disorders, such as AGS (85). As previously mentioned, all AGS-related genes are involved in nucleic acids metabolism or sensing and mutations in one of these genes determine an abnormal immune response (Figure 14).

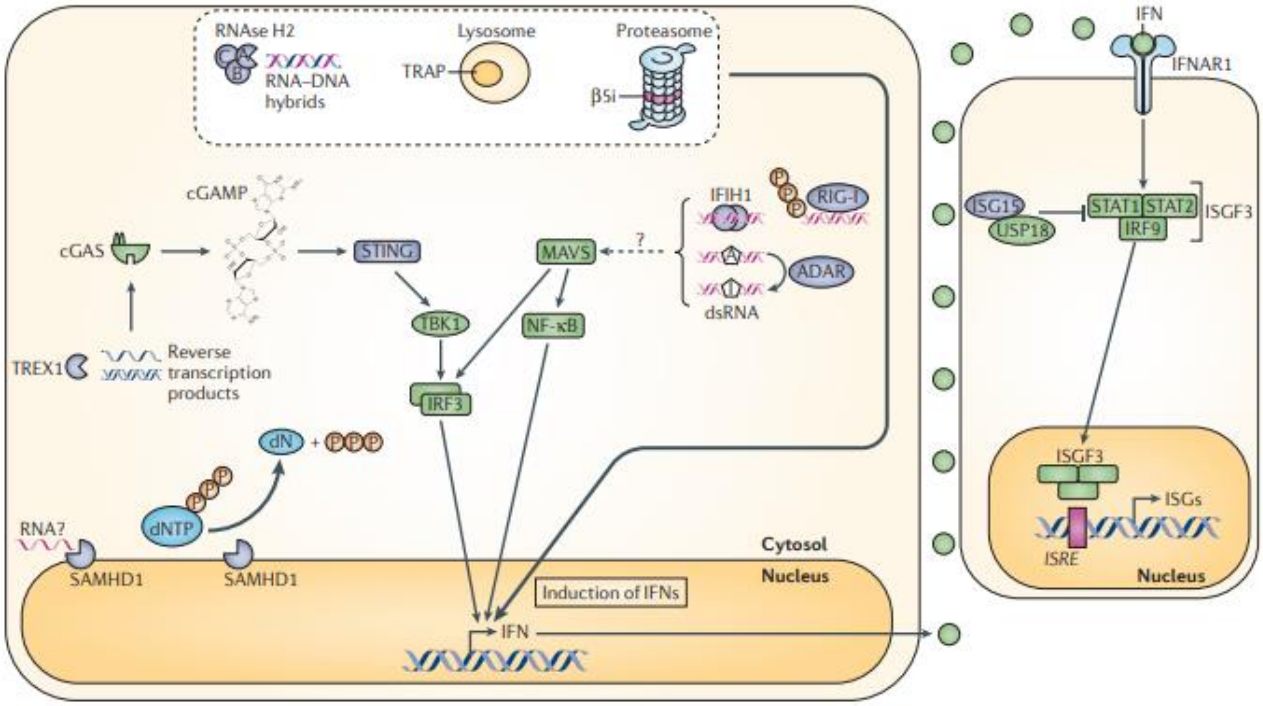

Figure 14. Innate immune signalling pathways impaired by mutations in AGS-related genes (36).

Loss of function mutations of TREX1, which encodes a DNA 3´ repair exonuclease 1, determine a cytoplasmatic accumulation of ssDNA and dsDNA, which in turn, triggers the cGAS-STING pathway with a consequent release of type I IFN. The same pathological mechanism can be found in SAMHD1 mutations. This enzyme hydrolyses dNTPs and may also degrade dsRNA, but mutations of this protein leads to accumulation of endogenous dsDNA that activates the cGAS-STING pathway. IFIH1 is as sensor for exogenous dsRNA, also known as MDA5. Gain of function mutations of this cytosolic sensors lead to a lower threshold of activation leading to the sensing of endogenous dsRNA as well. ADAR1 catalyses the deamination of adenosine to inosine and, when mutated, this enzyme leads to the accumulation of pathological nuclei acids which determine the activation of the immune response through the recruitment of MAVS (36).

Another pathological mechanism is also represented by mutations of the RNase H2 subunits. This enzyme can hydrolyse the RNA component of RNA:DNA hybrids and mutations in one of these three

subunits lead to an increased intracellular content of hybrids which can be sensed by cGAS or TLR9 (86,87).

1.5 Ribonuclease H

Ribonucleases H (RNases H) were discovered in 1969 and they are enzymes that hydrolyse the RNA portion of RNA:DNA hybrids (88) to generate 5′ phosphate and 3′ hydroxyl ends (89). They belong to the retroviral integrase superfamily (RISF) which comprehends a variety of enzymes involved in the metabolism of nucleic acids (90). There are two types of RNase H: Type I and Type II. This distinction is based on amino acid sequence similarities, common structural features and different substrates that are able to cleave (91,92). In *Archea* and bacteria, a third class of RNase H (RNase H3) can be found. It shows some structural similarities with RNase H2, although being more similar to RNase H1 in terms of substrates preference (91). All subtypes of RNase H, as well as all the enzymes belonging to the RISF family, present catalytic domains that adopt the so-called RNase H fold, whose key feature is represented by a mixed five-stranded β-sheet, where strand 2 always runs antiparallel to the others (90). The active site of RNases H is negatively charged and binds divalent metal ions in order to exert their catalytic activity. The hydrolysis is preferentially supported by Mg^{2+}, even if other ions, such as Mn^{2+} can be used (91).

Eukaryotes possess both RNase H1 and RNase H2. RNase H1 is also present in prokaryotes and in domains of reverse transcriptase and hydrolyses the RNA strand in RNA:DNA hybrids. In order to exert its cleavage activity, it needs at least four consecutive ribonucleotides (93). RNase H1 presents both affinity for RNA:DNA hybrids and dsRNAs, although it binds preferentially to RNA:DNA hybrids (94). At last, RNase H1 presents two isoforms that are localized in the nucleus and mitochondria (95) and plays an important role in mtDNA replication both in *in vivo* mouse models and humans (96,97).

The other major class of RNase H is represented by RNase H2 (91). Conversely from RNase H1, the key feature of this enzyme is the ability to remove single ribonucleotides misincorporated in genomic DNA (98) by hydrolyzing the 50-phosphodiester bond (99). This process represents the starting point of the pathway called ribonucleotide excision repair (100). RNase H2 is composed of three subunits and mutations in one of them are considered causative of AGS (55).

1.5.1 RNase H2

As already mentioned in the previous chapter, RNase H2 is one of the major sources of ribonuclease activity in eukaryotes (91). In prokaryotic organisms RNase H2 is represented by a single subunits, whereas its eukaryotic counterpart has evolved markedly and it is composed of three subunits which

are all equally important for the enzymatic activity (101). Eukaryotic RNase H2 is therefore composed of three subunits: RNASEH2A which is the catalytic subunit and shares about the 30% of amino acid sequence similarity with the prokaryotic enzyme (102); RNASEH2B and RNASEH2C which represent the two auxiliary subunits necessary to stabilise and form an enzymatically active heterotrimer (Figure 15) (103).

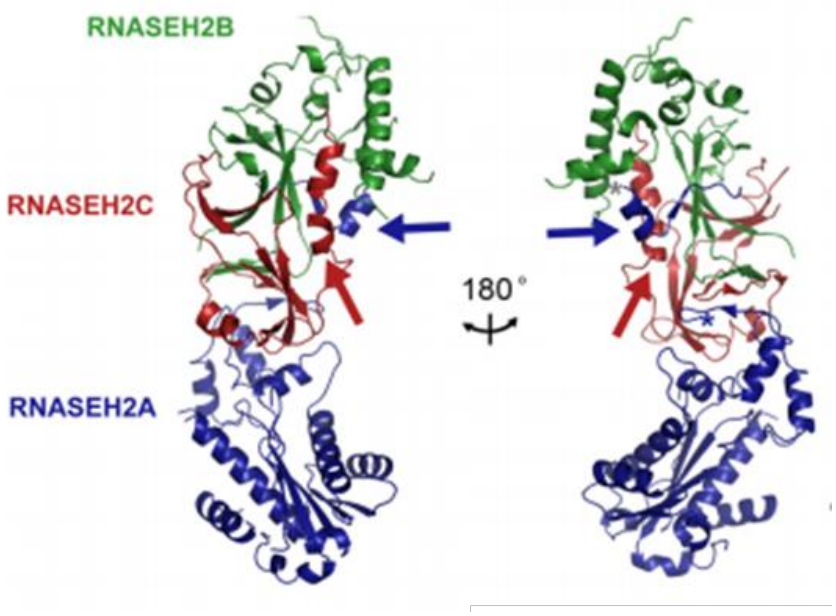

Figure 15. Crystal structure of the heterotrimeric RNase H2 complex. Ribbon diagram representation of human RNase H2 reveals a linear arrangement of subunits where the core of the catalytic domain (RNASEH2A; blue) is stacked on the interwoven auxiliary RNASEH2B (green) and RNASEH2C (red) subunits (103).

RNase H2 activity on RNA:DNA hybrids suggest its involvement in a variety of nucleic acids metabolism processes. During cell death, RNase H2 is involved in the degradation of RNA:DNA hybrids in order to prevent nucleic acid-mediated immune activation (55). RNase H2 is also suggested to possess a key role in the repression of endogenous retroelements (104) and in the resolution of RNA:DNA hybrids generated by RNA polymerases during transcription (93). This enzyme interacts with proliferating cell nuclear antigen (PCNA) forming a complex that act as a scaffold and catalyst for DNA-editing enzymes during DNA replication (105). This interaction also suggests a role in facilitating the Okazaki fragment processing (106) although this function is mainly exert by RNase H2 interaction with the endonuclease FEN-1. This complex is involved in the excision of ribonucleotide primers from an RNA:DNA hybrid during DNA replication (98).

Mutations in one of the three subunits of RNase H2 may cause AGS. According to the genetic location of the mutation, this may affect the protein in three different ways: impairment of substrate binding/hydrolysis, inhibition of complex formation and disruption of the interactions with potential

interacting proteins (107). In wider terms, mutations in RNase H2 enzyme determine an accumulation of nucleic acids derived from endogenous retroelements or from inefficient removal of ribonucleotides from genomic DNA and an increased DNA damage. All these scenarios ends with an abnormal stimulation of immunological pathways determining an increased release of IFN-α, which is one of the main features of AGS (Figure 16) (108).

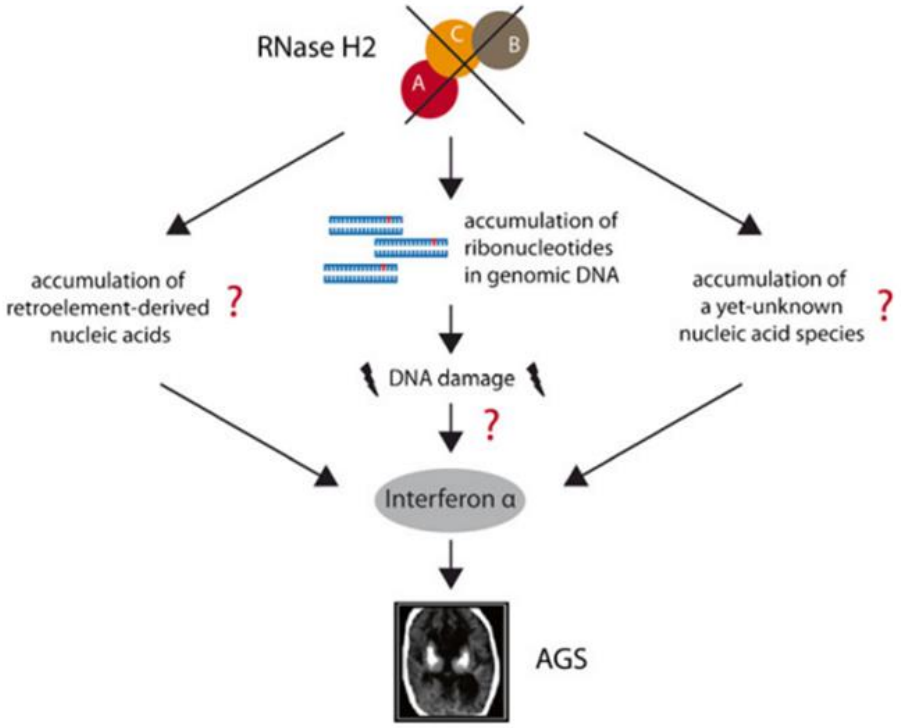

Figure 16. Possible mechanism underlying AGS pathogenesis in patients carrying mutations in one of the three subunits of RNase H2 enzyme (108).

RNase H2 deficiency in mammals is not compatible with life, explaining why all RNase H2 mutations found in AGS children are hypomorphic (55,106). RNase H2 knock-out mice models have been created by two different groups targeting RNase H2B and RNase H2C subunits (106) (56) and show an early embryonic death and an accumulation of misincorporated ribonucleotides. This accumulation represents the major cause of DNA damage (106,109). This genotoxic stress induces the release of nucleic acids in the cytoplasm of the cells where they are bound by DNA sensors, such as cGAS or TLRs, triggering an abnormal immune response associated with an excessive production of IFN-α (110,111,112). Surprisingly, mice models carrying the p.A177T variant in *RNASEH2B* gene, are viable, fertile, and do not display any phenotype similar to AGS, highlighting different pathological mechanism between humans and mice (106).

Patients with mutations in *RNASEH2B* and *RNASEH2A* show accumulation of ribonucleotides in genomic DNA and their cells also present impaired cell cycle progression with chronic activation of post-replication repair mechanisms (113,114,115).

1.6 RNA:DNA hybrids (R-loops)

R-loops have been described for the first time in 1976 and they consist of a three stranded structure composed of a RNA:DNA hybrid and a ssDNA (Figure 17) (116).

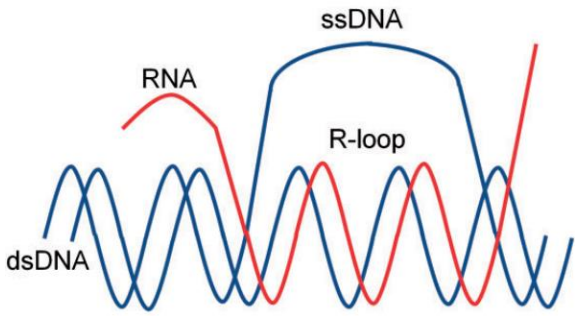

Figure 17. R-loop structure (117).

These structures usually arise during transcription from Guanine-rich clusters, since researchers demonstrated that RNA containing four or more consecutive guanine residues near the 5' end has a significantly higher rate of R-loop formation (118,119). Once they are formed, R-loops are very stable since RNA:DNA interactions are stronger than those between DNA:DNA (120). This R-loops are usually resolved by RNase H enzymes, but a loss of function of these enzymes lead to an accumulation of this nucleic acid species (93).

R-loops and RNA:DNA hybrids are found in a variety of physiological processes (Figure 18) such as transcription and DNA replication where RNA primers, synthesized by DNA polymerase α, are used by DNA polymerase δ to polymerize mature Okazaki fragment (121,122). Moreover, R-loops are present in mitochondrial origins of replication and, therefore, they are involved in mtDNA replication (123) and at the switch (S) region during immunoglobulin class switching recombination (124). These structures also occur at telomeres, where the telomerase, specifically recognizes telomere sequences through RNA:DNA base pairing in order to extend the ends preventing telomere erosion (125). Moreover, RNA:DNA hybrids can arise due to the incorporation of ribonucleotides monophosphates (rNMPs) into genomic DNA during DNA replication (126). This misincorporation may lead to genome instability, but also represents a useful tool used by the mismatch repair and non-homologous end-joining pathways to promote genome integrity (127,128,129). rNMPs resemble a signal to

discriminate and direct the repair of the misincorporated base on the newly synthetized strand. This type of hybrids are not considered R-loops since there is no displacement of the DNA strand (130). R-loops also have a different role in regulating transcription. They promote gene expression when they are located in downstream CpG island promoter regions by the inhibition of DNA methyltransferases (131) and they also can facilitate the binding of transcription factors to regulatory elements on DNA (132). At last, R-loops in G-rich sequences found downstream of the 3' polyadenylation (polyA) signal can induce antisense transcription, leading to the formation of dsRNA, to the recruitment of the RNA interference machinery promoting RNA Pol II pausing (133).

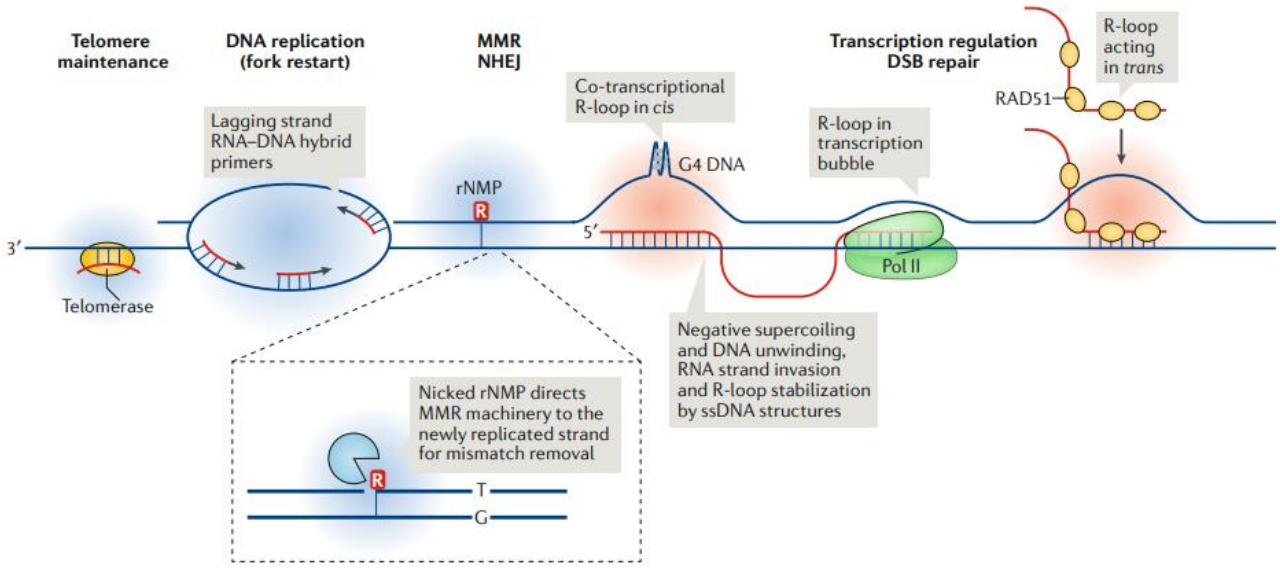

Figure 18. Roles of RNA:DNA hybrids (130).

Since R-loops present many physiological functions, researchers started to think that RNA:DNA hybrids formation may be a process which is regulated by the action of specific proteins. The RNA helicase DDX1 promotes R-loops accumulation to promote class switch recombination at the IgH locus (134) whereas DHX9 promotes the accumulation of R-loops in RNA splicing impairment (135). Although R-loops are important for many cellular processes, these nucleic acid species can also lead to genome instability and DNA damage. In the R-loop structure, the ssDNA is more exposed to the action of nucleases, genotoxics and transcription-associated mutagenesis (TAM) or transcription-associated recombination (TAR) (136). Chemical mutagens and DNA modifying factors, such as the Activation-induced cytidine deaminase (AID), may target the DNA strand of the R-loops creating lesions that in turn lead to point mutations or other deleterious effects (137). Genetic stress and changes in gene expression can also be induced by accumulation of R-loops at promoter and terminator regions of genes. Mutations in the THO complex lead to increased levels of RNA:DNA

hybrids that in turn prevent RNA Pol II processivity blocking the transcription elongation step (138,139). Moreover, genomic instability due to accumulation of R-loops usually results from the collision of the replicative fork and the transcriptional machinery (140). This impairment can determine a collapse of the fork, double strand breaks (DSBs), or incomplete replication before entry into mitosis (141). For example, genomic rearrangements have been identified after TOP1 inhibition. Human Top1-deficient cells accumulate DSBs at gene-rich genomic regions and show a slower progression of the replication fork due to R-loops (142).

R-loops formation and degradation are two processes well balanced and a disruption of this homeostasis has been described as causative of a variety of disorders, including cancer and neurological diseases (143). Mutations in the two tumor suppressor genes *BRCA1* and *BRCA2* genes lead to accumulation of R-loops. *Wild-type* BRCA1 recruits the helicase SETX to resolve R-loops and suppress DNA damage at transcription termination pause sites or sites of Negative Elongation Factor (NELF) (144) whereas BRCA2 can associate to the PCI-domain containing protein 2 preventing the co-transcriptional formation of R-loops (145) or it can act alone to avoid R-loops accumulation at DSB sites by inhibiting RF collapse and recruiting Rad51 (146).

Genes causative of Trinucleotide repeat disorders such as *HTT* (Huntington's Disease), *FXN* (Friedreich Ataxia), and *ATXN1/ATXN2* (Spinocerebellar Ataxias) present GC-rich trinucleotide expansions that form R-loops by different mechanisms (147,148). Regarding Friedreich Ataxia, the expansion of the first intron of FXN leads to R-loops formation and inhibition of Pol II mediated transcription (149). In the fragile X syndrome the expansion in the 5' UTR of the FMR1 gene determines the silencing of this region by increased DNA methylation (149) although depletion of DNA methylation does not completely restore FMR1 expression due to R-loops accumulation (150). Nucleotide expansions are also found in *C9ORF72* gene which is associated to Amyotrophic Lateral Sclerosis (ALS) and Fronto-Temporal Dementia (FTD) (151,152). C9ORF72 gene presents an hexanucleotide expansion, GGGGCC (G4C2), where, due to the G-richness of this sequence, R-loops formation is promoted together with RNA polimerase II stalling and decreased levels full-length mRNAs (153,154).

R-loops accumulation has also been observed in AGS patients. Mutations in *TREX1* and *RNASEH2* subunits lead to a global increase of RNA:DNA hybrids over intergenic or gene body regions (155). These particular locations of the hybrids suggest that these R-loops are probably different from those found in other neurological disease, which are usually located at 5′ or 3′ end of genes (143). Interestingly, mutations in *TREX1* and *RNASEH2B* genes are also causative of SLE (51,115) suggesting a possible role of R-loops in this autoimmune disease as well (143).

1.6.1 RNA:DNA hybrids and Aicardi-Goutières Syndrome

RNA:DNA hybrids may arise during transcription and after the misincorporation of ribonucleotides in genomic DNA during replication (126). As described in the previous chapter, RNases H are among the enzymes which exert a fundamental action in RNA:DNA hybrids removal (93). Impairment of RNase H activity may lead to an accumulation of this dangerous nucleic acid structures which can in turn be sensed by immunological pathways triggering a pathological production of type I IFN (156). Mutations in the *RNASEH2* genes have been observed in AGS patients (55) and lead to the accumulation of RNA:DNA hybrids (155). RNase H2 represents around the 90% of RNA:DNA hybrids cleavage activity and loss of function mutations in one of the three subunits of the enzyme lead to a reduced activity of the enzyme and, therefore, a significant accumulation of RNA:DNA hybrids both in human and yeast (106,157). The importance of RNase H2 in the pathogenesis of AGS and in RNA:DNA hybrids degradation is also highlighted by the fact that mutations in RNase H1 do not cause AGS and that R-loops arisen during replication may be inaccessible to RNase H1 (157,158). Studies on *RNASEH2A* and *RNASEH2B* mutated lymphoblastoid cell lines highlighted an accumulation of unrepaired rNMPs which remain embedded in genomic DNA leading to replication stress and genome instability. RNase H2 silencing in HeLa cells determined an impairment in cell proliferation with a high number of silenced cells stuck in S and G2-M phases. Moreover, these cells showed an accumulation of ubiquitylated PCNA, suggesting that RNase H2 depletion activates the post-replication repair pathway in order to overcome cell cycle impairment and conclude replication (113).

Moreover, R-loops accumulation have been observed also in fibroblasts derived from AGS patient mutated in *TREX1* and *SAMHD1* (155). Interestingly, RNA:DNA hybrids in AGS patients showed different localizations from the canonical sites of accumulation such as GC skews, transcription start sites and transcription termination sites (131). *RNASEH2A* and *RNASEH2B* mutated fibroblasts peaks were significantly increased at intergenic regions of the genome whereas *TREX1* and *SAMHD1* mutated cells presented an RNA:DNA hybrids enrichment at gene body regions. Moreover, in all AGS patients' fibroblasts was observed an accumulation of hybrids in genomic regions corresponding to long interspersed nuclear elements (LINE) and long terminal repeats (LTR) retrotransposons (155). An enrichment of RNA:DNA hybrids at retrotransposon elements has also been observed in yeast (159). Since *TREX1*, *SAMHD1* and *ADAR1* play an important role in nucleic acids processing derived from retroelements and in the suppression of retroelements expansion avoiding their sensing by the immune system (156), mutations in these genes can lead to the accumulation of RNA:DNA hybrids and, consequently, to an abnormal immune response (Figure 19).

Remarkably, a connection between RNase H2 and TREX1 activity in RNA:DNA hybrids removal has been proposed by researchers. According to them, the RNA component of the hybrids is degraded by RNase H2 whereas the remaining ssDNA is degraded by TREX1 (85,160).

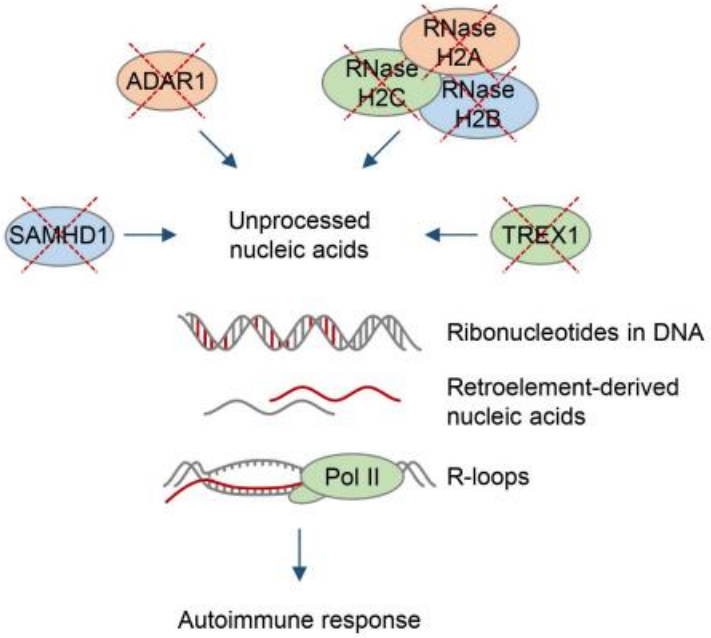

Figure 19. AGS is caused by mutations in genes involved in nucleic acid metabolism (*RNASEH2, TREX1, ADAR1 and SAMHD1*), which result in a response of the immune system (126).

1.6.2 RNA:DNA hybrids and immune system activation

The innate immune system has a key role in defending the host against pathogens. In order to exert its protective action, the innate immune system possesses a limited number of germline-encoded receptors, called pattern recognition receptors (PRRs) that sense molecular patterns associated to pathogens, also known as pathogen-associated molecular patterns (PAMPs) (161). PRRs include Toll-like receptors (TLRs), RIG-I-like receptors, Nod-like receptors (NLRs) and the DNA sensor cGAS (162,163).

It is of fundamental importance to distinguish between self and non-self nucleic acids and PRRs use two mechanism to specifically recognize nucleic acids of viral origin. The first one is represented by the identification of biochemical features that can only be found in viral, but not host, nucleic acids, whereas the second one is related to the ability of the host to restrict endogenous nucleic acids to specific locations inside the cell (163). When PRRs bind exogenous nucleic acids they start a vigorous antiviral response characterized by the induction of type I IFN release (164).

During tissue or cell damage, endogenous molecules may be release and recognize by PRRs triggering an inflammatory response. These molecules are called damage-associated molecular

patterns (DAMPs), highlighting the analogy with the acronym PAMPs. Therefore, DAMPs can initiate an inflammatory immune response in the absence of infections and these molecules have a central role in the development of autoimmune diseases (165).

AGS patients may present an accumulation of endogenous nucleic acids that trigger an abnormal immune response (36). In particular, *TREX1, RNASEH2* and *SAMHD1* mutated patients present an increased intracellular content of RNA:DNA hybrids (155). It has been demonstrated by two different research groups that RNA:DNA hybrids may be sensed by TLR9 and by the cGAS-STING pathway triggering a potent type I IFN response (86,87).

TLRs are the most characterized PRRs and they are highly expressed in immune cells and other cell types, such as fibroblasts, endothelial cells and chondrocytes (166). Ten subtypes of TLRs have been identified and they recognize different ligands and present different cellular localizations. TLR1, TLR2, TLR4, TLR5, TLR6, and TLR10 are located on cell membranes, whereas TLR3, TLR7, TLR8, and TLR9 are located in the endosomal compartments. The role of intracellular TLRs is to recognize nucleic acids derived from viruses, bacteria, and the host (167).

TLR9 was the first TLR to be discovered and it binds unmethylated CpG motifs and RNA:DNA hybrids (168) (86). TLR9 resides in the endolysosome where it is transported by the chaperon protein UNC93B1 (protein unc-93 homolog B1) (169). Once it reaches the endolysosome it undergoes a proteolytic cleavage of the ectodomain by proteases (170) and, therefore, the full-length TLR9 is only found in the endoplasmic reticulum. This cleavage is fundamental since it increases binding to unmethylated CpG motifs and allows the recruitment of the myeloid differentiation primary response 88 (Myd88), starting the signal transduction. Myd88 is an adaptor protein that leads to the activation of transcription factors, such as the nuclear factor kappa-light-chain enhancer of activated B cells (NF-κB), activating protein (AP)-1, or interferon response factor (IRF)-1, IRF-5, and IRF-7 (171,172,173). The expression of IFNs and other pro-inflammatory cytokines is then mediated and promoted by the translocation into the nucleus of these transcription factors (163).

More recently, a cytosolic DNA sensor able to induce a type I IFN response have been discovered (174,175). The cytosolic nucleic acid sensors include cyclic GMP-AMP (cGAMP) synthase (cGAS) binds to dsDNA in a sequence-independent manner (176,177). Upon dsDNA binding, cGAS uses ATP and GTP to synthesize a cyclic dinucleotide (CDN) molecule, known as cGAMP, which presents mixed 2′–5′ and 3′–5′ phosphodiester bonds (178-181). Then, the newly synthesized cGAMP molecule binds to STING which is located in the endoplasmic reticulum (182). Once activated, STING activates two protein kinases, IKK and TBK1, which activate the transcription factors NF-κB and IRF3, respectively. As previously described in the TLR9 signalling cascade, NF-kB and IRF3

translocate inside the nucleus in order to promote the expression of type I IFNs and other cytokines (87,183).

An aberrant accumulation of endogenous nucleic acids has been observed in AGS patients (36). In Trex1 knock-out mice models, cGAS has a central role in lethality and tissue destruction and the inhibition of cGAS in these trex1$^{-/-}$ mice resolves the lethal phenotype, diminishes tissue inflammation and reduces autoantibody production (184-186). Rnaseh2b$^{A174T/A174T}$ knock-in mice present a significant upregulation of interferon stimulated gene (ISG) transcript that resembles the interferon signature of AGS patients. This overexpression is dependent on the activation of the cGAS-STING pathway (187) which is triggered by endogenous RNA:DNA hybrids whose accumulation is due to *RNASEH2* mutations (Figure 20) (188).

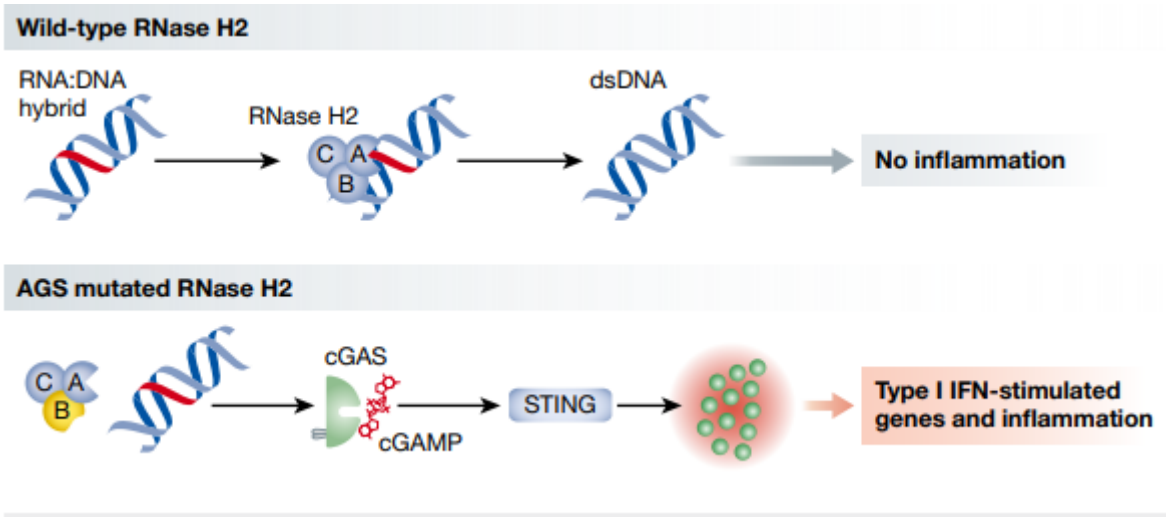

Figure 20. Mutations in RNase H2 complex result in RNA:DNA hybrids accumulation, which activate the cGAS-STING pathway and, consequently, a type I IFN response (188).

1.6.3 RNA:DNA hybrids degradation

RNA:DNA hybrids are often intermediate products of the replication process of the majority of microbial pathogens (189) and they can be delivered to endolysosomes in order to activate TLR9 or they may be transported into the lysosome following the autophagic process (190).

Intriguingly, a particular type of autophagy where lysosomes play a fundamental role, has been recently described and it has been defined with the term RNautophagy/DNautophagy (RDA). In this autophagic process, cellular RNAs and DNAs are directly engulfed and degraded by lysosomes in an ATP-dependent manner (Figure 21).

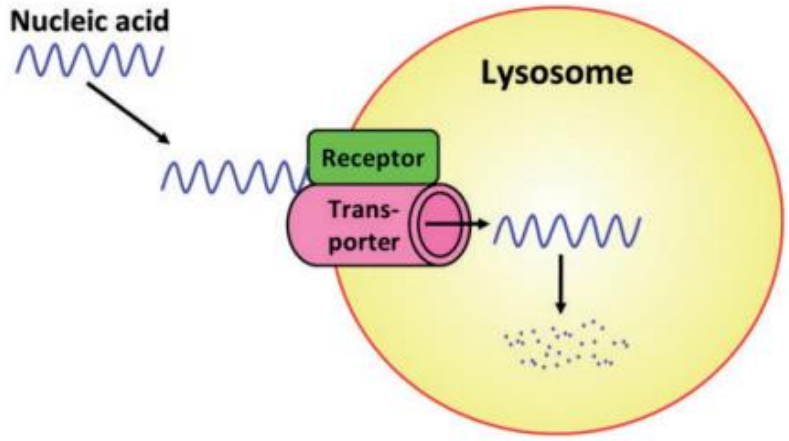

Figure 21. Model for the possible mechanism of RNautophagy/DNautophagy (191).

LAMP2C is a lysosomal membrane protein that can directly bind to nucleic acids and act as a receptor in RNautophagy and DNautophagy (192,193). LAMP2C is one of the three splice variant of LAMP2 gene (194), which is a major lysosomal membrane glycoprotein with a single transmembrane region. RNautophagy may have an important role in RNA homeostasis, especially in tissues that highly express LAMP2C, like the nervous system. This protein plays a key role in RDA since its overexpression leads to increased rates of RDA, whereas lamp2c knock-out mice show low levels of RDA. Interestingly, RDA in lamp2c knock-out mice is not completely abolished, suggesting that other proteins may have a role in RDA. Recently, Aizawa and colleagues found that SIDT2 may act as a nucleic acids transporter in lysosomes (195) (196). SIDT2 is a multipass membrane protein which is mainly localized in lysosomes (197). As described for LAMP2C, SID2T expression levels directly affect the rate of RDA. Intriguingly, an overexpression of SID2T in LAMP2 knock-out cells, stimulates RNautophagy even if LAMP2C activity is absent, highlighting that SID2T can exert its action independently from LAMP2C (195).

Therefore, RDA starts with an RNA substrate captured by an RNA-binding protein (RBP), that in turns binds the cytosolic tail of LAMP2C, located on the surface of the lysosomal membrane. At last, the substrate is incorporated into the lysosomal lumen in an ATP-dependent manner and the RNA is degraded by lysosomal enzymes, such as RNase T2 and DNase II, two endonucleases that cleaves single-stranded RNA (198) and double-stranded DNA (199), respectively.

RDA may also be involved in the entrapment of exogenous or viral nucleic acids into lysosomes or endosomes triggering an antiviral immune response mediated by TLRs (193). RNA:DNA hybrids are a molecular pattern that may be sensed by TLR9, which is located in the luminal region of endolysosomes and can induce a pro-inflammatory cytokine response triggering the innate immune

system activation (86). Thus, the endosomal sensing of RNA:DNA hybrids by TLR9 is physiologically relevant and these molecules may be degraded through RNautophagy/DNautophagy. These hybrids can also reach the lysosome through the canonical autophagic process (190). Autophagy, from the greek (from the Greek, "auto" oneself, "phagy" to eat) is an ancient and highly conserved mechanism first described by De Duve in 1967 (200). This process is responsible for the homeostatic turnover of great variety of intracellular compounds such as proteins, lipids, carbohydrates, nucleic acids, organelles and even intracellular pathogens (201). In mammalian cells, three types of autophagy have been described: microautophagy, macroautophagy and chaperone-mediated autophagy (CMA). Although they all present morphological differences, each of them ends with the delivery of the cargo to the lysosomes where it will be degraded and recycled (Figure 22) (202).

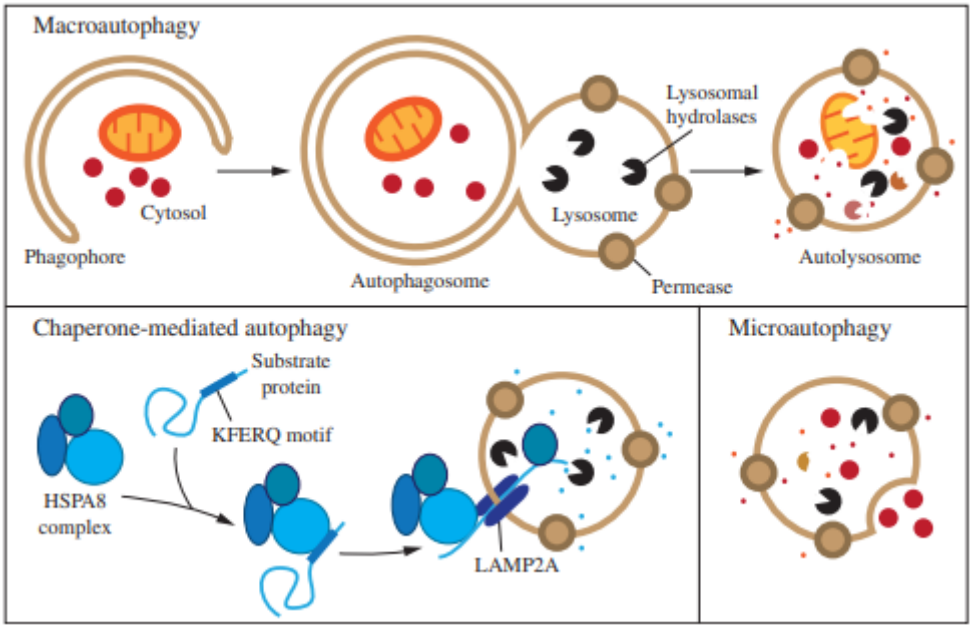

Figure 22. Three types of autophagy in mammalian cells (203).

Among these three kind of autophagic processes, macroautophagy is the best characterized and studied. The starting point of macroautophagy is represented by the formation of the phagophore, a small crescent-shaped structure. Its origin is still unknown, although different research groups have hypothesized that this structure could come from golgi apparatus (204), endoplasmic reticulum (205), mitochondria (206) and also the plasma membrane (207). This step is followed by the phagophore elongation where the cytoplasmic material is engulfed inside a double membrane autophagosome. Elongation is mediated by two conjugation systems involving ubiquitin-like (UBL) proteins (208). The first system involves the formation of the ATG12-ATG5-ATG16L1 complex whereas the second one involves the Atg8/LC3 system. LC3 is processed by ATG4, a cysteine protease, to expose a C-

terminal glycine (LC3-I). The ATG12-ATG5-ATG16L1 complex acts as an E3 ligase, mediating the conjugation of phosphatidylethanolamine (PE) with the C-terminal glycine of LC3-I, generating LC3-II (209-211). LC3-II subsequently associates with the phagophore and PE can be cleaved by ATG4 to release LC3 (212) (Fig. 5).

The step of maturation and closure is followed by the fusion between the autophagosome and lysosome in a process known as autophagosome maturation (213,214). The last step involves the degradation of the cargo by lysosomal enzymes. These last two step of maturation and degradation require the involvement of late endosome marker protein Rab7 and lysosomal membrane protein LAMP-2 (215).

Microautophagy is a non-selective lysosomal degradative process, where the cytoplasmic cargo is directly taken up by lysosomes or vacuoles. The lysosomal/vacuolar membrane is randomly invaginated and differentiated into autophagic tube to enclose parts of the cytoplasm. Among the main functions of microautophagy there are the maintenance of organellar size, membrane homeostasis, and cell survival under nitrogen restriction (216). Moreover, microauotophagy is coordinated with macroautophagy, chaperone mediated autophagy (CMA) and other forms of self-eating.

The third type of autophagy is the CMA which is a selective type of autophagy where cytosolic proteins enter in the lysosome for degradation through a protein translocation system located at the lysosomal membrane. In CMA only proteins amenable to unfolding can be internalized in lysosomes in a process similar to the protein transport system to other organelles (217). CMA starts with the binding of a cytosolic chaperone, the heat-shock cognate protein of 70 KDa (hsc70) to a consensus pentapeptide motif presents in the protein. The consensus peptide is Lys-Phe-Glu-Arg-Gln (KFERQ motif) and it is necessary and sufficient to target proteins to lysosomal degradation (218).

1.7 Treatments in AGS

AGS is a disease characterized by an abnormal response to endogenous nucleic acids and shares some features of both autoinflammatory and autoimmune disorders. More specifically, self-derived DNA is relevant for patients carrying mutations in *TREX1, RNASEH2* and *SAMHD1* genes, whereas in patients mutated in *ADAR1* and *IFIH1* the interferon response is driven by self-derived RNA (219). Therefore, some immune-modulating therapies have been empirically tested in a limited cohort of AGS patients, although the assessment of their efficacy could be difficult, because of the small number of treated patients and the diverse genotype involved, the different stages of the disease at which treatments were started and the different regimens employed. In wider terms, two strategies can be used to limit the pathological type I IFN response: the first approach is represented by the

hampering the production or improving the removal of endogenous nucleic acid stimuli; the second approach consists in blocking the downstream signaling of self-nucleic acid stimuli (219).

1.7.1 Reverse transcriptase inhibitors

Endogenous nucleic acids could arise from endogenous retroelements, suggesting that therapies with reverse transcriptase inhibitors (RTIs) could be beneficial for AGS patients. In a recent clinical trial, AGS patients mutated in *TREX1, RNASEH2A, RNASEH2B, RNASEH2C* or *SAMHD1* were treated with a combination of 3 RTIs (abacavir, lamivudine, and zidovudine) (220). Only 8 patients with mutations in *TREX1, RNASEH2A, RNASEH2B* and *SAMHD1* show a reduction of type I IFN signaling with no side effects. No clinical gains have been observed, but authors declared that all patients were already in an advanced stage of the disease with a significant neurological impairment at enrolment. Currently, researchers at the Children's Hospital of Philadelphia are exploring the efficacy and safety of other two RTIs (tenofovir and emtricitabine) administered to AGS children, although results are not yet available (221).

1.7.2 Janus Kinases inhibitors and antibody against IFN-α

Another therapeutic strategy in AGS is represented by Janus Kinases inhibitors (JAK inhibitors), such as ruxolitinib and baricitinib. JAK1 is an essential component of the type I IFN receptor complex and contributes to multiple cytokine signals. JAK1 inhibitors have already been used in the treatment of other type I interferonopathies such as familial chilblain lupus (222,223), CANDLE syndrome (chronic atypical neutrophilic dermatosis with lipodystrophy and elevated temperatures) (224) and SAVI (225,226). Regarding AGS, improvements have been observed in AGS patients with mutations in *RNASEH2B* (227), *SAMHD1* (228) and *IFIH1* (229) genes treated with ruxolitinib and baricitinib. Since IFN-α has a crucial role in AGS pathogenesis, the use of antibodies against the type I interferon receptor represents another strategy to stop the IFN-α activity. Currently, there are no clinical trial on AGS, but promising studies have been conducted in the context of SLE (230,231).

1.7.3 Hydroxychloroquine

Other therapeutic approaches can also involve molecules able to modulate the activity of nucleic acid receptors. Among these molecules, hydroxychloroquine (HCQ) is gaining more and more attention due to its immunomodulatory properties (232). HCQ sulfate is a 4-aminoquinoline firstly developed to treat malaria, although, due to its immunomodulatory properties, it is now widely used in the therapy of autoimmune diseases, such as SLE and rheumatoid arthritis (RA) (233). Antimalarial drugs

can affect lysosomal activity, autophagy and signalling pathways. Regarding lysosome activity and autophagy, it is well known that HCQ can interfere with both processes. Lysosomes are spherical vesicles that contain hydrolytic enzymes activated by the highly acidic pH. These organelles play an important role in recycling cell substrates, in antigen processing and MHC class II presentation and HCQ interferes with their activity by increasing their pH (234).

HCQ can also interfere with two immune signaling pathways: cGAS-STING and TLRs. In silico predictions identified several antimalarial drugs as inhibitors of DNA and cGAS binding and further analysis predicted that HCQ could interact with the DNA binding site of cGAS (232). Nonetheless it remains unclear if HCQ is able to inhibit cGAS by binding to dsDNA or to cGAS (235). Important clues about the inhibitory effect of HCQ came from studies on TLR9 signalling. HCQ reduces inflammatory responses by inhibiting TLRs activation and interfering with TLRs processing (170). Moreover, HCQ might block TLR9 signalling by steric blockade, inhibiting the interaction between TLRs and their ligand. Some research studies based on surface plasmon resonance and fluorescence spectroscopy demonstrated that this drug can alter the interaction between CpG and TLR9 (236) (Figure 23).

At last, HCQ play also an important role in reducing the release of pro-inflammatory cytokines from a variety of cells. In vitro, HCQ inhibits the production of TNF-α, IFN-γ and IL-6 by peripheral blood mononuclear cells (PBMCs) (237) and the release of TNF-α, IL-1β, and IL-6 in human monocytes (238).

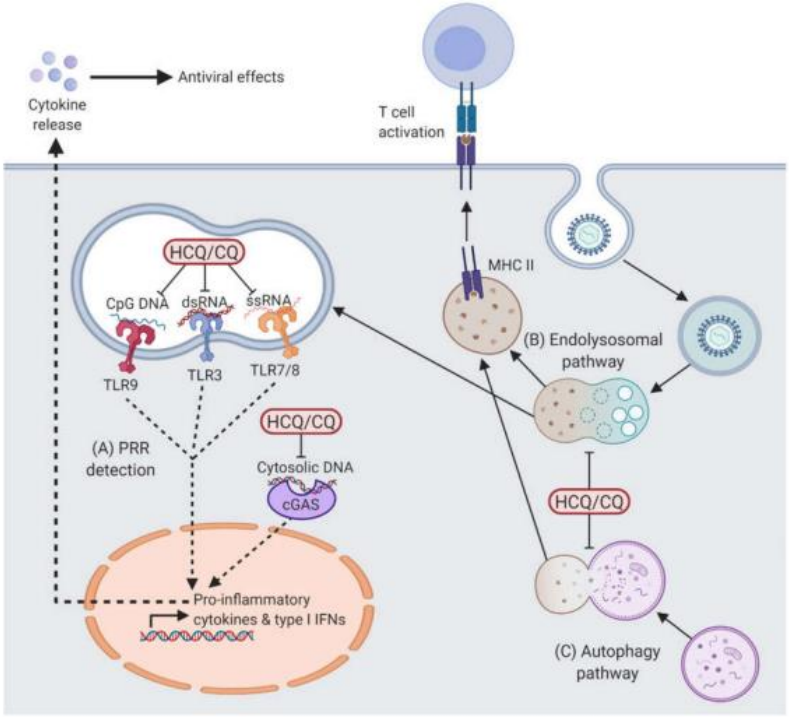

Figure 23. Molecular mechanisms of hydroxychloroquine and chloroquine during autoimmunity (235).

2. Aim of the work

Aicardi-Goutières Syndrome (AGS) is a rare, genetically determined encephalopathy with autosomal recessive and dominant inheritance, caused by mutations in 7 genes (*TREX1, RNASEH2A, RNASEH2B, RNASEH2C, SAMHD1, ADAR1* and *IFIH1*) and onset in the first year of life (2). Main features of this disorder are represented by acquired microcephaly (sometimes congenital), basal ganglia calcifications, white matter abnormalities, chronic lymphocytosis and raised IFN-α levels in CSF and in serum, together with bilateral spasticity, dystonia, ocular jerks and progressive brain atrophy. The clinical picture resembles congenital infections, even if the TORCH complex analysis always results negative (4,19). Although general knowledge about AGS is increasing, the real AGS incidence is still unknown. The first aim of our work was to characterize the Italian cohort of AGS patients, collecting both clinical and genetic information. We also decided to evaluate the interferon signature of some of our AGS patients, in order to identify a possible correlation between mutation and interferon score results.

Some genotype-phenotype association in AGS patients have been observed, as described in the introduction section. Nonetheless, in our cohort of patients, we observed some patients carrying the same mutation (p.A177T) but presenting either a classic phenotype or a mild phenotype characterized by normal IQ in almost all patients. Therefore, in order to understand the reason why patients carrying the same p.A177T mutation in *RNASEH2B* gene can develop a mild phenotype or a classic severe phenotype, we performed epigenetic analysis by studying their transcriptome and DNA methylation. Up to now, only one study has focused on this particular aspect of the disease and fibroblasts of patients mutated in *RNASEH2* subunits showed an upregulation of genes involved in inflammation, immune responses, chemokine signalling pathways and sensing of viral nucleic acids with a global decrease of genomic DNA methylation that impact almost all genomic compartments (155). Thus, in our project, we focused our analyses on the two subgroups of p.A177T *RNASEH2B* patients with the aim of discovering epigenetic perturbations that could possibly explain the phenotypic differences between these children.

Although it is known that the seven AGS-related genes are involved in nucleic acid metabolism and sensing and that mutations in one of these genes lead to an abnormal immune system activation and type I IFN release, the molecular mechanism underlying the syndrome are still controversial. We focused our project on the most frequently mutated gene in AGS patients: *RNASEH2*. RNase H2 is the major source of endonuclease activity in eukaryotes (91). This enzyme specifically degrades the RNA portion from RNA:DNA hybrids (88) and removes single ribonucleotides that can be mistakenly incorporated in genomic DNA (98) during the processes of DNA replication and repair. Genetic mutations in RNase H2 complex result in a loss of function of the enzyme and can lead to

the accumulation of intracellular nucleic acids fragments and RNA:DNA hybrids, that in turn activate the innate immune response. LCLs from patients with AGS carrying mutations in *RNASEH2A* and *RNASEH2B* genes presented an accumulation of misincorporated ribonucleotides in the DNA and impaired cell cycle progression, in association with chronic activation of post replication repair mechanisms (108,113). It has also been demonstrated that RNA:DNA hybrids can bind both TLR9 and cGAS sensor, possibly leading to a pathological activation of the immune system, however it was never demonstrated if in AGS patients carrying different mutations in *RNASEH2*, RNA:DNA hybrids can directly activate those diverse pathways. Thus, third aim of this work was to investigate the immune system activation by self-derived nucleic acids in lymphoblastoid cell lines (LCLs) derived from patients with mutations in RNase H2 subunits.

At last, since AGS is characterized by an abnormal immune response to self-derived nucleic acids and considering the inflammatory basis of the disease, two type of therapeutic approaches have been proposed. The first one has the aim of reducing the production or stimulating the removal of self-nucleic acid, whereas the second one has the objective of stopping the downstream signalling of self-nucleic acid stimuli (219). Recent studies demonstrated that antimalarial drugs, such as hydroxychloroquine, can inhibit immunological pathways activation and can also partially cross the blood brain barrier (239), paving the way to new opportunities for the treatment of interferonopathies. Indeed, HCQ is already used to treat other autoimmune diseases such as SLE and RA (233), and in this project we wanted to understand if HCQ is able to modulate the innate immune system activation also in AGS patients. Therefore, we decided to treat *RNASEH2B* and *RNASEH2A* mutated LCLs with HCQ in order to assess the impact of the drug on the inflammation process, due to its ability to compete with both cGAS and TLR9 for binding of nucleic acids and its role in endolysosomal activities, including autophagy, which has been proposed as a possible mechanism involved in RNA:DNA hybrids discard (86).

3. Materials and Methods

3.1 Patients' enrolment

Patients affected by AGS were enrolled at the IRCCS Mondino Foundation, Pavia, Italy. All patients are descendants of parents and grandparents of Italian nationality and Italian patients with even one foreign parent were excluded. The patients were diagnosed according to clinical suggestion guided by defined criteria (6,10,240). Healthy volunteers, free from any pharmacological treatment and pathology, were recruited at the Transfusion Centre of the IRCCS Policlinico S. Matteo Foundation in Pavia, Italy. This study was approved by the local ethics committee (approval n. 3549/2009 of 30/9/2009 and 11/12/2009, and n.20170035275 of 23/10/2017) of the IRCCS Mondino Foundation, Pavia, Italy and written informed consent was obtained from every participant or authorized relatives. Interferon signature analysis was performed in 18 out of 51 Italian AGS patients at IRCCS Mondino Foundation.

3.2 Genetic test

Blood samples from eight AGS patients (4 females and 4 males) were collected at IRCCS Mondino Foundation in vacutainers containing EDTA. Genomic DNA extraction was performed using a semi-automated method Maxwell® 16 System DNA Purification (Promega, Madison, WI, USA). DNA was quantified with NanoDrop ND1000 UV-Vis Spectrophotometer and Qubit® fluorometer (Thermo Scientific, Waltham, MA, USA). The genetic tests have been performed in different centers since 2006 initially using Sanger sequencing and then Next Generation Sequencing (NGS). For Sanger sequencing, we used a standard protocol to amplify AGS-related genes coding exons using primers located in adjacent intronic regions from genomic DNA by polymerase chain reaction (PCR). All amplicons were screened by direct sequencing using Big-Dye Terminator v3.1 sequencing kit (Applied Biosystems) and ABI 3130 Genetic Analyzer (Applied Biosystems, Foster City, CA, USA). Each fragment was sequenced on both strands. The alignment to the corresponding reference sequence was performed using Sequencher 4.8 software (Gene Codes Corporation, Ann Arbor, MI, USA). Latest genetic diagnoses was performed using Nextera Enrichment Sample Illumina (Illumina), according to the manufacturers' instructions. Five diagnoses were performed at IRCCS Mondino Foundation, 5 at Besta Foundation and 2 at Bambino Gesù Children's Hospital. In the panel were included *TREX1, RNASEH2B, RNASEH2C, RNASEH2A, ADAR1, SAMHD1, IFIH1* and *RNASET2* genes. DNA processing and DNA-seq analysis were carried out using Illumina MiSeq Sequencer. Samples were loaded on MiSeq instrument and the first steps of bioinformatic analysis (including base calling and demultiplexing) performed using MiSeq provided software (Real Time

Analysis RTA v.1.18.54 and Casava v.1.8.2, Illumina, Inc., San Diego, CA, USA). FastQ files provided for each sample, containing mate paired-end reads after demultiplexing and adapter removal, were used as input for an ad-hoc developed pipeline previously described (241). Variant annotation was performed using Annovar software (table_annovar.pl). Mutations were considered pathogenic if they were very rarely found in healthy controls (i.e., dbSNP, and 1000 Genomes databases), predicted to alter the sequence of the encoded protein (nonsynonymous, nonsense, splice-site, frameshift, and insertion/deletion mutations) and to adversely affect protein function, with the use of in silico prediction software (SIFT, PolyPhen, MutationTaster). Genetic regions with low coverage (less than 30×) and all identified variants were confirmed using Sanger sequencing (primer sequences and PCR conditions are available upon request).

3.3 Multiplex Ligation-Dependent Probe Amplification (MLPA)

In order to evaluate possible duplications or deletions, AGS-related genes were analyzed with SALSA MLPA P388-A2 Aicardi-Goutières syndrome probe mix kit (MRC-Holland, Amsterdam, The Netherlands). It consists of probes mapped on *TREX1, RNASEH2A, RNASEH2B*, *RNASEH2C* and *SAMHD1* genes. To perform data analysis, we used GeneScan ver.3.1. Data importation and elaboration have been made with the software Coffalyser (MRC-Holland, Amsterdam, the Netherlands). The changes were considered significant for values that presented a deviation greater than 30% compared to controls.

3.4 Interferon signature

Peripheral blood from 18 patients and 31 healthy controls were collected into PaxGene™ tubes (PreAnalytiX, Hombrechtikon, Switzerland) for RNA isolation. Tubes were kept at room temperature for 2 h and frozen at −80°C within 24 h. RNA extraction was performed according to the manufacturer's protocol and its concentration assessed using a NanoDrop ND1000 UV-Vis Spectrophotometer (Thermo Scientific, Waltham, MA, USA). For each sample we retrotranscribed 800 ng of RNA using kit iScript™ Reverse Transcription Supermix for RT-qPCR (Bio-Rad, Hercules, CA, USA). The expression analysis of six interferon-stimulated genes was performed using the TaqMan Universal PCR Master Mix (Applied Biosystems, Paisley, UK), and cDNA derived from 40 ng total RNA. The relative abundance of target transcripts was measured using TaqMan probes for *IFI27* (Hs01086370_m1), *IFI44L* (Hs00199115_m1), *IFIT1* (Hs00356631_g1), *ISG15* (Hs00192713_m1), *RSAD2* (Hs01057264_m1), and *SIGLEC1* (Hs00988063_m1), and normalized to the expression level of *HPRT1* (Hs03929096_g1) and *18S* (Hs999999001_s1) as described by Rice

and collaborators (24). To perform this assay, the LightCycler 480 (Roche) was used. AGS patient data were expressed relative to the average of 31 healthy controls. The median fold change of the six ISGs of the 31 normal controls plus two SDs (+2 SD), was used to create a score as reported in (242). In our case it was 2.216. For each patient, relative quantification (RQ) ($2^{-\Delta\Delta Ct}$) (243), i.e., the normalized fold change relative to the mean of each ISGs of the 31 controls, was calculated. The mean interferon score was given by the mean of the six genes and if it was above the score, it was designated as positive.

3.5 Cells isolation

Peripheral blood mononuclear cells (PBMCs) were immediately isolated from peripheral venous blood using Histopaque®-1077 (Sigma-Aldrich, St. Louis, MO, USA), following manufacturer's specifications. Briefly, blood samples were carefully posed in a centrifuge tube over an equal volume of Histopaque®-1077 and centrifuged at 1800 RPM for 30 minutes with low deceleration. PBMCs were then recovered from the intermediate phase using a glass Pasteur pipette and washed with 1X PBS (Sigma-Aldrich, St. Louis, MO, USA). Collected cells were centrifuged at 1600 RPM for 10 minutes and supernatants were discarded. All clinical information and samples were obtained with informed consent.

3.6 EBV-immortalization and cell culture

EBV-immortalization was performed by Doctor Chiara Baldo at Laboratorio di Genetica Umana, IRCCS Istituto Giannina Gaslini, Genoa. LCLs carrying mutations in *RNASEH2A* (p.R108W+p.F230L) and *RNASEH2B* (p.A177T) genes and healthy controls (CTRL) were analyzed. Cell lines were maintained in RPMI 1640 medium (CARLO ERBA Reagents S.r.l., Cornaredo, Italy), supplemented with 20% fetal bovine serum (FBS) (CARLO ERBA Reagents S.r.l., Cornaredo, Italy), 0.3 mg/L L-glutamine and 5% penicillin-streptomycin (CARLO ERBA Reagents S.r.l., Cornaredo, Italy), at 37 °C in a humidified atmosphere with 5% of CO2. At need, cells were pelleted by centrifugation, washed with 1X PBS and further processed as required. LCLs of healthy controls and mutated patients were treated with 25µM of hydroxychloroquine (Sigma-Aldrich, St. Louis, MO, USA) for 24h which represent the IC50 for this drug (232).

3.7 RNA extraction with Trizol reagent

RNA from LCLs was isolated with Trizol® reagent (Sigma-Aldrich, St. Louis, MO, USA) according to manufacturer's specifications. RNA was then quantified by NanoDrop ND1000 UV-Vis Spectrophotometer (Thermo Fisher Scientific, Waltham, MA, USA).

3.8 Transcriptome analysis

RNAs isolated from patient's LCLs were quantifed using a Nanodrop ND-1000 Spectrophotometer (Nanodrop Technologies, Wilmington, USA) and a 2100 Bioanalyzer (Agilent RNA 6000 Nano Kit, Waldbronn, Germany); RNAs with a 260:280 ratio of ≥1.5 and an RNA integrity number of ≥8 were subjected to deep sequencing. Sequencing libraries were prepared with the Illumina TruSeq Stranded RNA Library Prep, version 2, Protocol D, using 500-ng total RNA (Illumina). Qualities of sequencing libraries were assessed by 2100 Bioanalyzer with a DNA1000 assay and RNA processing was carried out using Illumina NextSeq. 500 Sequencing. FastQ files were generated via Illumina bcl2fastq2 (Version 2.17.1.14 - http://support.illumina.com/downloads/bcl2fastq-conversion-software-v217.html) starting from raw sequencing reads produced by Illumina NextSeq sequencer. Gene and transcript intensities were computed using STAR/RSEM software (244) using Gencode Release 19 (GRCh37.p13) as a reference, using the "stranded" option. Differential expression analysis for mRNA was performed using R package EBSeq (245). This tool was selected because of its superior performance in identifying isoforms differential expression (246). Differential expression analysis for long non-coding RNAs was performed with the R package DESeq. Coding and non coding genes were considered differentially expressed and retained for further analysis with |log2(disease sample/healthy control)|≥1 and a FDR≤0.1. We imposed minimum |Log2FC| of 1 and a FDR lower than 0.1 as thresholds to differentially expressed genes. This choice is motivated by the decision to maximize the sensitivity of this analysis, in order to perform a massive screening and identify candidate genes to be validated with a wider sample population with real-time analysis.

3.9 DNA methylation analysis

The Illumina Infinium Methylation EPIC BeadChip was used to interrogate DNA methylation in peripheral blood samples from patients carrying the p.A177T mutation with mild and severe patients and sex and age-matched healthy controls. Samples were randomized on the BeadChip in order to avoid batch effects. Data acquisition, preprocessing, quality control (QC), and normalization of methylation data have been performed using the R packages minfi and ChAMP (247,248). Genes showing a p-value < 0.05 and $\beta > |0.1|$ were considered differentially methylated. Gene Ontology analysis was done with the clusterProfiler package (249). Publicly available reference DNA

methylation signatures of flow sorted blood cell types were used to estimate blood cell type distribution for each of the study samples applying the method by Houseman et al. (250).

3.10 RIPA proteins extraction and quantification

Soluble protein samples were obtained with the extraction with RIPA (Radio Immuno Precipitation Assay) buffer was composed of 50mM Tris-HCl (pH 8.0), 150mM NaCl, 1% NP-40, 12mM Deoxycolic acid and supplemented with protease inhibitors. Protein concentration was determined using bicinchoninic acid (BCA) method (Sigma-Aldrich, St. Louis, MO, USA) and bovine serum albumin (BSA) (Sigma-Aldrich, St. Louis, MO, USA) as standard. Proteins quantification was determined using NanoDrop (Thermo Fisher Scientific, Waltham, MA, USA).

3.11 Western blot

Western Blotting analysis was performed by SDS–polyacrylamide gel electrophoresis (SDS-PAGE). Samples containing 30µg of proteins were loaded into 12.5% SDS-PAGE gel. Then, samples were transferred to PVDF membranes using a semidry transfer apparatus (Trans-blot Turbo, Bio-Rad Laboratories, Hercules, California, USA). Membranes were treated with a blocking solution, containing 5% of non-fat dry milk in 1X TBS-T buffer (10mM Tris-HCl, 100mM NaCl, 0.1% Tween, pH 7.5), for 1h and then incubated overnight with the primary antibodies at 4°C. Immunoreactivity was detected using the donkey anti-rabbit or anti-mouse secondary peroxidase-conjugated (GE Healthcare, UK) with 1:8000 dilution. The immunoreactive bands were visualized using the enhanced chemiluminescence detection kit (ECL Advance, GeHealthcare, UK). The following antibodies were used for western blot analysis: mouse monoclonal anti-cGAS (sc-515777, Santa Cruz Biotechnology, Dallas, Texas, USA, dilution 1:500), rabbit polyclonal anti-LC3 (L8918, Sigma-Aldrich, St. Louis, MO, USA, dilution 1:500), rabbit polyclonal anti-SQSTM1/p62 (ab91526, Abcam, Cambridge, UK, dilution 1:500), rabbit polyclonal anti-GAPDH (GTX100118, GeneTex, Irvine, CA, USA, dilution 1:10000), mouse monoclonal anti-TFAM (sc-376672, Santa Cruz Biotechnology, Dallas, Texas, USA, dilution 1:500), mouse monoclonal anti-LDH (sc-133123, Santa Cruz Biotechnology, Dallas, Texas, USA, dilution 1:1000), mouse monoclonal anti-COX IV (ab14744, Abcam, Cambridge, UK, dilution 1:1000).

3.12 Immunofluorescence

About $1x10^5$ cells were placed on a poly-L-Lysine slide (Thermo Fisher Scientific, Waltham, MA, USA) and incubated at room temperature (RT) for 20 minutes. Cells were stained with ER-Tracker™

(1μM) or Mito-Tracker™ (100nM) red dyes (Thermo Fisher Scientific Inc., Waltham, MA, USA) and then incubated for 30 minutes at 37°C. Cells were also stained with endolysosomal marker LysoTrackerTM red dye (Thermo Fisher Scientific Inc., Waltham, MA, USA) diluted in 1X PBS at final concentration of 75nM and then incubated for 1h and 30 minutes at 37°C. Cells were then fixed using a solution of 4% paraformaldehyde for 15 minutes at RT. Fixed cells were then permeabilized with 0.1% Triton™ X-100 (Sigma-Aldrich, St. Louis, MO, USA) for 10 minutes. Samples were treated with a blocking solution (0,05% Triton™ X-100, 1% BSA in 1X PBS) for 1h and were incubated with the primary antibody overnight at 4°C and incubated with secondary antibody for 1h at RT. For RNase H-treated cells, 2 IU of RNase H (NEB, Ipswich, MA, USA) with or without 1 μg RNase A (Roche) in PBS buffer for 1 hour at 37˚C was used prior to antibody incubation. They were finally washed 1X PBS, mounted with ProLong® Gold Antifade Reagent with DAPI (Thermo Fisher Scientific, Waltham, MA, USA), dried and nail-polished. Slides were analyzed with a confocal laser microscope using z-stack acquisition (Leica DM IRBE, Leica Microsystems Srl, Italy). The following antibodies were used for immunofluorescence: mouse monoclonal anti-S9.6 (MABE1095, Sigma-Aldrich, St. Louis, MO, USA, dilution 1:250), rabbit polyclonal anti-LC3 (L8918, Sigma-Aldrich, St. Louis, MO, USA, dilution 1:250), rabbit polyclonal anti-SQSTM1/p62 (ab91526, Abcam, Cambridge, UK, dilution 1:250).

3.13 RNA extraction with Trizol reagent

RNA from LCLs was isolated with Trizol® reagent (Sigma-Aldrich, St. Louis, MO, USA) according to manufacturer's specifications. RNA was then quantified by NanoDrop ND1000 UV-Vis Spectrophotometer (Thermo Fisher Scientific, Waltham, MA, USA).

3.14 Reverse transcription and Real-Time PCR

800ng of RNA was reverse transcribed using the iScript™ Reverse Transcription Supermix kit for RT-qPCR (Bio-Rad Laboratories, Hercules, CA, USA), according to the manufacturer's recommendations. 4μL of 5x iScript Reaction Mix, 1μL of iScript Reverse Transcriptase and Nuclease-free water were added to RNA in order to reach a total volume of 20μL. The relative abundance of target transcripts was measured using TaqMan probes (Applied biosystems, Foster City, CA, USA) for *IFI44L* and *IFIT1* (Hs00199115_m1 and Hs00356631_g1) and normalised to the expression level of *HPRT1* (Hs03929096_g1) as described in literature (242). To perform this assay, the CFX96™ Real-Time PCR Detection System (Bio-Rad Laboratories, Hercules, CA, USA) has been used.

For MYD88, NF-kB, IRF3 and IRF7 analysis, total RNA was reverse transcribed using the iScript cDNA synthesis kit (Bio-Rad Laboratories, Hercules, CA, USA) according to the manufacturer's protocol. The reaction mix was incubated for 5 min at 25°C, for 30 min at 42°C and for 5 min at 85°C. The cDNA samples were stored at −20°C. qPCR reactions included 200 nM of each oligonucleotide, 1 ul of SYBR Green SuperMix (BioRad, Richmond, CA), and 1 µL of cDNA template (or water control). Primers are indicated in Table 1.

Cycle threshold (Ct) values were automatically recorded for each replicate qPCR reaction, and mean Ct values were normalized against those determined for GAPDH. Fold-expression differences relative to healthy controls were determined using the 2-ΔΔCt method.

Gene symbol	**Forward sequence**	**Reverse sequence**
MYD88	TGTCTGCGACTACACCAACC	ACAACGAAAGGAGGAGGCAG
NF-kB	ACAGCTGGATGTGTGACTGG	TCCTCCGAAGCTGGACAAAC
IRF3	GAGGTGACAGCCTTCTACCG	TGCCTCACGTAGCTCATCAC
IRF7	ATGGGCAAGTGCAAGGTGTA	GATGGTATAGCGTGGGGAGC
GAPDH	ATGGAAATCCCATCACCAT	CGCCCCACTTGATTTTGG

Table 1. Primers sequences

3.15 Flow cytometry

About $1x10^6$ cells were collected for each condition. For viability staining, Zombie Violet dye solution (BioLegend, San Diego, California, USA) (1:500 in 1X PBS) was used. Cells were then labelled with anti-CD19 APC-H7 or isotype control antibody (0.25µg/mL) (BD Biosciences, Franklin Lakes, New Jersey, USA). Both tubes were centrifuged at 1600 RPM for 5 minutes, the supernatant was removed and a permeabilizing factor (1X BD FACS) (BD Biosciences, Franklin Lakes, New Jersey, USA) was added at RT. Cells for each tube were rinsed with a washing buffer (1X PBS, Perm/wash 1X, 2% FBS) and centrifuged twice at 1600 RPM for 5 minutes. The resulting pellets were resuspended with the perm/wash solution and labelled with anti-S9.6 PE and isotype control for 1h at room temperature. S9.6 labelled with PE has been obtained with PE / R-Phycoerythrin Conjugation Kit (Abcam, Cambridge, UK). For viability, necrosis and apoptosis assessments, Annexin V and 7-Amino-Actinomycin (7-AAD) vital dye have been used to identify dead cells (BD Biosciences, Franklin Lakes, New Jersey, USA). Samples were analysed immediately after labelling, using a BD FACS Canto II with BD FACS Diva software (BD Biosciences, Franklin Lakes, New Jersey, USA).

3.16 Immuno-gold labelling of anti-RNA:DNA antibody

Approximately 3×10^6 cells were washed in 1X PBS (Sigma-Aldrich, St. Louis, MO, USA) and incubated with the fixing solution (2.5% glutaraldehyde and 2% paraformaldehyde in cacodylate buffer, pH 7.3) at 4°C for 4 hours, followed by a post-fixation step in 1.5% osmium tetroxide for 1 hour at room temperature and Epon-Araldite embedding (251). Ultra-thin Lowicryl sections were mounted on formvar nickel grids and washed in 5% BSA (1X PBS, 0.05% Triton X-100) for 10 min. Then the grids were incubated with the anti-RNA:DNA hybrid antibody diluted 1:300 in 1X PBS for 1 h at room temperature. After washing in 1X PBS, they were floated in protein A conjugated to 10-nm colloidal gold particles (Sigma-Aldrich, St. Louis, MO, USA), diluted 1:25 in PBS for 45 min at room temperature. They were washed in 1X PBS and then bidistilled water. Finally, the sections were counterstained with 5% uranyl acetate and observed in a Hitachi EM H-600-2 at 75 kV (252).

3.17 mtDNA isolation and real-time PCR

DNA isolation from LCLs have been performed by using the QIAamp DNA Mini Kit (QIAGEN, Germany) following manufacturer's instructions. DNA was then quantified by NanoDrop ND1000 UV-Vis Spectrophotometer (Thermo Fisher Scientific, Waltham, MA, USA). The relative abundance of target transcripts was measured using primers for MT-ND (Forward: ATGGCCAACCTCCTACTCCT; Reverse: TAGATGTGGCGGGTTTTAGG) and normalised to the expression level of β2M (Forward: CAAATTCAAACCCAGCCTGT; Reverse: TCCTGCCTGGAACTCTCTGT). To perform this assay, the CFX96™ Real-Time PCR Detection System (Bio-Rad Laboratories, Hercules, CA, USA) has been used.

3.18 Statistical analysis

Values were expressed as means ± S.D. Statistical analysis was performed by One-Way Analysis of Variance (ANOVA) followed by Tukey's Test as a post-hoc test (GraphPad Prism version 5 (USA)). Values were considered statistically significant when p-values were < 0.05.

4. Results

4.1 Characterization of the Italian cohort of AGS patients

Up to now, the real incidence of AGS is still unknown. IRCCS Mondino Foundation is the Italian reference centre for AGS and, with this project, we decided to describe for the first time the genetic landscape and the ISGs expression of our large cohort of patients (Table 2).

Number of patients	Mean Age	Sex
51	12.44 ± 7.34	32 males 19 females

Table 2. Italian population with Aicardi-Goutières Syndrome.

The NGS analysis allowed us to identify mutations in AGS-related genes in 94% of AGS patients, whereas the remaining 6% of patients presented a clear AGS phenotype, although no mutations in one of the seven AGS genes were found. As described by Figure 1, 59% of Italian AGS patients had mutations in *RNASEH2B*, 11% in *IFIH1*, 8% in *TREX1*, 8% in *SAMHD1*, 4% in *RNASEH2A*, 2% in *RNASEH2C* and 2% in *ADAR1* (Figure 24). Interestingly, three patients were phenotypically diagnosed with the infantile onset of AGS but no mutation in any of the AGS-related genes was identified. After NGS, compound heterozygous mutations have been observed in *RNASET2* gene and both variants were predicted to be damaging by *in silico* analyses (Mutation Taster). A summary of mutations identified in each gene is reported in table 3.

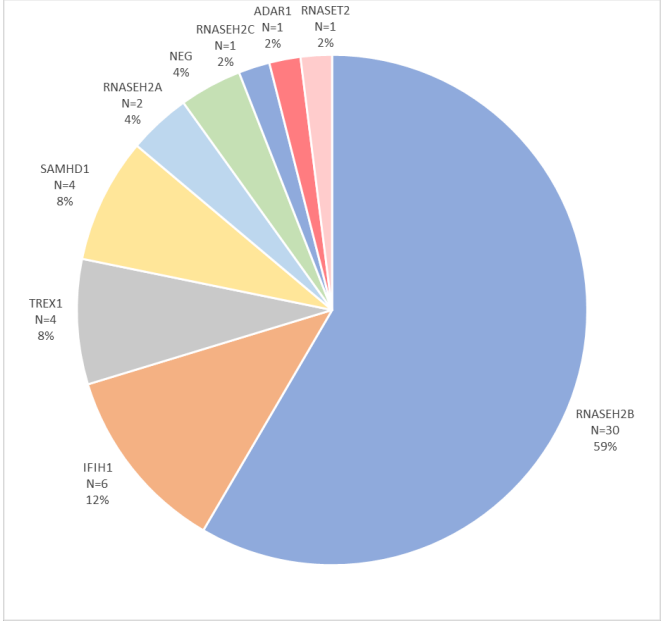

Figure 24. Numbers and percentages of patients with Aicardi–Goutières syndrome with or without mutations in *TREX1, RNASEH2A, RNASEH2B, RNASEH2C, SAMHD1, ADAR1, IFIH1* and *RNASET2* genes (253).

Gene	Mutation	Homozygous/Heterozygous [%]	MAF [£] (ExAC)
TREX1	p.S88Kfs*	0/1	NA
	p.R97H	0/1	T = 0.000008/1
	p.R114H	1/1	A = 0.0002/19
	p.N51Gfs*50	1/0	NA
	p.P290_A295del	0/1	- = 0.00007/8
	p.R169H	0/1	A = 0.0002/19
RNASEH2A	p.R108W	0/1	A = 0.000008/1
	p.F230L	0/1	A = 0.000008/1
	p.R186W	0/1	NA
	p.V23V	0/1	A = 0.00002/3
RNASEH2B	p.W73L	0/2	NA
	p.T163I	0/7	NA
	p.A177T	17/12	A = 0.0013/158
	p.V185G	1/0	NA
	p.A212V	0/1	NA
	p.Ex9_Ex11del	0/1	NA
	c.64+1G>A	0/1	NA
RNASEH2C	p.D39Y	0/1	NA
	c.173-1G>C	0/1	
SAMHD1	p.D137G	2/0	T = 0.000008/1
	p.Q465*	0/1	NA
	c.1410+5G>C	0/1	NA
	p.Ex12_Ex16del	1/0	NA
ADAR1	p.P193A	0/1	C = 0.0021/260
	p.A870T	0/1	NA
IFIH1	p.D393V	0/1	C = 0.000008/1
	p.R720Q	0/1	NA
	p.R824K	0/1	NA
	p.R779H	0/2	NA
	p.M854K	0/1	NA
RNASET2	p.K133del	0/1	- = 0.00002/2
	p.E49*	0/1	NA

[%] Heterozygous/Homozygous: Number of families with a heterozygous/homozygous change. [£] MAF: Frequency of the allele/number of times the SNP has been observed in the studied population.

Table 3. Summary of identified mutations (253).

We also assessed the so-called interferon signature of 18 AGS patients. We evaluated the expression levels of six ISGs (*IFI27, IFI44L, IFIT1, ISG15, RSAD2* and *SIGLEC1*) normalized to the expression levels of two housekeeping genes (*HPRT1* and *18S*) (Figure 25) and eleven patients tested positive, whereas seven subjects presented a negative interferon score (Figure 26A). Among positive patients, seven were mutated in *RNASEH2B*, one in *RNASEH2C*, one in *SAMHD1* and two in *IFIH1*. Regarding negative patients, five were mutated in *RNASEH2B*, one in *RNASET2* and the last one presented all the symptoms associated with AGS though the patient carried no mutations in the seven AGS-related genes. Interestingly, all negative patients mutated in *RNASEH2B* carried the p.A177T, which is the most common mutation found in AGS patients (Figure 26B).

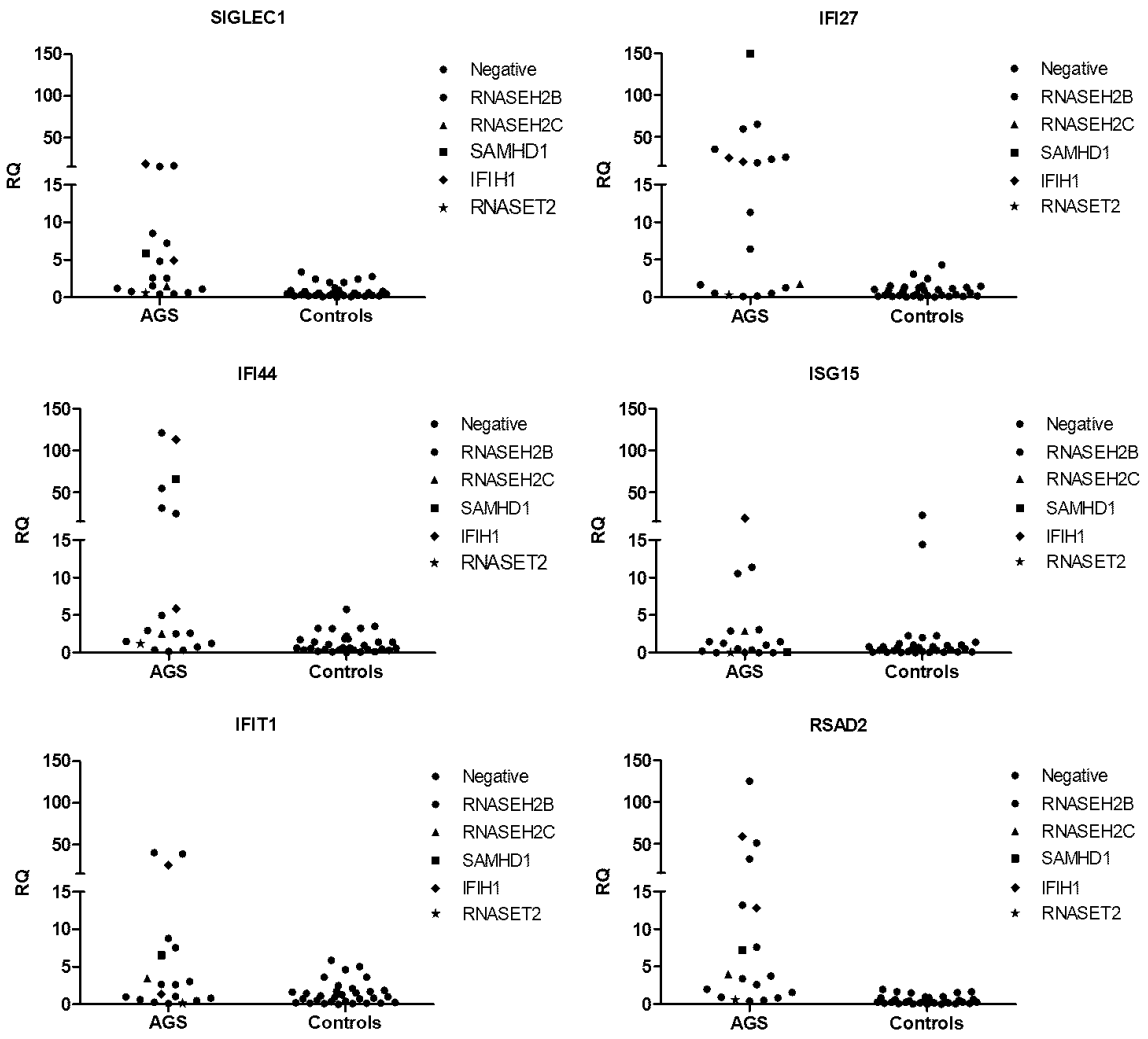

Figure 25. Median fold expression of six interferon-stimulated genes ISGs *IFI27, IFI44, IFIT1, ISG15, RSAD* and *SIGLEC1* according to the genotype of 18 AGS patients and 31 controls (253).

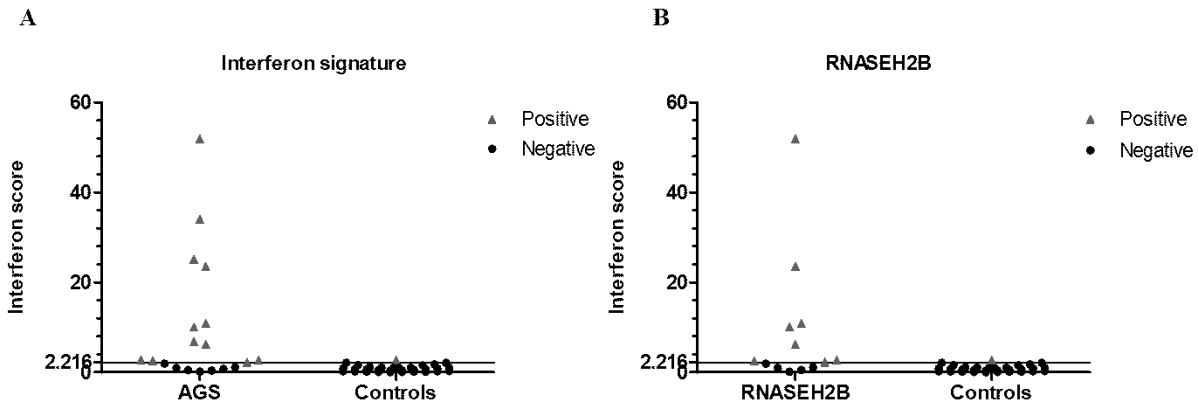

Figure 26. Interferon signature results of 18 AGS patients. (A) Quantitative reverse transcription PCR of six ISGs *IFI27, IFI44, IFIT1, ISG15, RSAD2* and *SIGLEC1* in whole blood measured in 18 patients with Aicardi-Goutières syndrome and 31 controls. The threshold is calculated at 2.216: Higher values are considered positive, whereas lower scores are negative. (B) Interferon scores of 12 *RNASEH2B* mutated patients and 31 healthy controls. Scores above the threshold are considered positive (253).

4.2 Transcriptomic and epigenetic analysis of p.A177T *RNASEH2B* mutated patients

All the previous studies allowed us to identify some molecular differences between *RNASEH2A* and *RNASEH2B* mutated patients. Intriguingly, in our cohort of patients we have a considerable number of *RNASEH2B* mutated patients, with the same homozygous common mutation p.A177T but with very different clinical phenotypes. Therefore, we decided to perform a whole transcriptome analysis on LCLs derived from mild and severe p.A177T patients and healthy controls and a whole methylome analysis on peripheral whole blood samples derived from mild and severe patients and healthy controls.

4.2.1 Transcriptome analysis of LCLs derived from severe and mild p.A177T *RNASEH2B* patients and healthy subjects

The Principal Component Analysis (PCA) show clearly the separation between the two subgroups of *RNASEH2B* mutated patients and also between all *RNASEH2B* mutated patients and healthy controls. Mild patients are closer to healthy controls (green) than those affected by a severe phenotype, highlighting a lower transcript deregulation in patients with a mild phenotype. The same result is also confirmed by the heatmap on the right (Figure 27).

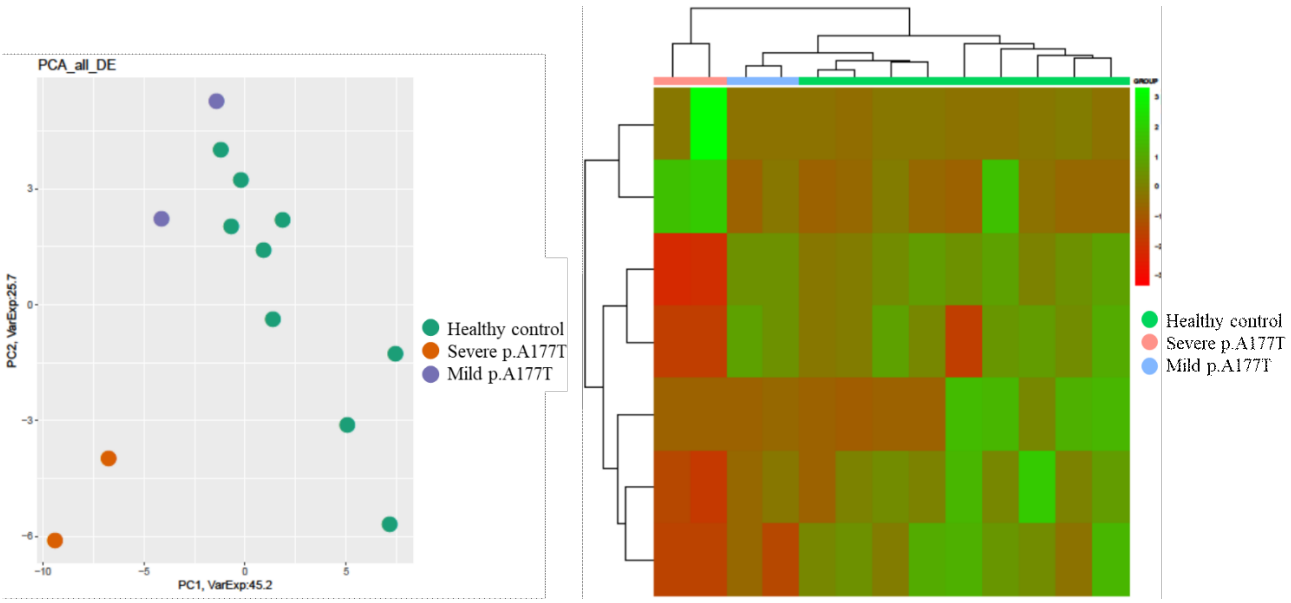

Figure 27. PCA of the DE genes from LCLs from healthy controls (green), AGS patients carrying p.A177T mutation on *RNASEH2B* with mild (purple) and severe phenotype patients (orange). Heatmap of the 60 most deregulated genes. All comparisons are given between the disease state and the control samples.

Severe patients showed a downregulation of mRNAs involved in GABA receptor activity, in the DNA and RNA helicase activity. Among the downregulated transcripts, we found AC009950.1 which is an antisense of SP110. SP110 is linked to STAT1, transcription activator that mediates cellular responses to IFNs and to DDX58 (DExD/H-Box Helicase 58), RNA helicases which are involved in viral double-stranded (ds) RNA recognition and the regulation of immune response (254) (Table 4). Mild patients showed an upregulation of RAB40B which is involved in protein ubiquitination and, consequently, in the proteasomal degradation of target proteins. It is also involved in metalloproteinases 2 and 9 (MMP2 and MMP9) trafficking and these two MMPs could cause the leakage of brain barrier (255).

Deregulated genes in severe patients

	log2FoldChange	gene_name	gene_biotype
ENSG00000134545	7,620477	KLRC1	protein_coding
ENSG00000127955	4,799084	GNAI1	protein_coding
ENSG00000204681	-2,16339	GABBR1	protein_coding
ENSG00000237550	-2,73489	RPL9P9	transcribed_processed_pseudogene
ENSG00000283460	-8,42339	RAD54B	protein_coding
ENSG00000280755	-8,88879	AC009950.1	protein_coding
ENSG00000283143	-21,8617	AL358113.1	protein_coding

Deregulated genes in mild patients

	log2FoldChange	gene_name	gene_biotype
ENSG00000141542	2,165588143	RAB40B	protein_coding
ENSG00000283143	-21,72854573	AL358113.1	protein_coding
ENSG00000211685	-23,71476196	IGLC7	IG_C_gene

Table 4. Statistically significant differentially expressed mRNAs in LCLs from severe and mild p.A177T patients compared to healthy controls.

4.2.2 Epigenetic analysis of white cells derived from whole blood samples of mild and severe p.A177T *RNASEH2B* mutated patients and healthy subjects

The Illumina Infinium MethylationEPIC BeadChip, which targets > 850,000 CpG sites across the genome, was used to interrogate DNA methylation in DNA isolated from whole peripheral blood samples of patients carrying the p.A177T mutation but with mild or severe phenotypes and age and sex-matched healthy controls. We started our analysis by estimating the blood cell type distribution using the method elaborated by Houseman et al. (250). Thanks to this approach we have been able to

estimate the relative proportions of lymphocytes, monocytes, B-cells, T-cells and granulocytes (Figure 28). Both subtypes of patients presented lower numbers of granulocytes and higher levels of B cells and CD4+ T cells when compared to healthy controls. No differences have been identified in the monocytes and CD8+ T cells proportions. A slight decrease in the distribution of NK cells has been highlighted in p.A177T severe patients (p=0.06) (Figure 18).

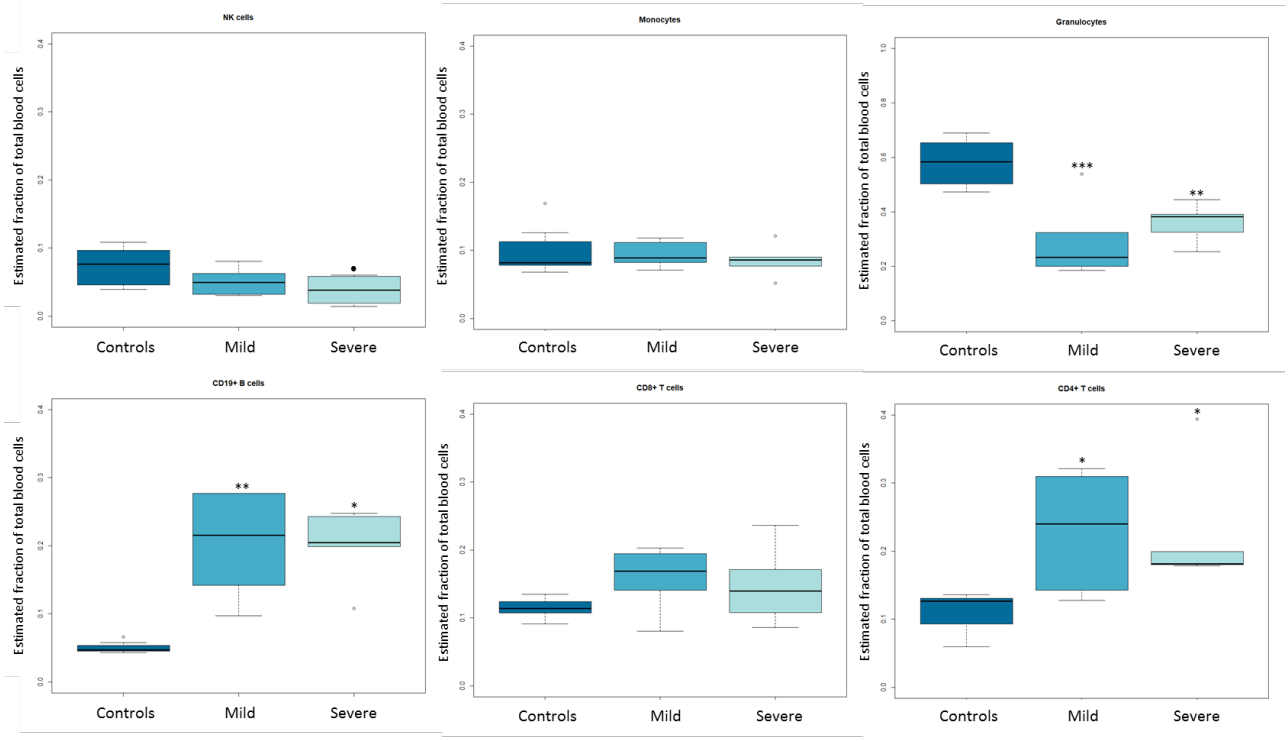

Figure 28. Boxplots representing estimated cell type fractions in whole blood samples from healthy controls (n=6), and AGS patients with "mild" (n=6) or "severe" disease (n=5) (all *RNASEH2B* p.A177T). One-way ANOVA analysis has been performed and Tukey post-hoc test has been used. •p=0.06; *p<0.05, **p<0.01; ***p<0.001.

4.2.3 Levels of DNA methylation and identification of differentially methylated positions (DMPs) of mild and severe p.A177T *RNASEH2B* mutated patients and healthy subjects

We started the DNA methylation analysis by comparing the β-values of controls and mild and severe patients. Both subtypes of p.A177T *RNASEH2B* patients presented an increased DNA methylation when compared to healthy controls (Figure 29).

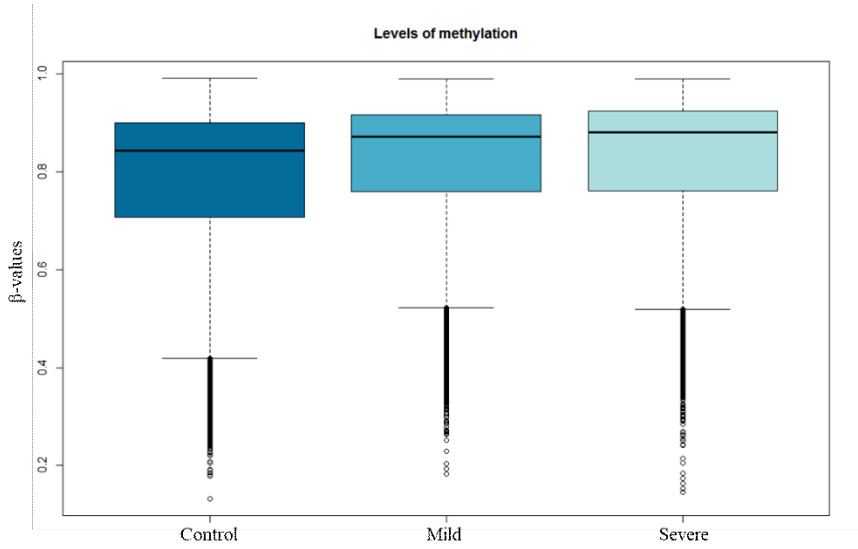

Figure 29. Levels of DNA methylation in healthy controls, mild p.A177T patients and severe p.A177T patients.

We then focused on statistically significant differentially methylated positions (DMPs) located in the promoter regions of genes. In order to achieve this result we compared the β-values of healthy controls and the β-values of mild and severe patients, respectively.

When comparing mild patients and healthy controls β-values, we obtained a total 5280 DMPs (4170 showing hypermethylation and 1110 hypomethylation) in promoter regions. We continued with a comparison between severe patients and healthy controls and, considering only the promoter regions of genes, we identified 5242 DMPs (4432 showing hypermethylation and 810 hypomethylation).

Then we wondered whether some DMPs may be in common between the two subgroups of p.A177T mutated patients or may be specifically associated to one of the two subgroups. Taking into consideration all the DMPs observed in mild and severe patients (6064 DMPs), we observed that patients with a severe phenotype and patients with mild phenotype presented almost the same number of unique DMPs (784 DMPs vs 822 DMPs, respectively), whereas both subtypes of p.A177T patients shared 4458 DMPs (Figure 30).

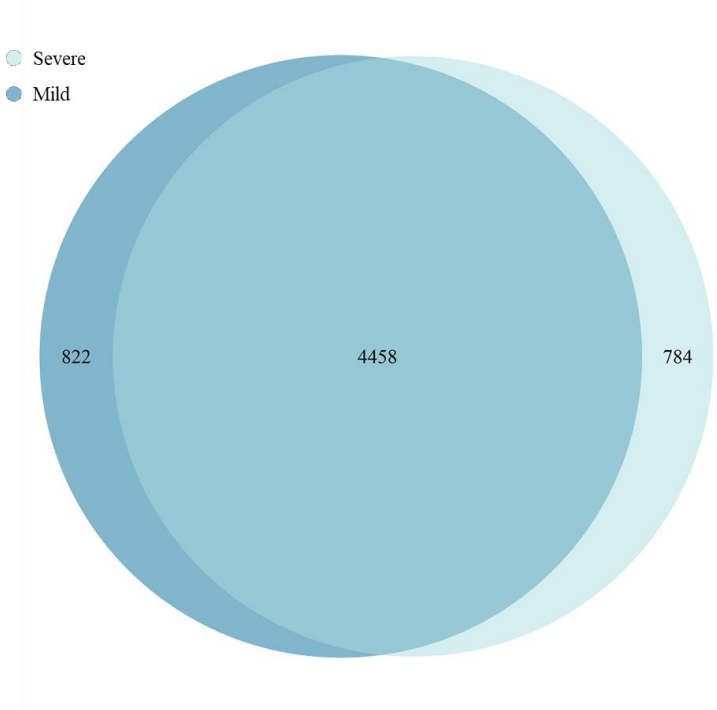

Figure 30. Venn diagram representing shared and unique DMPs observed in mild and severe p.A177T patients compared to healthy controls.

We continued analysing the unique and shared DMPs, but this time we decided to subdivide them in hypermethylated and hypomethylated positions. Our results showed that the number of hypermethylated positions (n = 4865) (Figure 31A) is four times as much the number of hypomethylated positions (n = 1199) (Figure 31B). Nonetheless, the number of hypermethylated positions specifically associated to a severe AGS phenotype and the number of hypermethylated positions uniquely associated to a mild phenotype is very similar (Figure 31A). Interestingly, if we consider only the hypomethylated positions, mild patients present a number of hypomethylated positions (n = 389) which is four times as much the number of hypomethylated positions specifically associated to a severe phenotype (n = 89) (Figure 31B).

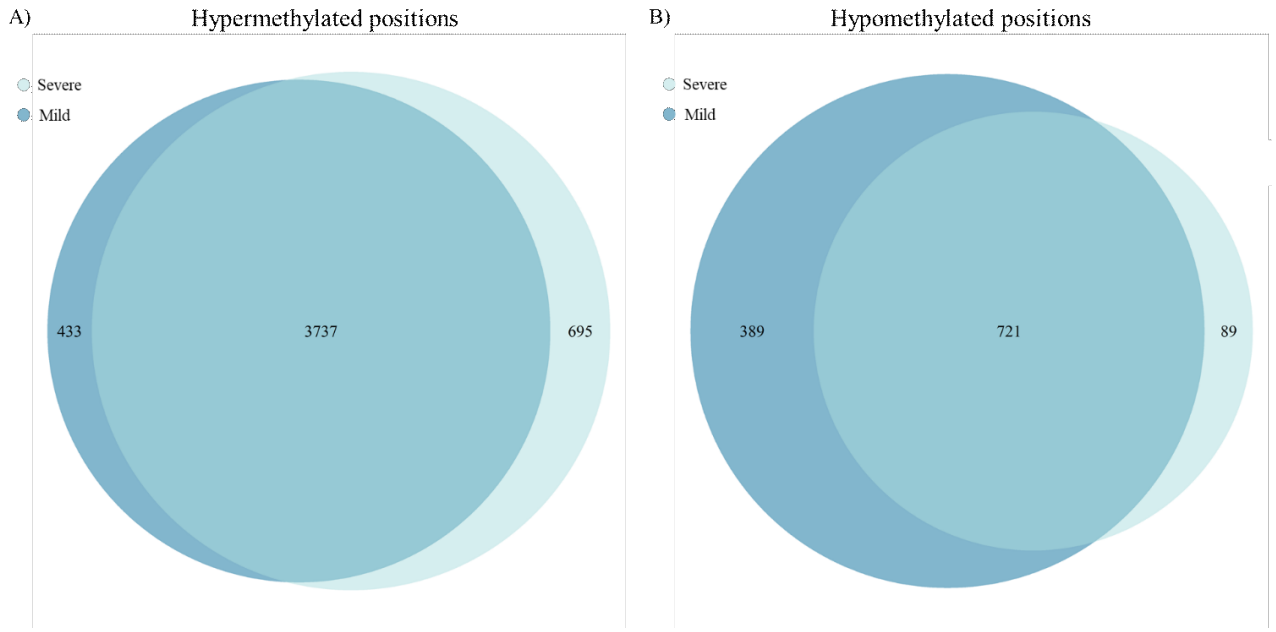

Figure 31. Venn diagrams representing shared and unique (A) hyper- and (B) hypomethylated positions observed in mild and severe p.A177T patients compared to healthy controls.

Therefore, we decided to investigate which genes presented the same methylation pattern in the two phenotypes and to analyse all the genes whose methylation patterns were specifically associated to one of the two phenotypes. At first, we performed a gene enrichment analysis taking into consideration only hypomethylated or hypermethylated genes which were in common between the two AGS phenotypes (Figure 32). The gene enrichment analysis was performed on all unique genes which presented shared DMPs in mild and severe patients, and both subtypes of p.A177T patients showed an hypermethylation in genes involved in neutrophil activation, mediated immunity, degranulation and neutrophil activation involved in immune response, regulation of GTPase activity, RAS protein signal transduction and response to lipopolysaccharide. On the other hand, a hypomethylation of genes involved in the T cell activation and differentiation, regulation of cell-cell adhesion, leukocyte cell-cell adhesion and cell-cell adhesion via plasma-membrane adhesion molecules. Enriched genes and their links with all the pathways are described in the cnetplots on the bottom of figures 32A and 32B.

A)

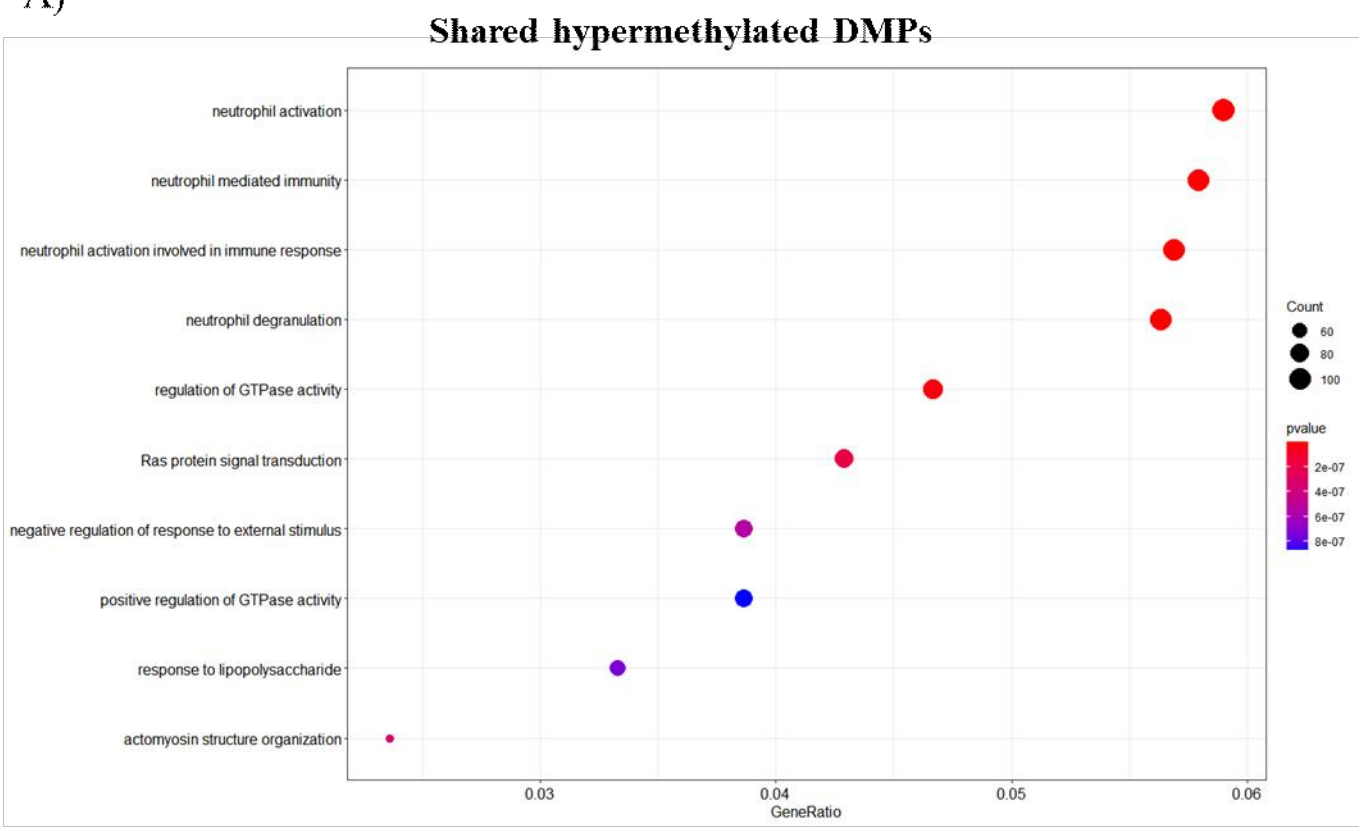
Shared hypermethylated DMPs
neutrophil activation
neutrophil mediated immunity
neutrophil activation involved in immune response
neutrophil degranulation
regulation of GTPase activity
Ras protein signal transduction
negative regulation of response to external stimulus
positive regulation of GTPase activity
response to lipopolysaccharide
actomyosin structure organization
0.03
0.04
0.05
0.06
GeneRatio
Count
60
80
100
pvalue
2e-07
4e-07
6e-07
8e-07

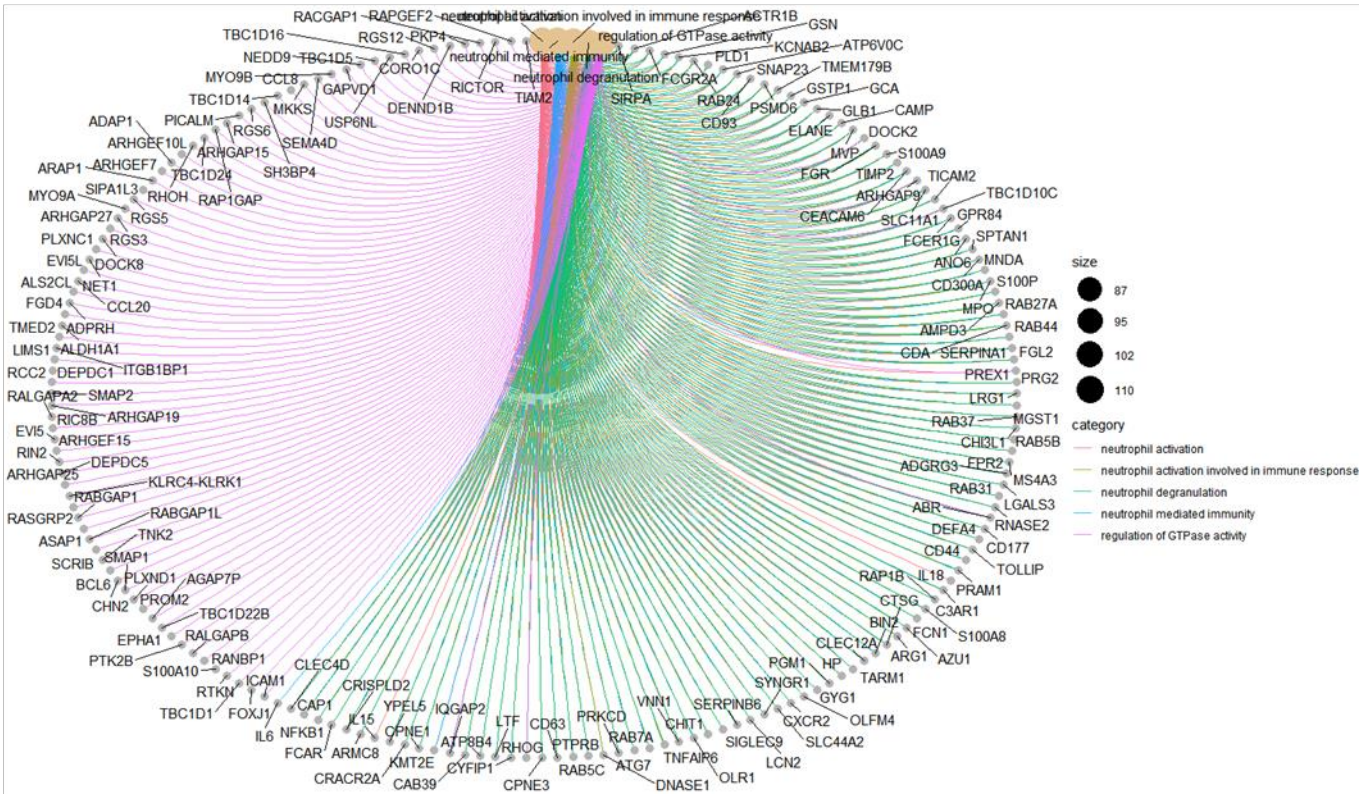
size
87
95
102
110
category
neutrophil activation
neutrophil activation involved in immune response
neutrophil degranulation
neutrophil mediated immunity
regulation of GTPase activity

B)

Figure 32. Gene Enrichment analysis of (A) hypermethylated and (B) hypomethylated shared DMPs identified in patients with a mild and a severe phenotype. Dotplots displaying the most significant enriched GO terms and cnetplots describing the linkages of genes and GO terms as a network.

We performed the same gene enrichment analysis considering only the hypermethylated genes uniquely found in p.A177T severe and mild patients. Severe patients showed an hypermethylation of genes involved in the regulation of cell-cell adhesion, leukocyte differentiation, regulation of hemopoiesis, T-cell activation and response to osmotic stress (Figure 33A), whereas in mild patients a hypermethylation was found in genes involved in neutrophil degranulation and activation, neutrophil mediated immunity and homophilic cell adhesion via plasma membrane adhesion molecules (Figure 33B).

A)

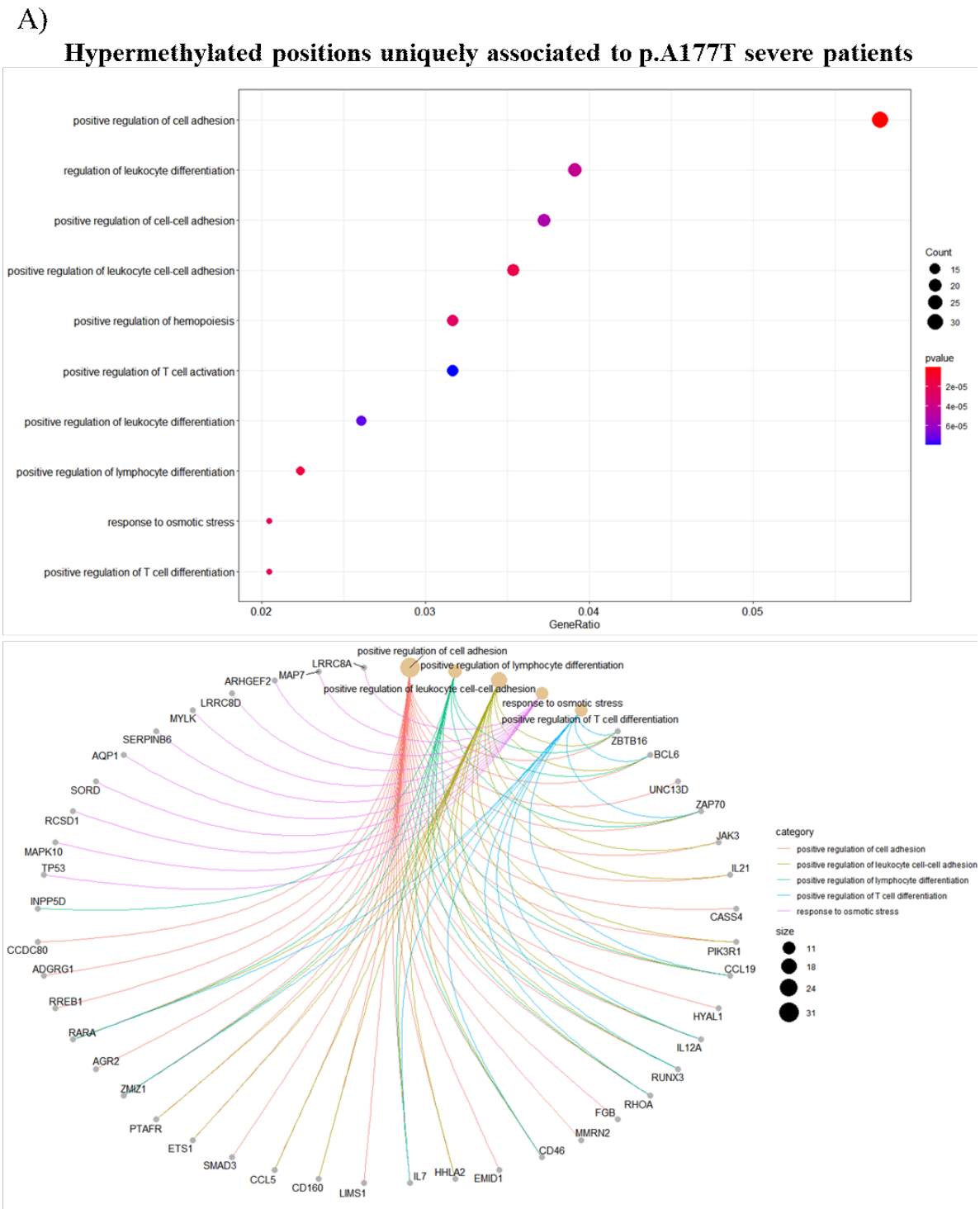

B)

Hypermethylated positions uniquely associated to p.A177T mild patients

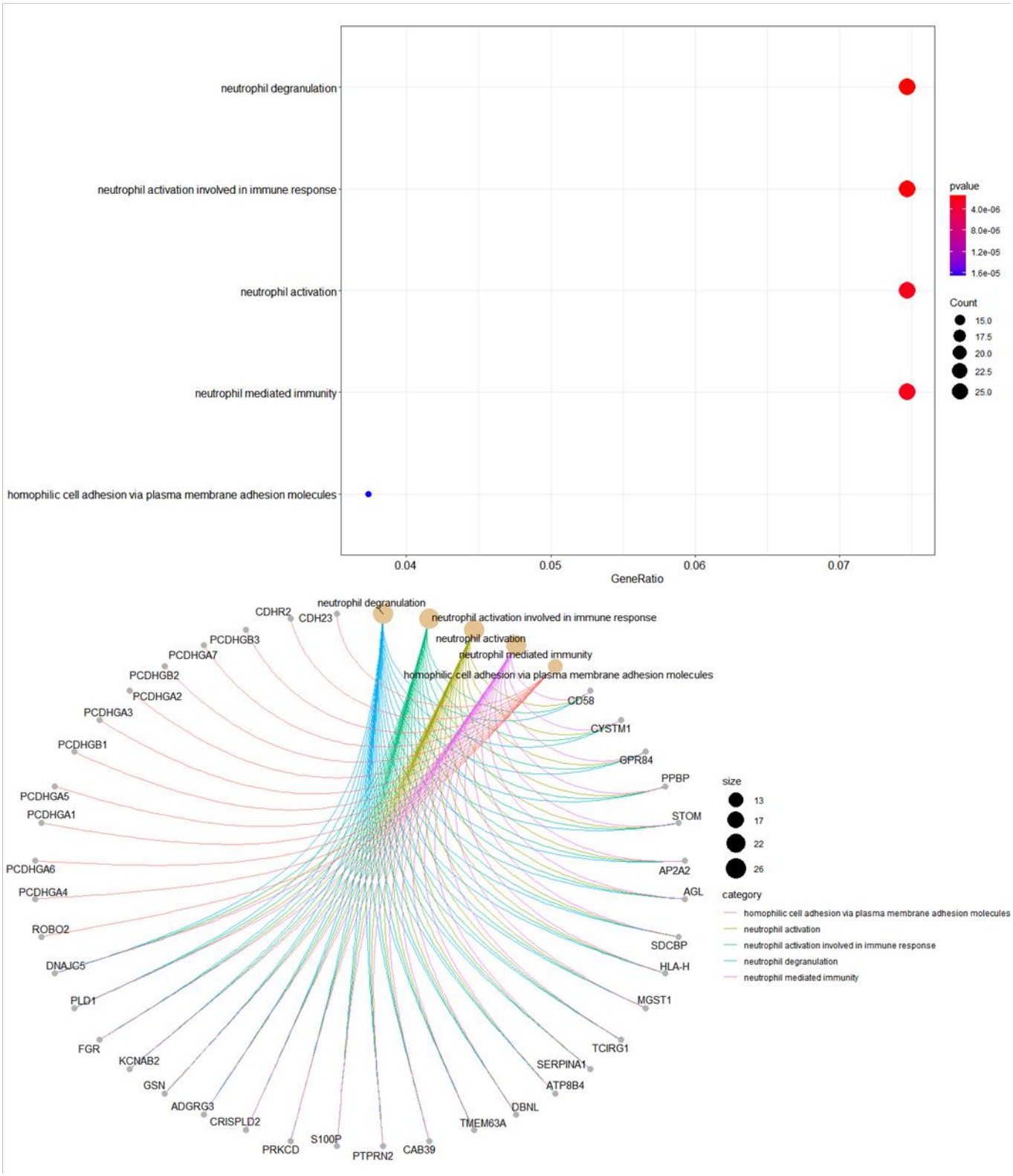

Figure 33. Gene Enrichment analysis of hypermethylated genes identified uniquely in patients with a (A) severe and a (B) mild phenotype, respectively. Dotplots displaying the most significant enriched GO terms and cnetplots describing the linkages of genes and GO terms as a network.

At last, we characterised the unique hypomethylated positions found in severe and mild patients. We performed a gene enrichment analysis of the genes carrying a mild-specific hypomethylation and this analysis allowed us to identify T-cell activation, lymphocyte differentiation, leukocyte cell-cell adhesion, regulation of antigen receptor-mediated signalling pathway and regulation of B cell receptor signalling pathway (Figure 34).

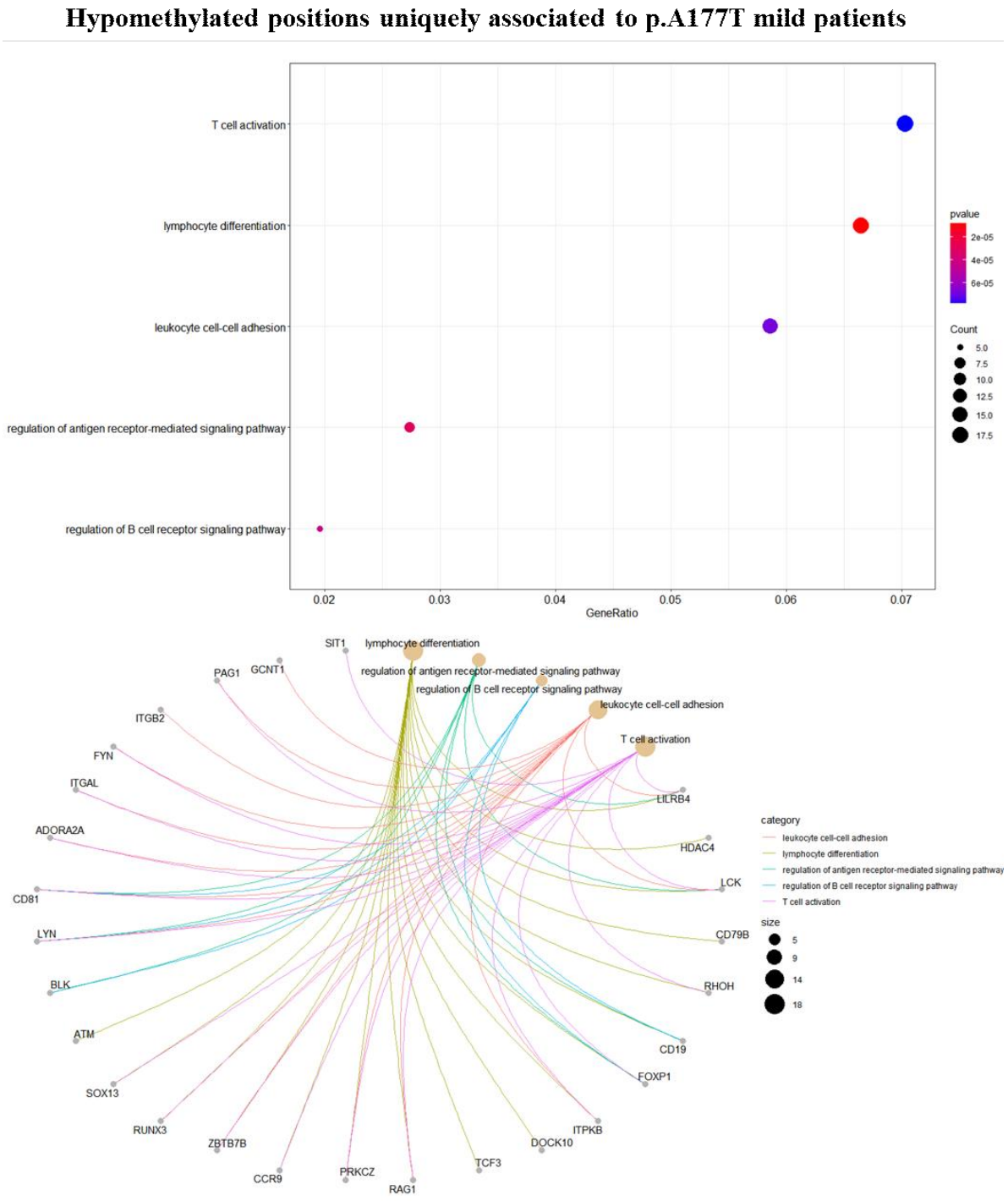

Figure 34. Gene Enrichment analysis of hypomethylated genes identified uniquely in patients with a mild phenotype. Dotplot displaying the most significant enriched GO terms and cnetplot describing the linkages of genes and GO terms as a network.

Since only 89 hypomethylated positions were found uniquely associated to p.A177T severe patients, we could not performed a gene enrichment analysis which was statistically significant. Therefore we will show the most hypomethylated positions uniquely associated to severe patients in table 5. These genes are involved in regulation of viral life cycle, regulation of NF-kB activity, mesodermal cell fate commitment, T-helper cell differentiation and regulation of IL-5, IL-13, IL-10 release.

Top 10 hypomethylated positions in severe patients

CpG site	Gene	Gene name	Δβ Severe-Ctrl
cg24577455	PRKCZ	Protein kinase C zeta type	-0.168600489512061
cg22862003	MX1	Interferon-induced GTP-binding protein Mx1	-0.163800497061138
cg10067510	GTF2A1L	TFIIA-alpha and beta-like factor	-0.16178417171349
cg11856929	NOSIP	Nitric oxide synthase-interacting protein	-0.149992979999781
cg06489385	STEAP2-AS1	Metalloreductase STEAP2 antisense	-0.147108296798339
cg06489385	STEAP2	Metalloreductase STEAP2	-0.147108296798339
cg05701418	TRIM15	Tripartite motif-containing protein 15	-0.146194890748057
cg18387107	PARP11	Protein mono-ADP-ribosyltransferase PARP11	-0.144453207697106
Cg12350592	PYY	Peptide YY	-0.143280078060042
cg26359730	TNR	Tenascin-R	-0.143633658063787

Table 5. Top 10 hypomethylated positions uniquely associated to p.A177T severe patients.

Among the most hypomethylated genes we found *IFI44L* which is one of the ISGs of the interferon signature. The levels of DNA methylation were lower in both subtypes of patients, although severe patients presented a stronger hypomethylation than mild patients (Figure 35A). Moreover, when comparing mild and severe patients we identified different DMPs at the promoter region of the *LIG4* gene. This gene was more hypomethylated in mild patients than severe patients (Figure 35B), suggesting a higher expression of this ligase involved in the DNA non-homologous end joining and required for double-strand break repair.

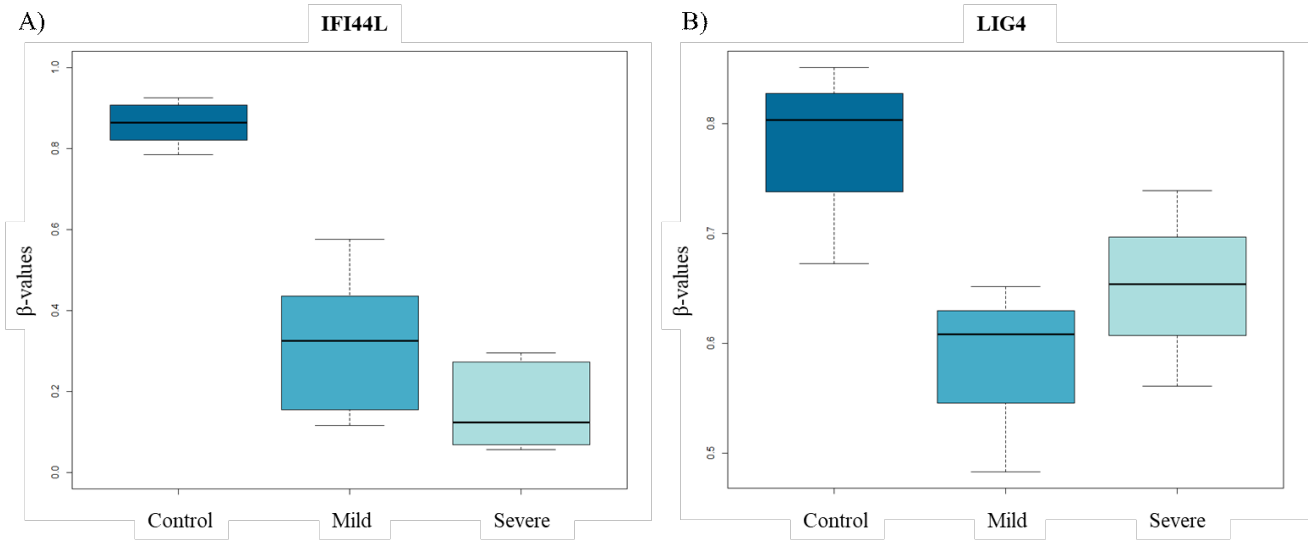

Figure 35. Box plots of DNA methylation levels at (A) IFI44L and (B) LIG4 in controls, p.A177T mild and p.A177T severe patients.

4.2.4 Identification of differentially methylated regions (DMRs) of mild and severe p.A177T *RNASEH2B* mutated patients and healthy subjects

Differentially methylated regions (DMRs) are genomic regions which present a different DNA methylation status and they are considered regions involved in the regulation of gene transcription. Moreover DMRs are more highly associated with disease when compared to DMPs (256). Therefore, we also investigate DMRs in severe and mild patients and healthy controls. Using *DMRcate* package we identified 74 DMRs. They were mainly located in genomic regions associated with small nucleolar RNAs and with genes involved in regulation of ganglioside metabolic process, viral life cycle, regulation of nitric oxide synthase and substantia nigra development. Besides, here we report a hypomethylated region in the genomic region of *IFITM1* gene which plays a key role in anti-viral activity, immunity, cell adhesion and proliferation (257) (Figure 36).

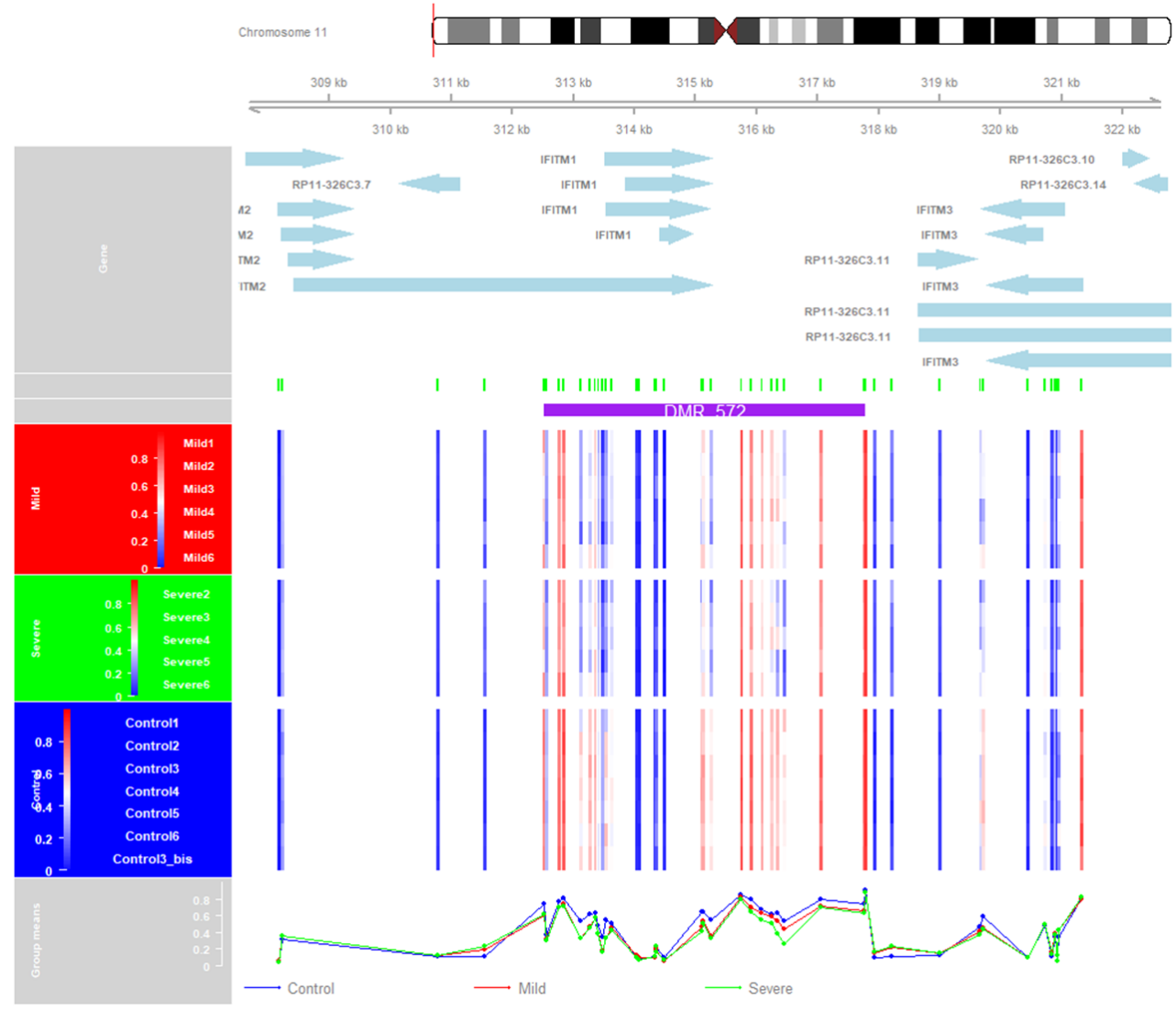

Figure 36. DMR in *IFITM1*. Both mild and severe patients present with hypomethylation in the genomic region of *IFITM1*, a gene involved in the immune response.

4.3 Characterization of lymphoblastoid cell lines derived from patients with mutations in *RNASEH2A* and *RNASEH2B* genes

Since mutations in *RNASEH2* subunits are the most frequent both in the Italian and in the worldwide cohort of AGS patients, we decided to study molecular mechanism associated with mutations in these genes. In this work of thesis we used lymphoblastoid cell lines (LCLs) derived from patients mutated in *RNASEH2B* and *RNASEH2A* genes. In fact, for the rareness of the disease and the very young age of all AGS patients who are regularly followed-up by IRCCS Mondino Foundation, it is difficult to obtain blood samples regularly. The LCLs instead are immortalized cell lines obtained by the infection of patients' B cells with the Epstein Barr virus (258). We concentrated our work on two mutations: the homozygous mutation p.A177T in *RNASEH2B* and the compound heterozygous

mutation p.R108W+p.F230L in *RNASEH2A*. Firstly, we decided to assess the viability of this cell model by trypan blue exclusion assay and all the three cell lines did not show differences (Figure 37). Then, to verify if the mutations in *RNASEH2B* and *RNASEH2A* genes may affect RNase H2 subunits protein levels, we performed a western blot on total cell lysates (Figure 38).

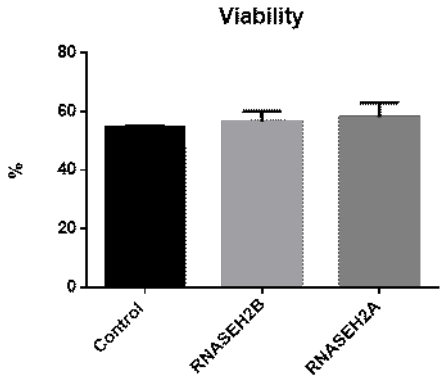

Figure 37. Cell viability of the healthy control and *RNASEH2A* and *RNASEH2B* mutated LCLs. The bar graph represents the mean±SEM of three biological experiments.

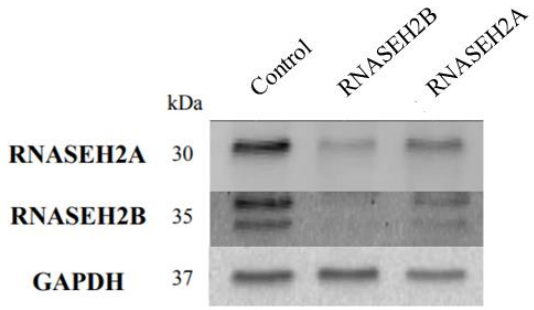

Figure 38. Western Blot analysis of RNase H2 subunits protein level of *RNASEH2A* and *RNASEH2B* mutated LCLs and a healthy control.

4.3.1 DNA damage and accumulation of RNA:DNA hybrids

RNase H2 is an enzyme involved in the removal of misincorporated ribonucleotides in the genome. Mutations in one of the three subunits may lead to DNA damage and to RNA:DNA hybrids accumulation. We studied DNA damage in the three cell lines by immunofluorescence staining with γ-H2AX antibody and we observed an increase γ-H2AX signal in both mutated cell lines when compared to the healthy control (Figure 39).

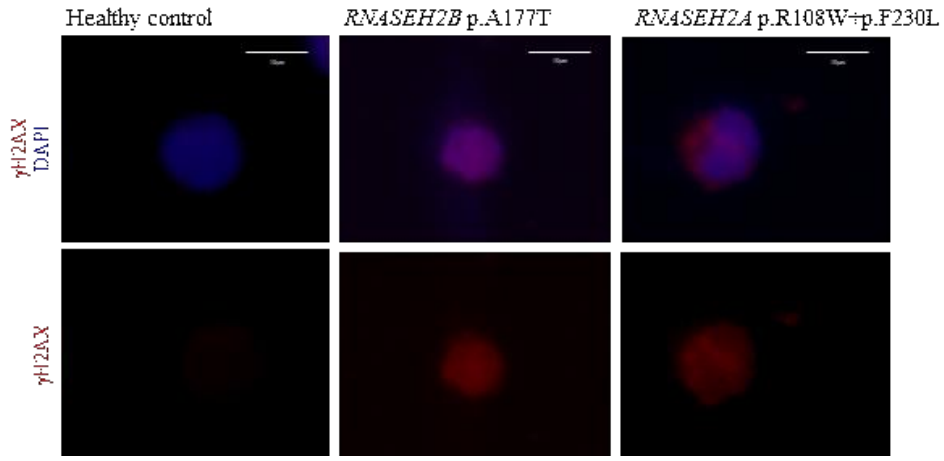

Figure 38. γ-H2AX signal in *RNASEH2A* and *RNASEH2B* mutated LCLs and a healthy control. LCLs were stained with monoclonal γH2AX antibody (red) and nuclear blue dye DAPI and images were acquired with a confocal laser microscope (Leica DM IRBE, Leica Microsystems Srl, Italy).

Then we also analysed if there was an accumulation of RNA:DNA hybrids. LCLs have been stained with S9.6 antibody and we investigated a possible accumulation of RNA:DNA hybrids by flow cytometry. As shown in figure 39, increased level of RNA:DNA hybrids have been identified in *RNASEH2B* mutated cell lines. Interestingly, *RNASEH2A* mutated LCLs shown as much RNA:DNA hybrids as the healthy control.

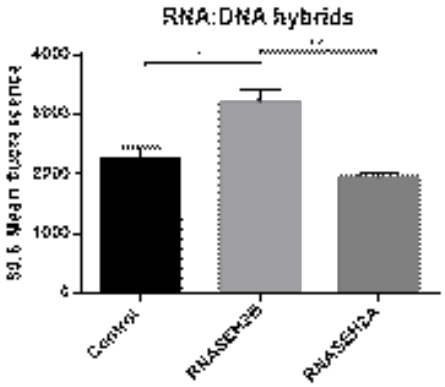

Figure 39. Quantification of S9.6 mean fluorescence for *RNASEH2A* and *RNASEH2B* mutated LCLs and for the healthy control. The bar plot represents the mean±SEM of three biological experiments. ANOVA test and post-hoc analysis with Tukey's test has been performed. *p<0.05, **p<0.01.

After discovering an increased RNA:DNA hybrids level content in *RNASEH2B* mutated LCLs, we wanted to identify their location inside the cells. We stained the RNA:DNA hybrids with S9.6 in red and nuclei with DAPI in blue. RNA:DNA hybrids are mainly localized in the cytoplasm of all the three cell lines (Figure 40A) and *RNASEH2B* mutated LCLs seem to accumulate this nucleic acid species in a specific area of the cytoplasm (white arrow, Figure 40A). To confirm these results we

also performed an immunogold staining of RNA-DNA hybrids and we analysed the cells by transmission electron microscopy (TEM). As shown in Figure 40B, each dot represents S9.6 binding to RNA:DNA hybrids and they are mainly localised in the cytoplasm, even if they may also be found in the nucleus, especially in *RNASEH2B* mutated LCLs (white arrows, figure 40B).

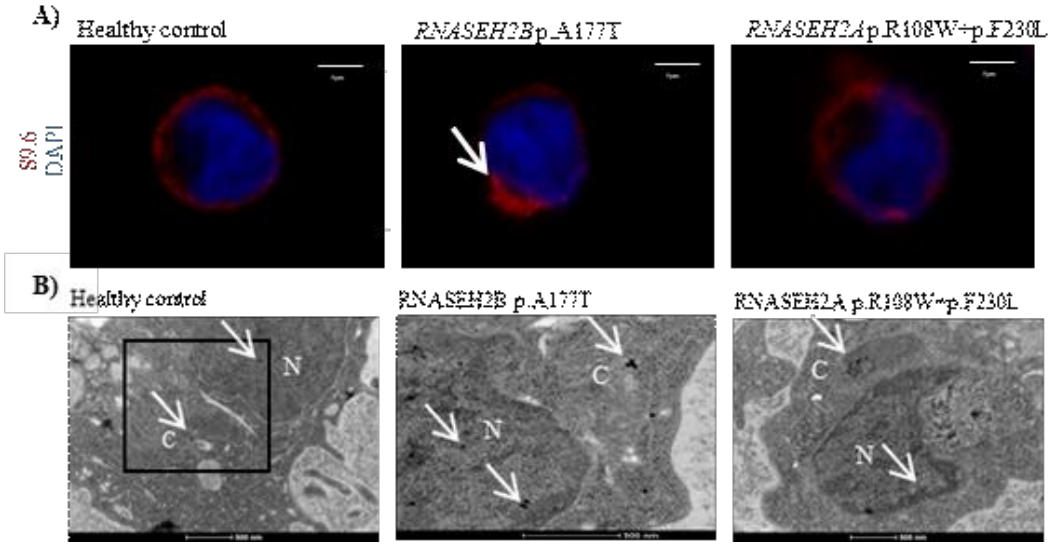

Figure 40. RNA:DNA hybrids are mainly localised in cells' cytoplasm. (A) Healthy control, *RNASEH2A*, *RNASEH2B* mutated LCLs were stained with RNA:DNA hybrids (S9,6 in red) in the presence of DAPI (blue, nuclear stain). Images were acquired with a confocal laser microscope (Leica DM IRBE, Leica Microsystems Srl, Italy) from three technical replicates (B) Representative immunogold electron microscopy localization of RNA:DNA hybrids in the cytoplasm of *RNASEH2* mutated and healthy control LCLs. Frozen sections of fixed and gelatin embedded *RNASEH2* mutated and healthy control LCLs were incubated with human anti-S9.6 and then post-immunolabeled with protein A-gold (10 nm).

Different studies have shown that S9.6 may also bind dsRNA with a lower affinity than RNA:DNA hybrids (K_D of 0.6 nM for DNA:RNA hybrids against a K_D of 2.7 nM for dsRNA) (259) and, thus, treatments with RNase H, which selectively degrade the RNA strand of RNA:DNA hybrids, became inevitable to evaluate S9.6 specificity (260).

After RNase H treatment, the red signal of RNA:DNA hybrids underwent a considerable decrease in *RNASEH2B* LCLs, the only cell line which presented a significant accumulation of RNA:DNA hybrids (Figure 41). No differences were observed before and after RNase H treatment in both control and *RNASEH2A* LCLs. Since RNase A degrades free RNA (261), we also performed an additional treatment with RNase A. The use of this enzyme, removed the S9.6 signal in CTRL and *RNASEH2A* mutated LCLs confirming that the signal is represented by dsRNA (Figure 41).

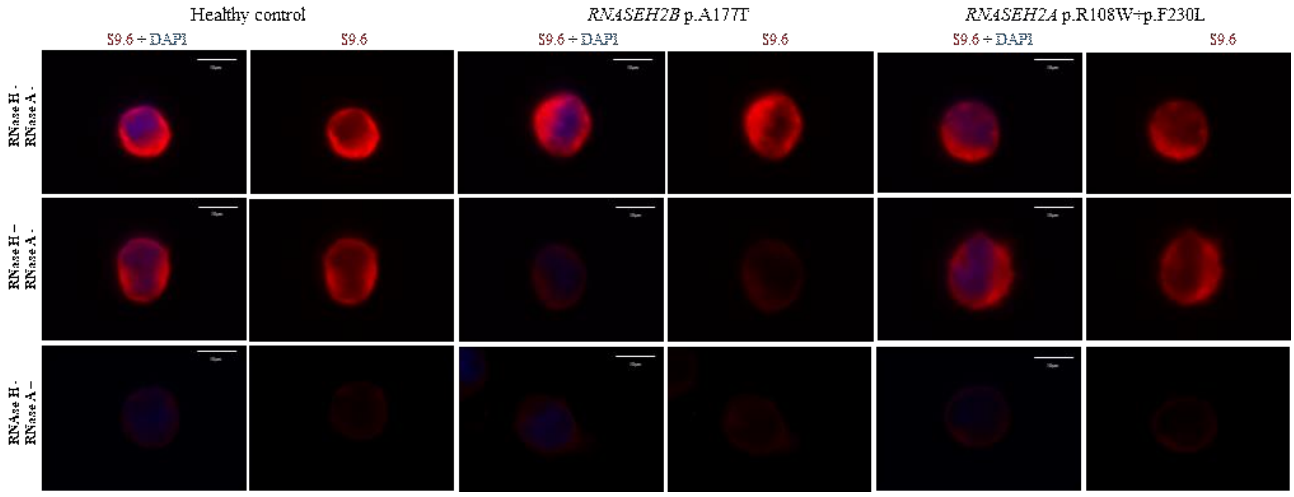

Figure 41. Treatment with RNase H degrades specifically RNA:DNA hybrids in LCLs. Immunofluorescence of LCLs derived from a healthy control and AGS patients mutated in *RNASEH2B* and *RNASEH2A* stained with S9.6 antibody (red) and DAPI (blue) before and after treatments with RNase H and RNase A.

4.3.2 RNA:DNA hybrids presence in mitochondria, endoplasmic reticulum and endolysosomes of *RNASEH2* mutated lymphoblastoid cell lines

From this starting point, we carried on investigating the subcellular localization of RNA:DNA hybrids among the main organelles of the cell, and we studied their localization in the endoplasmic reticulum (ER), mitochondria and endolysosomes. Cells have been stained with monoclonal S9.6 antibody and with the mitochondria-specific vital dye MitoTracker^{TM}, the ER-specific marker ER-Tracker^{TM}, the endolysosomal marker LysoTracker^{TM} and the nuclear blue dye DAPI (Figure 42). No colocalized signals have been identified between RNA:DNA hybrids and mitochondria or ER for all cell lines. On the other hand, we found a colocalization of RNA:DNA hybrids and endolysosomes in *RNASEH2B* mutated LCLs.

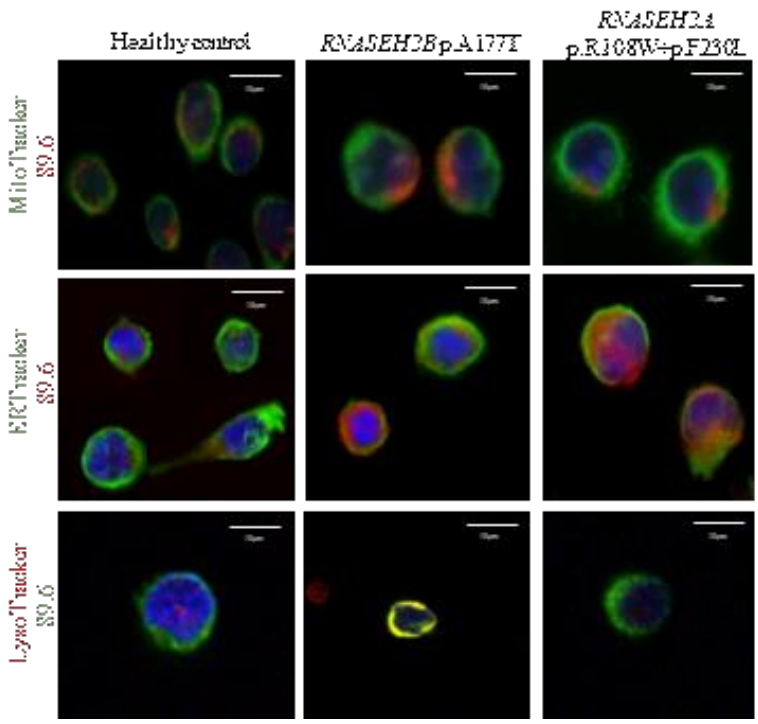

Figure 42. Immunofluorescence of LCLs derived from AGS patients carrying mutations in *RNASEH2* subunits genes and a healthy control. LCLs were stained with monoclonal S9.6 antibody and MitoTracker, ERTracker (green) and LysoTracker (red) and nuclear blue dye DAPI and images were acquired with a confocal laser microscope (Leica DM IRBE, Leica Microsystems Srl, Italy). Images from three biological experiments (Mitotracker and ER-Tracker) and two technical replicates (Lysotracker).

4.3.3 Immunological pathways activation in *RNASEH2A* and *RNASEH2B* mutated LCLs

Due to the accumulation of nucleic acids in the cytoplasm and in particular in the endolysosomes of *RNASEH2B* mutated LCLs we wondered whether they were able to trigger an immune response or not and which pathway could be involved in their sensing. It is known from the literature that cytoplasmatic nucleic acids may trigger the activation of PRRs (165). Therefore, we started studying the levels of cGAS protein which is involved in the cGAS-STING pathway and is able to bind RNA:DNA hybrids. No differences were found between the healthy control and the two mutated patients (Figure 43A). Then, to confirm this result, we also studied NF-kB and IRF3 transcripts levels by Real-Time PCR. No significant alteration were found between the healthy control and the two patients, even if we can observe a slight increase of IRF3 expression levels in *RNASEH2A* mutated LCLs (Figure 43B, 43C).

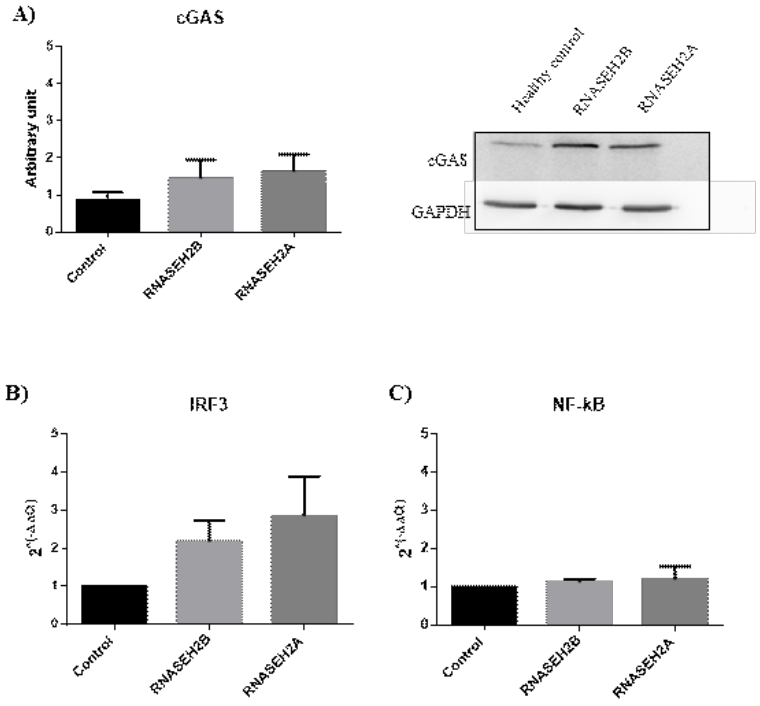

Figure 43. cGAS-STING pathway involment in RNA:DNA hybrids sensing. (A) Representative histogram and Western Blot of the cGAS protein level in LCLs derived from healthy control and AGS patients. (B,C) mRNA expression of NF-kB and IRF3 which are involved in cGAS-STING signaling in healthy control and AGS patients.

Thus, we focus on TLRs since TLR-9 has been described as capable of binding not only dsDNA but also RNA:DNA hybrids (86). We analysed the expression of genes involved in the downstream signalling of TLR-9 pathway. Interestingly, we found an increased expression of MYD88 ($p<0.05$) and we also observed the same trend in the expression levels of IRF7 ($p<0.07$) in *RNASEH2B* mutated LCLs. Conversely, no differences could be found in the *RNASEH2A* patient LCLs (Figure 44A, 44B).

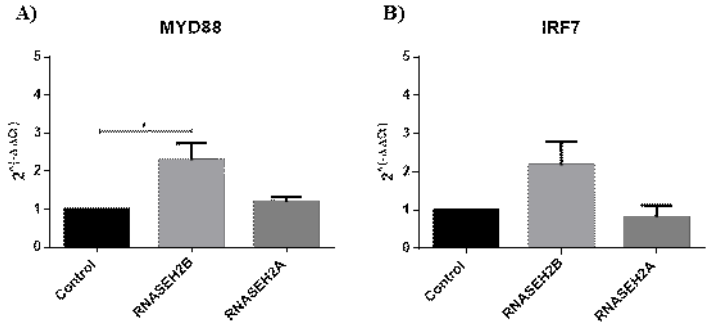

Figure 44. Activation of downstream signalling of TLRs pathways. (A, B). mRNA expression of MYD88 and IRF7 which are involved in TLRs signalling in healthy control and AGS patients (*RNASEH2B* and *RNASEH2A* mutated). Bar plots represent the mean±SEM of three biological experiments. ANOVA test and post-hoc analysis Tukey's Test have been performed. *$p<0.05$.

Some AGS patients present an increased interferon signature which is calculated by considering the expression levels of 6 interferon stimulated genes. We analysed by Real Time PCR the expression levels of two of the 6 ISGs that compose the interferon signature, *IFI44* and *IFIT1*, because they are the most expressed in LCLs. Both ISGs are significantly upregulated in *RNASEH2B* mutated LCLs (*IFIT1* $p<0.01$ and *IFI44* $p<0.001$) when compared to the healthy control, whereas the transcript levels of these two genes are very similar between the control and *RNASEH2A* mutated patient (Figure 45).

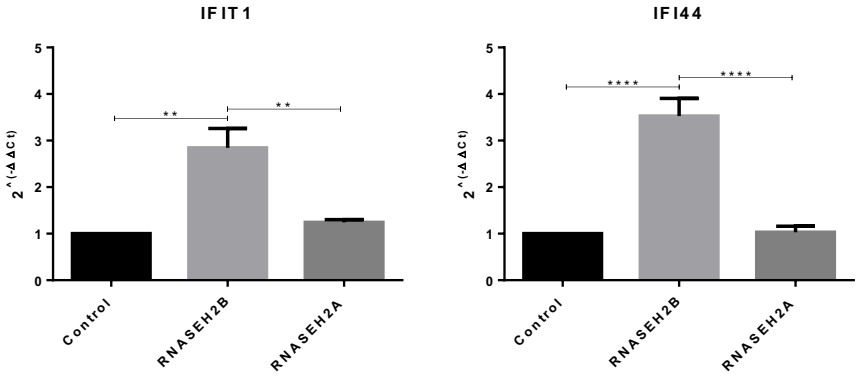

Figure 45. Interferon stimulated genes expression is increased in *RNASEH2B* mutated LCLs. mRNA expression levels of *IFIT1* and *IFI44* interferon stimulated genes in healthy control and AGS patients (*RNASEH2B* and *RNASEH2A* mutated). The histogram represents the mean of three biological experiments. ANOVA test and post-hoc analysis Tukey's Test have been performed. **p<0.01, ****p<0.0001.

4.4 Mitochondria as a source of DAMPs which may be able to activate TLR-9

It is known from literature that TLR-9 can bind either RNA:DNA hybrids (86) or mtDNA (262). Mitochondria are a source of Damage-Associated Molecular Patterns (DAMPs) and among them we find mtDNA and the mitochondrial transcriptional factor A (also known as TFAM). These two DAMPs are strictly correlated to each other and their alterations have been linked to autoimmune and neurological diseases (263,264). Usually decreased levels of TFAM are associated with decreased levels of mt-DNA (263).

4.4.1 Correlation between mitochondrial DNA and TFAM protein in patients' LCLs

Since mtDNA may trigger an immune response driven by the TLR-9 activation, we firstly decided to assess mtDNA copy number in patients and control's LCLs. We performed a Real-Time PCR in order to evaluate the amount of mtDNA in *RNASEH2A*, *RNASEH2B* and control's LCLs. We compared the mitochondrial gene MTND1 and the nuclear encoded gene β2M and surprisingly we observed a reduced level of mitochondrial DNA in both mutated LCLs (Figure 46).

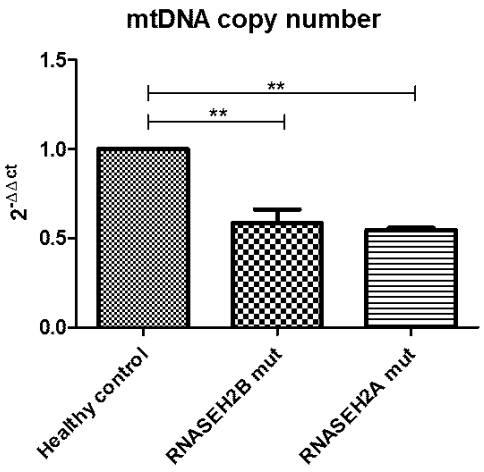

Figure 46. *RNASEH2A* and *RNASEH2B* mutated LCLs present reduced mtDNA copy number. Representative bar plot of mtDNA copy number in a healthy control and in *RNASEH2A* and *RNASEH2B* mutated LCLs. MT-ND1 transcript levels have been evaluated by Real-Time PCR and they have been normalised with the genomic housekeeping β2-Microglobulin. ANOVA test and post-hoc analysis Tukey's Test have been performed **p<0.01.

We studied TFAM protein level by WB analysis in different cellular fractions (cytoplasm and mitochondrion) and in total cell lysates (Figure 47). Both *RNASEH2A* and *RNASEH2B* mutated cell lines presented decreased TFAM protein levels when considering the whole cell lysate or the mitochondrial fraction. Conversely, if we consider only the cytoplasmatic fraction we can find the presence of TFAM only in AGS patients, where it is usually found. Taken together, these data suggest a possible release of this immunostimulatory protein in the cytoplasm of *RNASEH2A* and *RNASEH2B* mutated patients. This result is well related to the decreased mtDNA levels in mitochondria of both patients. Moreover, a TFAM deficiency may cause mitochondrial stress and mtDNA mispackaging and these alterations taken together can in turn determine mitochondrial ejection into the cytoplasm (265). Both molecules are then able to trigger an immune response which is likely to be connected with a TLR-9 activation as suggested by our previous data and also by the literature (262,265,266).

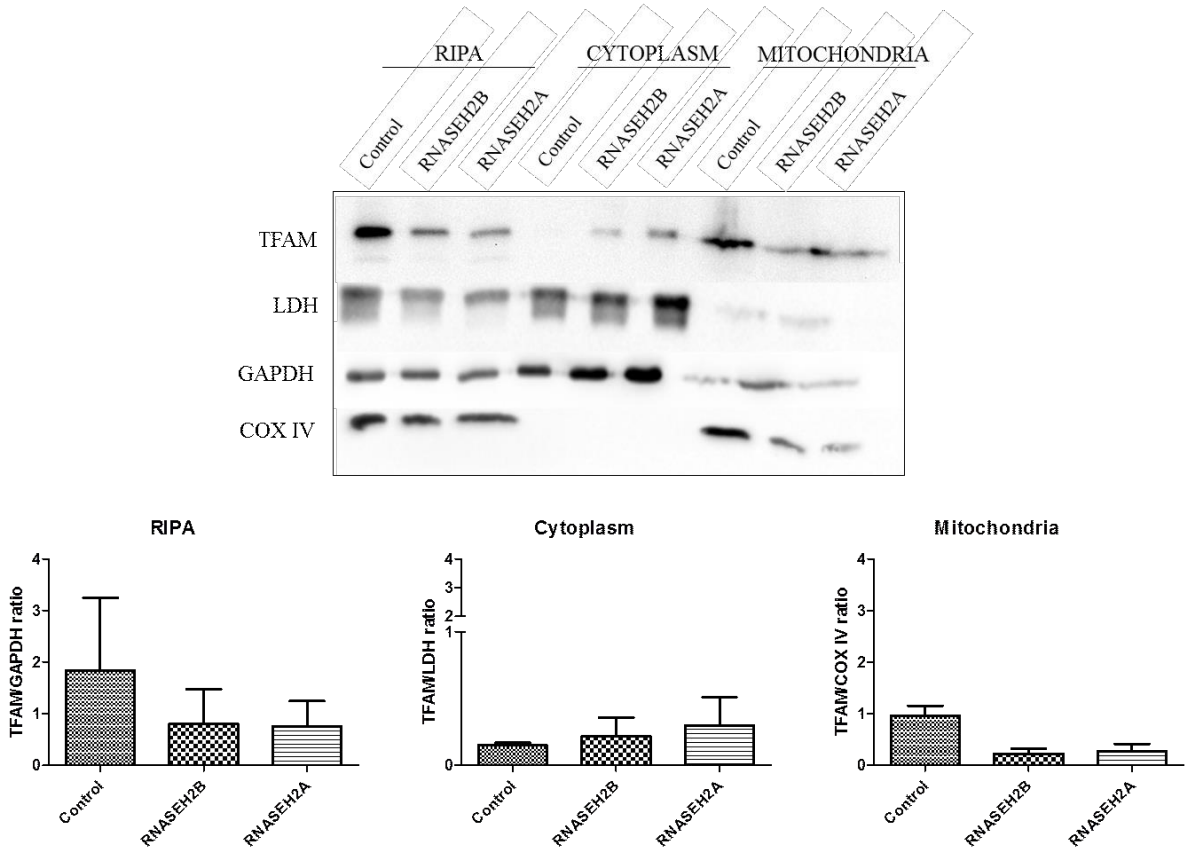

Figure 47. *RNASEH2A* and *RNASEH2B* mutated LCLs present reduced TFAM protein levels in mitochondria. Representative western blot of TFAM protein levels in a healthy control and *RNASEH2B* and *RNASEH2A* mutated LCLs. Representative bar plot of TFAM protein levels in a healthy control and in *RNASEH2A* and *RNASEH2B* mutated LCLs. TFAM protein levels have been evaluated by WB and they have been normalised with housekeeping genes specifically associated to each cellular fraction (GAPDH, LDH and COX IV).

4.4.2 Mitochondrial damage in AGS patients' LCLs

Since in neurodegenerative diseases, reduced TFAM protein levels may be accompanied by reduced nuclear mitochondria biogenesis, altered number of mitochondria, abnormal mitochondrial morphogenesis and alteration in mitochondrial fission and fusion (263), we decided to investigate if some of these abnormalities may be found also in LCLs derived from AGS patients.

Thanks to TEM experiments on patients' and control's LCLs, we identified an abnormal morphology of AGS patients' mitochondria (Figure 48). Both mutated patients presented mitochondria with an altered structure, as indicated by the black arrows in figure 48C and 48F, with compact cristae and a dense matrix compartment, as described by red arrows in figure 48C, 48D and 48F. Moreover, some mitochondria have an elongated shape (yellow arrows, figures 48C and 48F) whereas other organelles seem to be swollen and to present a loss of mitochondrial cristae, as indicated by asterisks in figure 48E.

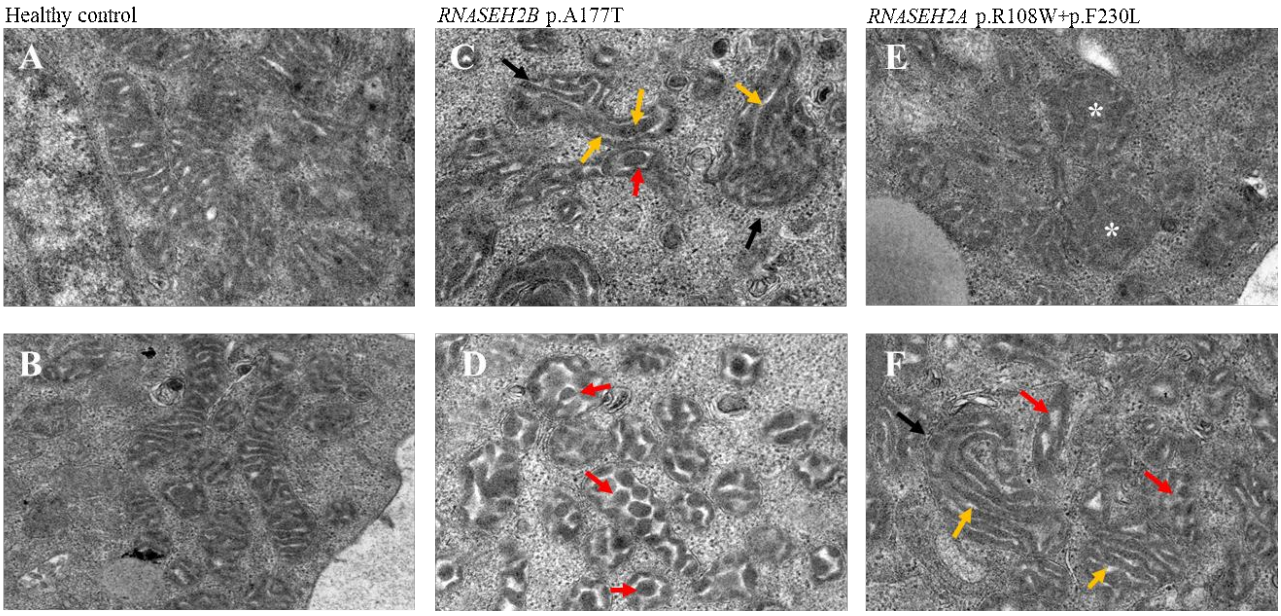

Figure 48. Mitochondria morphology of *RNASEH2* mutated LCLs and healthy control. Representative images of mitochondria from AGS patients shows alteration of normal morphology. They have unusual shapes (black arrows) (C and F) with packed cristae or overlaid layers of membranes (red arrows) or with a longitudinal shape (yellow arrows), Some mitochondria are enlarged and there are loss of cristae (asterisks) (E).

4.5 HCQ treatment of *RNASEH2* mutated LCLs reduces RNA:DNA hybrids

HCQ has been first developed to treat malaria, but due to its immunomodulatory properties it is also widely used in clinical practice of autoimmune diseases such as Systemic Lupus Erythematosus (SLE) and Rheumatoid Arthritis (RA) (267,268). Since HCQ is able to inhibit cGAS and TLR-9 signalling through the direct binding to nucleic acids (232) we wondered if it could represent a useful therapeutic approach also for AGS patients. We started identifying the most adequate HCQ concentration for LCLs treatment. We evaluated cell viability by trypan blue staining and early and late apoptosis by checking Annexin V (a probe for phosphatidylserine on the outer membrane of apoptotic cells) and 7-Aminoactinomycin (7-AAD, a fluorescent DNA dye that discriminates between live cells as well as early and late apoptosis) by flow cytometry before and after a 24h treatment with different concentrations of HCQ (25µM, 50µM and 100µM). Samples treated with a concentration of 25µM were viable around 48%, while cells treated with concentrations of 50µM and 100µM were viable around 44% and 36%, respectively. If we compare these results with the samples without HCQ treatment (viability 57%), the concentration of 25µM of HCQ resulted the one which determined the highest cell viability (Figure 49A). We also assessed the level of apoptosis (Figure 49B) and cell death (Figure 49C) in the three types of LCLs by flow cytometry. The apoptosis level for samples without treatment was around 20%, for samples treated with 25µM of HCQ was around 26%, while samples treated with 50µM and 100µM had an apoptosis level around 29% and 33% respectively. Finally, the percentage of dead cells treated with the concentrations of 25µM, 50µM

and 100µM of HCQ was around 26%, 29% and 33% respectively, while the cells without treatment showed a mortality of 20%. Based on these results we chose 25µM of HCQ for cell treatment.

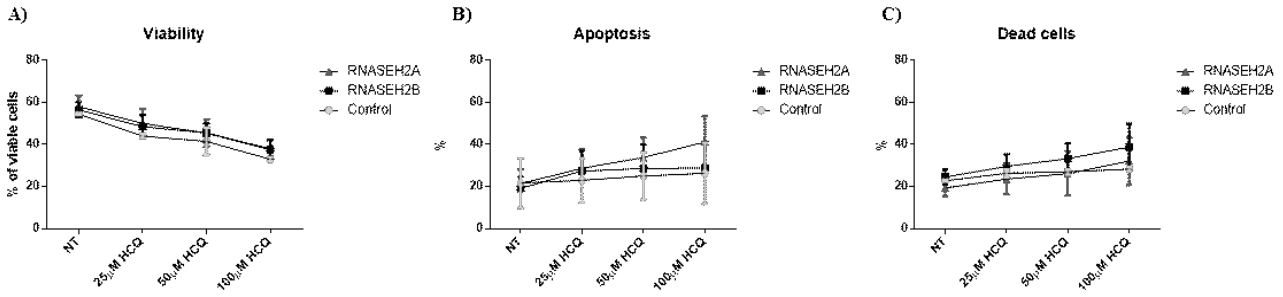

Figure 49. LCLs viability, apoptosis and cell death after treatments with different HCQ concentrations. (A) Cell viability was evaluated with trypan blue staining after 25µM, 50µM and 100µM treatment with HCQ for 24h in healthy control, *RNASEH2A* and *RNASEH2B* mutated LCLs (B, C). Apoptosis and cell death was assessed by flow cytometry using Annexin V or 7ADD staining respectively.

4.5.1 HCQ treatment of *RNASEH2* mutated LCLs reduce RNA:DNA hybrids

Since patients carrying mutation in *RNASEH2B* presented an accumulation of RNA:DNA hybrids that seem to trigger an abnormal immune response, we started evaluating if RNA:DNA hybrids levels change after a treatment with 25µM HCQ for 24h in the three cell lines. We found that RNA:DNA hybrids decreased after HCQ treatment mainly in the *RNASEH2B* ($p<0.05$), while *RNASEH2A* mutated LCLs did not show any significant changes (Figure 50A).

Moreover, we had previously described that endolysosomes can internalize RNA:DNA hybrids, and, therefore, we decided to investigate if 25µM HCQ for 24h may change the localization of RNA:DNA hybrids in *RNASEH2A* and *RNASEH2B* LCLs. We stained LCLs with monoclonal S9.6 hybrids antibody (green), the endolysosomal marker LysoTrackerTM (red) and the nuclear dye DAPI (blue) (Figure 50B). First of all, we observed a decreased lysosomal signal after the 25µM HCQ treatment for 24h. This result is in accordance with the literature suggesting that the drug lead to an alkalization of lysosomes which, in turn, results in a loss of their functions (269). Moreover colocalization between endolysosomes and RNA:DNA hybrids identified in *RNASEH2B* LCLs was lost after treatment.

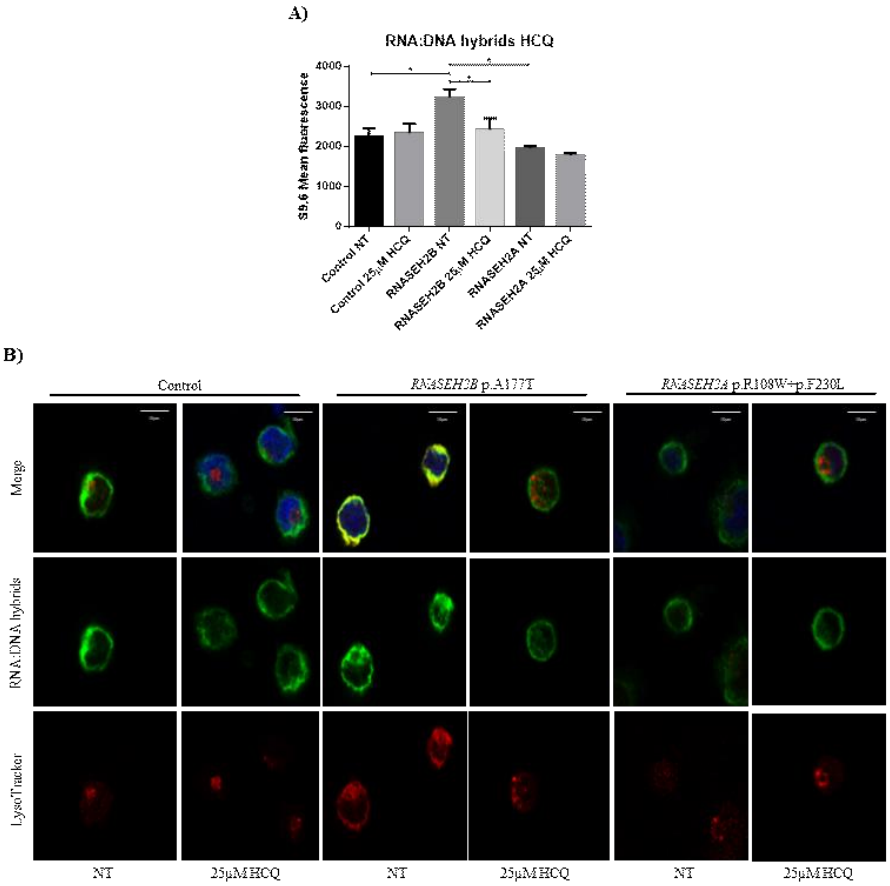

Figure 50. HCQ reduced RNA:DNA hybrids in *RNASEH2B* LCLs and changes localization. (A) Histogram of three biological experiments of RNA:DNA hybrids mean fluorescence of a healthy control and *RNASEH2A* and *RNASEH2B* mutated LCLs with (25µM HCQ) and without (NT) HCQ treatment. Paired t test has been performed. *p<0,05. (B) Immunofluorescence of LCLs derived from a healthy control and AGS patients with mutations in *RNASEH2A* and *RNASEH2B* genes before (NT) and after HCQ treatment (25µM) for 24h. RNA:DNA hybrids stained with S9.6 specific antibody (green), lysosomes stained with endolysosomal marker LysoTracker™ (red) and nuclear DAPI (blue).

4.5.2 Role of HCQ treatment on RNA:DNA hybrids removal by autophagy

It is known from the literature that HCQ also interferes with the autophagy process (270) (271), therefore, we investigated if autophagy can be involved in RNA:DNA hybrids removal after HCQ treatment. During autophagy, LC3I is converted in LC3-II and the LC3-II/LC3-I ratio is used to assess the autophagic flux (272). Therefore, we evaluated LC3II/LC3I protein levels in LCLs derived from a healthy control and AGS patients mutated in *RNASEH2A* and *RNASEH2B* genes. Without HCQ treatment we could not identify a difference in LC3II/LC3I ratio between patients and control. Conversely, after a treatment with 25µM HCQ for 24h, we observed an increase in the LC3II/LC3I ratio between the treated and the untreated sample for each cell line, especially for *RNASEH2B* mutated LCLs (Figure 51A) with a statistically significant p-value <0.001. We also assessed the localization of RNA:DNA hybrids and they colocalize with LC3 in the healthy control and in

RNASEH2B mutated LCLs at the basal level. After HCQ treatment the LC3 signal increased and it still colocalizes with RNA:DNA hybrids (Figure 51B).

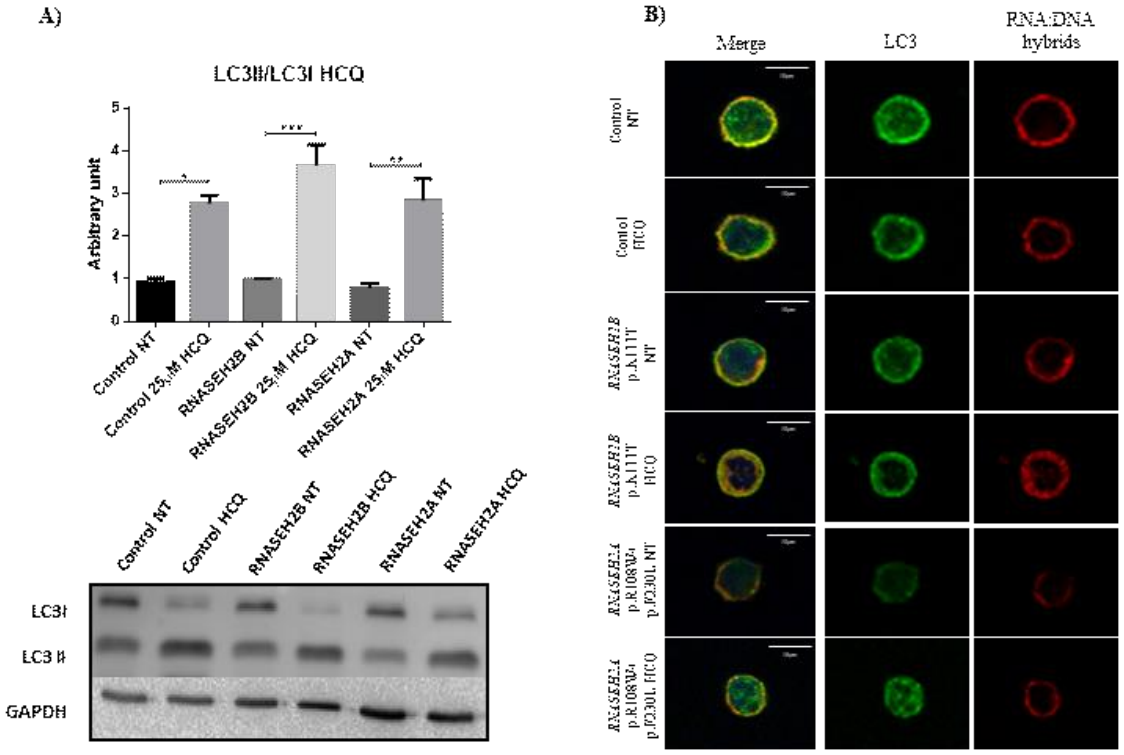

Figure 51. HCQ determines an accumulation of LC3. (A) Western Blot analysis of LC3 protein level in LCLs derived from a healthy control and AGS patients carrying mutations in *RNASEH2* subunits genes before and after HCQ treatment (25µM for 24h). The histogram represents the mean of three biological experiments. ANOVA test and post-hoc analysis Tukey's Test have been performed. * $p<0.05$, ** $p<0.01$, *** $p<0.001$. (B) Immunofluorescence of LCLs derived from AGS patients carrying mutations in *RNASEH2* subunits genes and a healthy control before and after HCQ treatment. LCLs stained with monoclonal S9.6 antibody (red), anti-LC3 (green) and nuclear blue dye DAPI.

These results were also confirmed by the evaluation of p62, another marker of autophagosome formation. We firstly assessed p62 protein level in LCLs from the healthy control and mutated *RNASEH2A* and *RNASEH2B* AGS patients. Once again, without HCQ treatment there were no differences in p62 expression between patients and control. Conversely, after a treatment with 25µM HCQ for 24h, we observed a slight increase in p62 protein levels between the treated and the untreated sample for each cell line (Figure 52A). We can still clearly observe that RNA:DNA hybrids colocalized with p62 strengthening the hypothesis that RNA:DNA were stuck in autophagosomes because HCQ inhibited the fusion of autophagosomes with lysosomes (Figure 52B). This colocalization between RNA:DNA hybrids and p62 is stronger and more evident in *RNASEH2B* mutated LCLs, which also presented more p62 foci than the healthy control and *RNASEH2A* mutated patient.

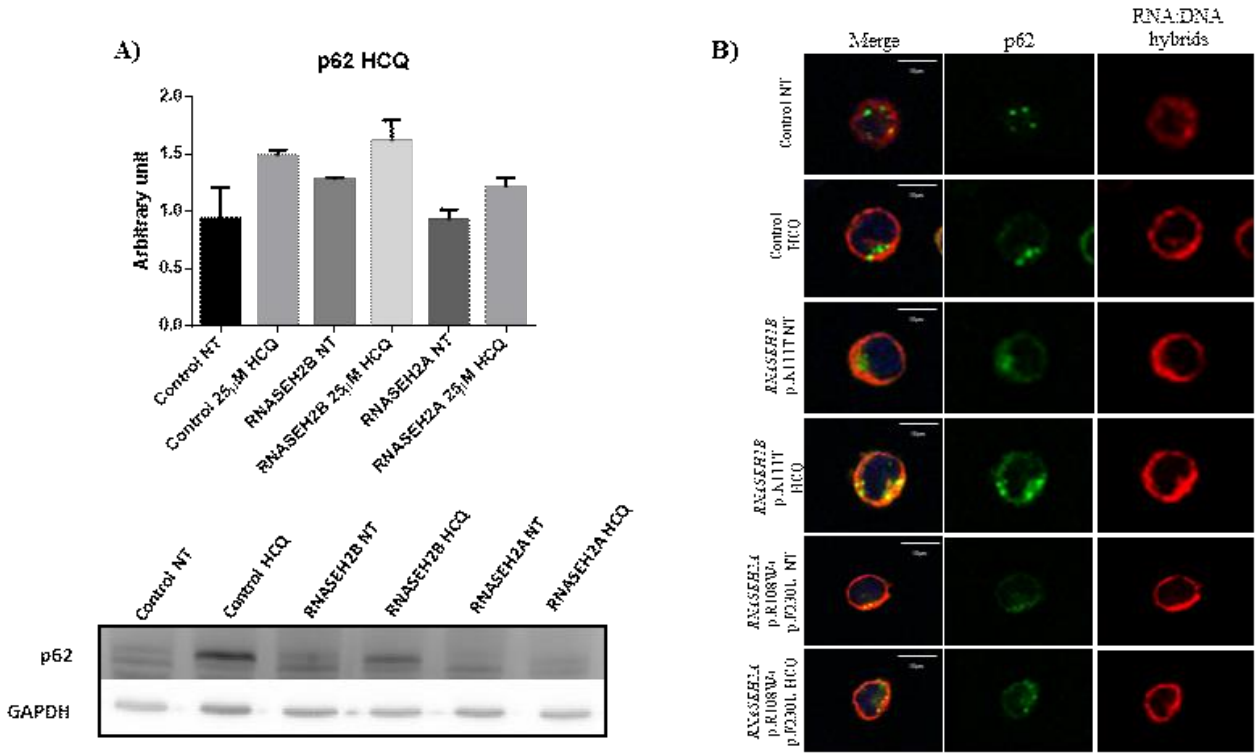

Figure 52. HCQ determined an increased expression of p62 and a colocalization of p62 and RNA:DNA hybrids in mutated LCLs (A) Western Blot analysis of p62 protein level in LCLs derived from an healthy control and AGS patients carrying mutations in *RNASEH2* subunits genes before and after HCQ treatment (25µM for 24h). The histogram represent the mean of three biological experiments. ANOVA test has been performed, but no significance has been identified (B) Immunofluorescence of LCLs derived from AGS patients carrying mutations in *RNASEH2* subunits genes and a healthy control. LCLs stained with monoclonal S9.6 antibody (red), anti-p62 (green) and nuclear blue dye DAPI. Cells were treated with HCQ at a concentration of 25µM for 24h.

4.5.3 HCQ effect on TLRs and cGAS pathways and on ISGs in *RNASEH2* mutated LCLs

After identifying a reduction of RNA:DNA hybrid content in *RNASEH2B* mutated LCLs, we wondered if this reduction induced by HCQ could have an effect on cGAS-STING and TLRs pathways activation. We evaluated the differences in cGAS protein levels and transcript levels of TLRs-related proteins. By Western Blot analysis we studied cGAS protein levels in the healthy control and in the two patients before and after HCQ treatment (Figure 53A). No differences have been identified between the control and patients and before and after treatment in each cell line, even if cGAS protein level was slightly decreased in *RNASEH2B* patient. Moreover, no difference was detected in the expression levels of IRF3 and NF-kB, which are two proteins involved in the downstream signalling of the cGAS-STING pathway (Figure 53B). When considering the expression levels of the serine/threonine protein kinase TBK1 before and after HCQ treatment by flow cytometry (Figure 53C).

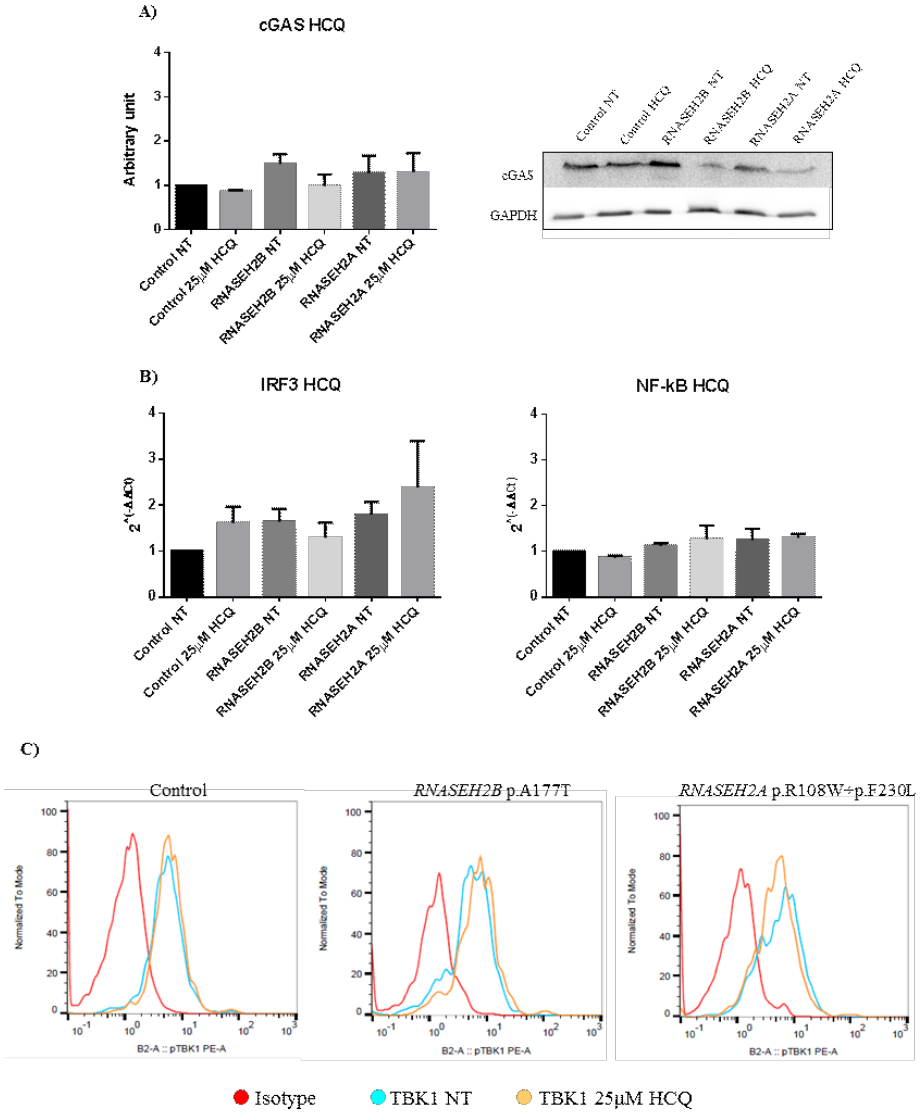

Figure 53. cGAS-STING pathway shows no significant modifications after HCQ treatment (A) Representative histogram and Western Blot of the cGAS protein level in LCLs derived from healthy control and AGS patients carrying mutation on *RNASEH2A* and *RNASEH2B* genes without and with HCQ treatment (25µM for 24h). (B) mRNA expression of NF-kB and IRF3 which are involved in cGAS-STING signaling in healthy control and AGS patients. (C) Flow cytometry analysis of TBK1 levels in healthy control and *RNASEH2* mutated LCLs with anti-TBK1 conjugated with PE. The red peak represent the isotype control, light blue peak the untreated sample and the yellow peak the HCQ treatment (25µM).

Conversely, when considering MYD88 and IRF7 few differences could be highlighted. After HCQ treatment (25µM for 24h) we observed a decrease MYD88 and IRF7 transcripts levels, especially in *RNASEH2B* mutated LCLs (Figure 54).

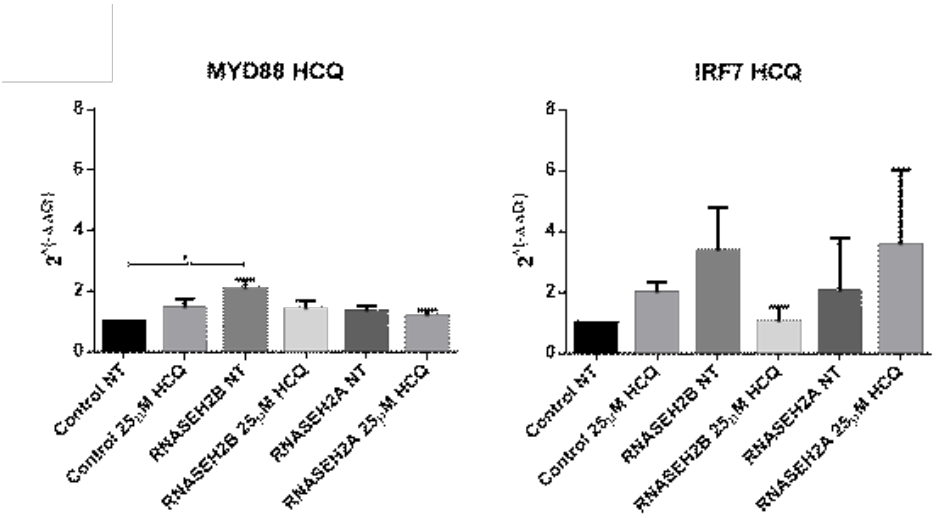

Figure 54. HCQ action on MYD88 and NK-kB. mRNA expression of MYD88 and IRF7 which are involved in TLRs signalling in healthy control and AGS patients before and after HCQ treatment (25µM for 24h). The histograms represent the mean of three biological experiments ANOVA test and post-hoc analysis Tukey's Test have been performed *p<0.05.

At last, we also evaluated how the expression of two ISGs, *IFI44* and *IFIT1*, changed in *RNASEH2A* and *RNASEH2B* mutated LCLs after HCQ treatment (25µM for 24h). The *IFI44* and, mostly, *IFIT1* expression level decreased after HCQ treatment in *RNASEH2B* mutated cell line with a significant p-value <0.01 and <0.05, respectively. No differences in *RNASEH2A* mutated LCLs have been observed (Figure 55).

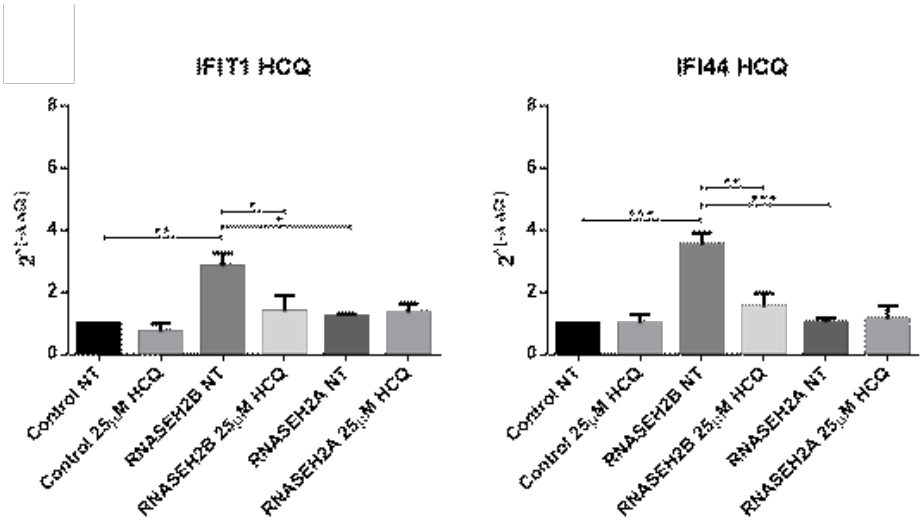

Figure 55. HCQ inhibits type I interferon response. *IFIT1* and *IFI44* mRNA expression levels in healthy control and AGS patients before and after HCQ treatment. The histograms represent the mean of three biological experiments. ANOVA test and post-hoc analysis Tukey's Test have been performed *p<0.05, **p>0.01, ***p<0.001.

5. Discussion

AGS is a rare, genetically determined encephalopathy with autosomal recessive and dominant inheritance and onset in the first year of life. Since 2000, 7 genes involved in the pathogenesis have been discovered: *TREX1, RNASEH2A, RNASEH2B, RNASEH2C, SAMHD1, ADAR1* and *IFIH1*. Mutations in the first six genes are suggested to determine an accumulation of undigested endogenous nucleic acids that consequently lead to the activation of an abnormal innate immune response, which is usually triggered by viral nucleic acids. Same result, but different situation in the case of *IFIH1* mutations. This gene encodes a protein (MDA5) that acts as a cytoplasmic sensor of the nucleic acids and, when mutated, this sensor binds more "avidly" to the cytoplasmic RNA causing an excessive activation of the type I interferon response (2,19).

In our study we observed that the Italian AGS population presented different mutation percentages compared to the frequency reported in a larger international cohort (2). The most frequently mutated genes in our cohort of AGS patients are *RNASEH2B* and *IFIH1* (59% versus 36% globally, and 12% versus 3%, respectively), whereas the frequency of mutations in TREX1 gene was lower than the global cohort (8% versus 22%). The percentage of mutations in the remaining AGS-related genes was instead quite similar to the one found in the global AGS population.

Moreover, thanks to our analysis we also identified five novel mutations in *RNASEH2B, SAMHD1* and *IFIH1* genes and three patients with a complete AGS phenotype, but without mutations in one of the seven AGS-related genes, highlighting how general knowledge about AGS is still limited and how other genetic factors are likely to be involved in the pathogenesis of this disease. Intriguingly, one patient presented two heterozygous mutations in *RNASET2*, a gene involved in ribosomal RNA metabolism and in the regulation of the immune response, both aspects usually altered in AGS patients (273,274). The association between mutations in *RNASET2* gene and Aicardi-Goutières syndrome is still controversial, but few cases mutated in this gene have already been described in a recent work by Tonduti and colleagues (45).

We have also evaluated the interferon signature in eighteen AGS patients and thirty-one healthy controls. Our results showed that eleven out of eighteen patients were positive, whereas the remaining seven subjects were negative. Since *RNASEH2B* is the most frequently mutated gene in AGS, we exclusively took these patients into consideration (thirteen on the whole) and we observed that eight were positive to the IS (61.5%) and five resulted negative (38.5%). These data are in accordance with the literature, since, as previously reported, 31% of patients carrying mutations in *RNASEH2B* showed negative results to the IS (2). Due to the heterogeneity of our results, it is difficult to consider the expression levels of ISGs as a possible biomarker of AGS, although this test undoubtedly represents a useful tool to address genetic tests and diagnosis.

The most frequent *RNASEH2B* mutation in our cohort of patients was p.A177T, as well as in the global AGS population (2). This mutation was associated with heterogeneity in the clinical phenotype, since the 60% of Italian patients showed a classic phenotype with or without extraneurological involvement, whereas the remaining showed a mild phenotype characterized by normal IQ in almost all patients and mild hemiparesis in two of them. The onset of the disease was predominantly within the first year of life, but later presentation was reported in the 18% of cases (253). No correlation between the interferon signature results and the clinical presentation of *RNASEH2B* patients has been observed. The transcriptomic and epigenetic analysis of p.A177T mild and severe patients performed in our study facilitated the identification of common or severity-specific molecular signatures. Regarding the transcriptomic analysis, severe patients presented a higher global deregulation than mild patients. Both subtypes of patients presented a deregulation of the antisense RNA of *SP110*, an interferon-induced gene, and deregulation of these genes have already been observed in another study by Lim and colleagues (155). Interestingly, a reduced expression of Rad54b was uniquely observed in patients with a severe phenotype. In a physiological status, this protein is involved in DNA repair and mitotic recombination and a downregulation of Rad54b is associated with inhibition of cell proliferation, induction of G1/S cell cycle arrest and chromosome instability (275,276). These features have also been described by Pizzi and collaborators in 2015 (113), and our data suggested that the impairment of cell proliferation and chromosome instability may determine a worse outcome of the disease, since this deregulation has been identified only in severe patients. Moreover, mild patients showed an overexpression of Rab40b that is not observed in severe patients. This protein may be a substrate-recognition component of an Elongin-Cullin-SOCS-box protein E3 ubiquitin ligase complex which mediates the ubiquitination and subsequent proteasomal degradation of target proteins. The number of patients included in the analysis have to be implemented.

Regarding DNA methylation, we can observe a general hypermethylation in both subtypes of patients (six mild and five severe) when compared to healthy controls. In literature, only one paper focused on DNA methylation of AGS patients and researchers highlighted a broad DNA hypomethylation in fibroblasts derived from four patients carrying mutations in four different AGS-related genes: *TREX1, RNASEH2A, RNASEH2B* and *SAMHD1*.

We identified a widespread shared epigenetic background between mild and severe patients, underlining that both cohorts of patients present a common pathological mechanism that contributes to AGS manifestation. Indeed, all patients show a strong hypomethylation of interferon regulated genes such as *IFI44L*, *IFITM1* and *MX1*. All of them are more hypomethylated in severe patients, probably highlighting a deeper involvement of the immune system in this subgroup of patients.

Remarkably, *IFI44L*, which is the most hypomethylated gene in both cohort of children, is also part of the interferon signature, one of the proposed biomarker of AGS (80). Moreover, all the main enriched terms for hypermethylated shared pathways include neutrophils' functions, cells that play an important role in the pathogenesis of systemic autoimmune diseases (277).

When considering only DMPs specifically associated to mild or severe phenotypes we can observed that different pathways are involved. Enriched terms for hypermethylated positions uniquely associated to severe patients, which comprehend leukocyte cell adhesion and lymphocyte differentiation whereas mild patients show a dysregulation of neutrophils' main functions. Interestingly, enriched terms for hypomethylated pathways specifically associated to mild patients and include lymphocytes differentiation and leukocyte cell adhesion, the same pathways that were hypermethylated in severe patients. Mild patients also showed a higher hypomethylation of *LIG4*, a DNA ligase involved in non homologous end joining and double strand breaks repairs. It is known from literature that cells depleted for RNase H2 show an activation of pathways involved in the maintenance of genome integrity (113) and an overexpression of this ligase in iPSCs have been linked to a reduction in the accumulation of DSBs (278).

In broader terms, pathways of differentially methylated genes in mild patients follow those found in both subtypes of patients, probably highlighting that a common pathological mechanism underlies both phenotypes. Remarkably, different methylation patterns are observed in severe patients, suggesting that further mechanisms contribute to the deterioration of their clinical conditions.

Since our data showed that *RNASEH2* subunits represent the most frequently mutated genes in AGS patients (253), we continue our project focusing on *RNASEH2B* and *RNASEH2A* mutated LCLs. RNase H2 represents the major source of cellular ribonuclease activity in eukaryotes and when the complex is mutated in one of its subunits, RNA:DNA hybrids accumulate in the cell cytoplasm leading to an inappropriate innate immune system activation, with high expression of type I IFN (6) (36). There is no evidence in the literature of the accumulation of RNA:DNA hybrids in *RNASEH2* mutated LCLs and if there is a different compartmentalization of the hybrids in these cells. We observed that RNA:DNA hybrids accumulate in *RNASEH2B* LCLs compared to the healthy control and these data are in accordance with the literature since Lim et al. showed that fibroblasts from patients mutated in *RNASEH2B* showed a pronounced increase in ribonucleotides (155). Surprisingly, no accumulation of hybrids have been observed in *RNASEH2A* mutated LCLs. These cells carry mutations at non conserved positions of RNase H2A that determine an impairment of the enzyme activity that is not as severe as other mutations found in highly conserved positions (279). This could possibly explain the lack of a significant hybrids accumulation and other pathological mechanism are being evaluated at the moment.

RNA:DNA hybrids in *RNASEH2B* LCLs presented a cytoplasmic localization and in literature it has been reported that nucleic acids released in the cytoplasm may be taken up and degraded by lysosomes in an ATP dependent manner (280). We found a colocalization of the hybrids with endolysosomes in LCLs mutated in *RNASEH2B* gene, suggesting that in this phenotype RNA:DNA hybrids accumulate in the cytoplasm and may be degraded by lysosomes. Rigby and colleagues described an accumulation of RNA:DNA hybrids in the cytosol and endosomes of B3T3 fibroblasts infected with the retrovirus Moloney Murine Leukaemia Virus (MMLV), which mimic retroviral infection (86). This can happen according to a mechanism similar to the novel type of autophagy, the RNautophagy/DNautophagy pathway, suggested by Fujiwara and colleagues where nucleic acids are degraded by lysosomes after being directly taken up in an ATP-dependent manner (192). Since both TLR9 and cGAS have been described as able to bind RNA:DNA hybrids we also assessed a possible activation of protein involved in the downstream signalling of these two pathway. *RNASEH2B* patients showed higher levels of MYD88 and IRF7 transcripts, suggesting the activation of TLRs in these patients. In parallel to this, we also assessed the expression level of two ISGs (*IFIT1* and *IFI44*) which are significantly higher in *RNASEH2B* mutated cell line, strengthening the evidence of an abnormal immune response in this patient. Moreover, since this activation has not been observed in *RNASEH2A* mutated LCLs, the involvement of TLRs is likely to be mutation-specific, since only *RNASEH2B* mutated patients showed an activation of this pathway. RNA:DNA hybrids accumulation activates the innate immune system and takes advantage of a nucleic acid sensor, the cyclic GMP-AMP synthase (cGAS), and its adaptor, STING, that lead to type I IFN production and transcription of ISGs (87). Surprisingly, we found that in both *RNASEH2B* and *RNASEH2A* mutated LCLs there were no significant differences in the activation of this immunological pathway.

Beside RNA:DNA hybrids, TLR9 can also sense dsDNA rich in unmethylated CpG motifs which is usually represented by bacterial DNA (281) or mtDNA, that contains CpG DNA repeats as well (282). Therefore, we started with the study of mitochondria morphology by TEM in AGS patients and we found a complete loss of the normal morphology of these organelles in both *RNASEH2B* and *RNASEH2A* LCLs. Remarkably, abnormalities in the morphology of mitochondria have been already found in patients affected by neurodegenerative diseases such as Parkinson disease, Alzheimer disease and Huntington disease (283). Damages to the structure of the mitochondrion can lead to the release of mtDNA at the cytoplasmic level (284) that can be sensed by both TLR9 and cGAS (265). Moreover, it is reported in the literature that in the presence of damaged organelles, a correlation between the content of mtDNA and the expression levels of a binding factor known as TFAM can be observed (263). We evaluated the expression levels of TFAM in the two mutated LCLs and in the healthy control, demonstrating its reduction in the mitochondrial compartment and the related

decrease in mtDNA content as reported in the literature. This lead us to hypothesize that fragmented mtDNA may be released outside the cell and detected by the sensors of the immune system (263). Further studies are needed to demonstrate this pathological mechanism, although mtDNA may represent another sources of immunostimulatory endogenous nucleic acid that accumulates in AGS cells.

Therapies in AGS are usually targeted to reduce the activation of the immune system by endogenous nucleic acids that accumulate in patients carrying mutations in AGS1-6 genes. In our study we used HCQ as a new therapeutic approach that has already been used to treat other autoimmune diseases such as SLE and RA. We observed that a 24h treatment with HCQ decreases the RNA:DNA hybrids content of *RNASEH2B* LCLs suggesting that this drug can also intercalates in hybrids, and not only in dsDNA as described in literature (271). HCQ therefore presents a greater effect on the *RNASEH2B* LCLs, that had a higher ISGs expression and presence of RNA:DNA hybrids. We also found that after the HCQ treatment the colocalization between lysosomes and RNA:DNA hybrids previously seen in LCLs mutated in *RNASEH2B* was no longer present. This is probably linked to the HCQ ability to alter the lysosomal acidification and stability increasing lysosomes' pH and leading to a loss of their functions (269). Moreover, HCQ is an established inhibitor of endosomal TLR-nucleic acid binding (236) and this can indicate that hybrids activate TLR9 in the endosomal compartment of *RNASEH2B* LCLs. The results regarding *MYD88* and *IRF7* expression suggest that the activation of TLRs pathway is likely to be mutation-specific, since only *RNASEH2B* LCLs showed an activation of this pathway. In parallel to this, the expression level of both the ISGs that we have studied, *IFIT1* and *IFI44*, decreased significantly after HCQ treatment only in *RNASEH2B* LCLs, suggesting that the drug can actively interfere with the immune response in this phenotype. Thus promising, these results need to be confirmed by further experiments on a larger cohort of LCLs derived from patients mutated in *RNASEH2B* and *RNASEH2A*.

As expected, after the treatment with HCQ, we also found out a statistically significant increase of LC3 protein level, confirming its ability to block the autophagic process and leading to the accumulation of the autophagic factors. It is known that blocking autophagy by using inhibitors such as HCQ may result in the activation of the exosome pathway (285). So, it is possible that when autophagy is inhibited, cells may get rid of RNA:DNA hybrids through exosomes, but further investigations are needed.

In summary, we characterized for the first time the Italian cohort of AGS patients from a genetic and a clinical point of view, highlighting the fundamental importance of an integrated approach in the diagnosis of this rare disease. Although it is known that mutations in all AGS-related genes lead to an abnormal immune system activation, molecular mechanisms associated to each mutation are still

controversial. We demonstrated that in *RNASEH2B* LCLs derived from an AGS patient there is an accumulation of undigested RNA:DNA hybrids that trigger an innate immune response probably driven by the endosomal TLR9. This mechanism seems to be mutation specific since the same activation is not observed in *RNASEH2A* LCLs, although further studies are needed to better characterize this hypothesis. Hence, the transcriptomic and DNA methylation experiments performed in this project contributed to a deeper understanding of pathological mechanisms underlying AGS severity in *RNASEH2B* mutated patients. Both of them allowed us to identify a dysregulation of IFN-induced genes, underlining once again the importance of the immune system activation in the pathogenesis of this disease. Moreover, we identified some biological pathways that are specifically impaired in severe patients and that will address further researches in the AGS field. The discovery of various deregulated molecular mechanisms in mild and severe patients could also be fundamental to identify the more appropriate therapeutic approach for these patients. Remarkably, in our project we demonstrated that HCQ, a European Medicines Agency (EMA) approved drug, could represent an efficient therapeutic approach in patients that present an overexpression of ISGs, as observed in *RNASEH2B* LCLs, opening new scenarios in a personalized medicine approach in AGS.

6. Bibliography

1. **Tolmie JL, Shillito P, Hughes-Benzie R, Stephenson JB.** *The Aicardi-Goutières syndrome (familial, early onset encephalopathy with calcifications of the basal ganglia and chronic cerebrospinal fluid lymphocytosis).* J Med Genet. 1995 Nov;32(11):881-4. doi: 10.1136/jmg.32.11.881.

2. **Crow YJ, Chase DS, Lowenstein Schmidt J, et al.** *Characterization of Human Disease Phenotypes Associated With Mutations in TREX1, RNASEH2A, RNASEH2B, RNASEH2C, SAMHD1, ADAR, and IFIH1.* Am J Med Genet A. 2015 Feb;167A(2):296-312. doi: 10.1002/ajmg.a.36887.

3. **Aicardi J, Goutières F.** *A Progressive Familial Encephalopathy in Infancy With Calcifications of the Basal Ganglia and Chronic Cerebrospinal Fluid Lymphocytosis.* Ann Neurol. 1984 Jan;15(1):49-54. doi: 10.1002/ana.410150109.

4. **Goutières F.** *Aicardi-Goutières Syndrome.* Brain Dev. 2005, 27(3):201-6. doi: 10.1016/j.braindev.2003.12.011.

5. **Crow YJ, Jackson AP, Roberts E, et al.** *Aicardi-Goutières syndrome displays genetic heterogeneity with one locus (AGS1) on chromosome 3p21.* Am. J. Hum. Genet. 2000, 67(1):213-21.

6. **Orcesi S, La Piana R, Fazzi E.** *Aicardi-Goutieres Syndrome.* Br Med Bull. 2009, 89:183-201. doi: 10.1093/bmb/ldn049.

7. **Vogt J, Agrawal S, Ibrahim Z, et al.** *Striking Intrafamilial Phenotypic Variability in Aicardi-Goutières Syndrome Associated With the Recurrent Asian Founder Mutation in RNASEH2C.* Am J Med Genet A. 2013, 161A(2):338-42. doi: 10.1002/ajmg.a.35712.

8. **Ramantani G, Maillard LG, Bast T, et al.** *Epilepsy in Aicardi-Goutières syndrome.* Eur J Paediatr Neurol. 2014 Jan;18(1):30-7. doi: 10.1016/j.ejpn.2013.07.005.

9. **Rice G, Patrick T, Parmar R, et al.** *Clinical and molecular phenotype of Aicardi-Goutieres syndrome.* Am J Hum Genet. 2007 Oct;81(4):713-25. doi: 10.1086/521373.

10. **Tonduti D, Panteghini C, Pichiecchio A, et al.** *Encephalopathies with intracranial calcification in children: clinical and genetic characterization.* Orphanet J Rare Dis. 2018 Aug 16;13(1):135. doi: 10.1186/s13023-018-0854-y.

11. **Zhang L, Hu XZ, Li H, Li X, Smerin S, Benedek DM, Ursano R.** *Startle response related genes.* Med Hypotheses. 2011 Oct;77(4):685-91. doi: 10.1016/j.mehy.2011.07.018.

12. **Abdel-Salam GM, El-Kamah GY, Rice GI, et al.** *Chilblains as a diagnostic sign of aicardi-goutières syndrome.* Neuropediatrics. 2010 Feb;41(1):18-23. doi: 10.1055/s-0030-1255059.

13. **Yarbrough K, Danko C, Krol A, Zonana J, Leitenberger S.** *The importance of chilblains as a diagnostic clue for mild Aicardi-Goutières syndrome.* Am J Med Genet A. 2016 Dec;170(12):3308-3312. doi: 10.1002/ajmg.a.37944.

14. **Kolivras A, Aeby A, Crow YJ, Rice GI, Sass U, André J.** *Cutaneous histopathological findings of Aicardi-Goutières syndrome, overlap with chilblain lupus.* J Cutan Pathol. 2008 Aug;35(8):774-8. doi: 10.1111/j.1600-0560.2007.00900.x.

15. **Crow YJ, Livingston JH.** *Aicardi-Goutières syndrome: an important Mendelian mimic of congenital infection.* Dev Med Child Neurol. 2008 Jun;50(6):410-6. doi: 10.1111/j.1469-8749.2008.02062.x.

16. **La Piana R, Uggetti C, Roncarolo F, et al.** *Neuroradiologic patterns and novel imaging findings in Aicardi-Goutières syndrome.* Neurology. 2016 Jan 5;86(1):28-35. doi: 10.1212/WNL.0000000000002228.

17. **Østergaard JR, Christensen T.** *Aicardi-Goutières syndrome: neuroradiological findings after nine years of follow-up.* Eur J Paediatr Neurol. 2004;8(5):243-6. doi: 10.1016/j.ejpn.2004.06.003.

18. **Abdel-Salam GM, Zaki MS, Lebon P, Meguid NA.** *Aicardi-Goutières syndrome: clinical and neuroradiological findings of 10 new cases.* Acta Paediatr. 2004 Jul;93(7):929-36. doi: 10.1111/j.1651-2227.2004.tb02691.x.

19. **Lanzi G, Fazzi E, D'Arrigo S, et al.***The natural history of Aicardi-Goutières syndrome: follow-up of 11 Italian patients.* Neurology. 2005 May 10;64(9):1621-4. doi: 10.1212/01.WNL.0000159864.05826.08.
20. **van Heteren JT, Rozenberg F, Aronica E, Troost D, Lebon P, Kuijpers TW.** *Astrocytes produce interferon-alpha and CXCL10, but not IL-6 or CXCL8, in Aicardi-Goutières syndrome.* Glia. 2008 Apr;56(5):568-78. doi: 10.1002/glia.20639.
21. **Blau N, Bonafé L, Krägeloh-Mann I, Thöny B, Kierat L, Häusler M, Ramaekers V.** *Cerebrospinal fluid pterins and folates in Aicardi-Goutières syndrome: a new phenotype.* Neurology. 2003 Sep 9;61(5):642-7. doi: 10.1212/01.wnl.0000082726.08631.e7.
22. **Viaccoz A, Ducray F, Tholance Y, et al.** *CSF neopterin level as a diagnostic marker in primary central nervous system lymphoma.* Neuro Oncol. 2015 Nov;17(11):1497-503. doi: 10.1093/neuonc/nov092.
23. **Dale RC, Brilot F, Fagan E, Earl J.** *Cerebrospinal fluid neopterin in paediatric neurology: a marker of active central nervous system inflammation.* Dev Med Child Neurol. 2009 Apr;51(4):317-23. doi: 10.1111/j.1469-8749.2008.03225.x.
24. **Rice GI, Forte GM, Szynkiewicz M, et al.** *Assessment of interferon-related biomarkers in Aicardi-Goutières syndrome associated with mutations in TREX1, RNASEH2A, RNASEH2B, RNASEH2C, SAMHD1, and ADAR: a case-control study.* Lancet Neurol. 2013 Dec;12(12):1159-69. doi: 10.1016/S1474-4422(13)70258-8.
25. **Aicardi J, Goutières F.** *Systemic lupus erythematosus or Aicardi-Goutières syndrome?* Neuropediatrics. 2000 Jun;31(3):113. doi: 10.1055/s-2000-7533.
26. **De Laet C, Goyens P, Christophe C, Ferster A, Mascart F, Dan B.** *Phenotypic overlap between infantile systemic lupus erythematosus and Aicardi-Goutières syndrome.* Neuropediatrics. 2005 Dec;36(6):399-402. doi: 10.1055/s-2005-873058.
27. **Baechler EC, Batliwalla FM, Karypis G, et al.** *Interferon-inducible gene expression signature in peripheral blood cells of patients with severe lupus.* Proc Natl Acad Sci U S A. 2003 Mar 4;100(5):2610-5. doi: 10.1073/pnas.0337679100.
28. **Rönnblom L, Eloranta ML.** *The interferon signature in autoimmune diseases.* Curr Opin Rheumatol. 2013 Mar;25(2):248-53. doi: 10.1097/BOR.0b013e32835c7e32.
29. **Isaacs A, Lindenmann J.** *Pillars Article: Virus Interference. I. The Interferon. Proc R Soc Lond B Biol Sci. 1957. 147: 258-267.* J Immunol. 2015 Sep 1;195(5):1911-20.
30. **Baron S, Tyring SK, Fleischmann WR Jr, et al.** *The interferons. Mechanisms of action and clinical applications.* JAMA. 1991 Sep 11;266(10):1375-83. doi: 10.1001/jama.266.10.1375.
31. **Belardelli F, Gresser I.** *The neglected role of type I interferon in the T-cell response: implications for its clinical use.* Immunol Today. 1996 Aug;17(8):369-72. doi: 10.1016/0167-5699(96)10027-X.
32. **Gutterman JU.** *Cytokine therapeutics: lessons from interferon alpha.* Proc Natl Acad Sci U S A. 1994 Feb 15;91(4):1198-205. doi: 10.1073/pnas.91.4.1198.
33. **Manry J, Laval G, Patin E, et al.** *Evolutionary genetic dissection of human interferons.* J Exp Med. 2011 Dec 19;208(13):2747-59. doi: 10.1084/jem.20111680.
34. **Swiecki M, Colonna M.** *Type I interferons: diversity of sources, production pathways and effects on immune responses.* Curr Opin Virol. 2011 Dec;1(6):463-75. doi: 10.1016/j.coviro.2011.10.026.
35. **Niewold TB, Clark DN, Salloum R, Poole BD.** *Interferon alpha in systemic lupus erythematosus.* J Biomed Biotechnol. 2010;2010:948364. doi: 10.1155/2010/948364.
36. **Crow YJ, Manel N.** *Aicardi-Goutières syndrome and the type I interferonopathies.* Nat Rev Immunol. 2015 Jul;15(7):429-40. doi: 10.1038/nri3850.
37. **Borden EC, Sen GC, Uze G, Silverman RH, Ransohoff RM, Foster GR, Stark GR.** *Interferons at age 50: past, current and future impact on biomedicine.* Nat Rev Drug Discov. 2007 Dec;6(12):975-90. doi: 10.1038/nrd2422.

38. **Lieberman AP, Pitha PM, Shin HS, Shin ML.** *Production of tumor necrosis factor and other cytokines by astrocytes stimulated with lipopolysaccharide or a neurotropic virus.* Proc Natl Acad Sci U S A. 1989 Aug;86(16):6348-52. doi: 10.1073/pnas.86.16.6348.
39. **Akiyama H, Ikeda K, Katoh M, McGeer EG, McGeer PL.** *Expression of MRP14, 27E10, interferon-alpha and leukocyte common antigen by reactive microglia in postmortem human brain tissue.* J Neuroimmunol. 1994 Mar;50(2):195-201. doi: 10.1016/0165-5728(94)90046-9.
40. **Akwa Y, Hassett DE, Eloranta ML, et al.** *Transgenic expression of IFN-alpha in the central nervous system of mice protects against lethal neurotropic viral infection but induces inflammation and neurodegeneration.* J Immunol. 1998 Nov 1;161(9):5016-26.
41. **Bauer JW, Petri M, Batliwalla FM, et al.** *Interferon-regulated chemokines as biomarkers of systemic lupus erythematosus disease activity: a validation study.* Arthritis Rheum. 2009 Oct;60(10):3098-107. doi: 10.1002/art.24803.
42. **Dall'era MC, Cardarelli PM, Preston BT, Witte A, Davis JC Jr.** *Type I interferon correlates with serological and clinical manifestations of SLE.* Ann Rheum Dis. 2005 Dec;64(12):1692-7. doi: 10.1136/ard.2004.033753.
43. **Briggs TA, Rice GI, Daly S, et al.** *Tartrate-resistant acid phosphatase deficiency causes a bone dysplasia with autoimmunity and a type I interferon expression signature.* Nat Genet. 2011 Feb;43(2):127-31. doi: 10.1038/ng.748.
44. **Sase S, Takanohashi A, Vanderver A, Almad A.** *Astrocytes, an active player in Aicardi-Goutières syndrome.* Brain Pathol. 2018 May;28(3):399-407. doi: 10.1111/bpa.12600.
45. **Tonduti D, Orcesi S, Jenkinson EM, et al.** *Clinical, radiological and possible pathological overlap of cystic leukoencephalopathy without megalencephaly and Aicardi-Goutières syndrome.* Eur J Paediatr Neurol. 2016 Jul;20(4):604-10. doi: 10.1016/j.ejpn.2016.03.009.
46. **Crow YJ, Jackson AP, Roberts E, et al.** *Aicardi-Goutières Syndrome Displays Genetic Heterogeneity with One Locus (AGS1) on Chromosome 3p21.* Am J Hum Genet. 2000 Jul;67(1):213-21. doi: 10.1086/302955.
47. **Crow YJ, Hayward BE, Parmar R, et al.** *Mutations in the gene encoding the 3'-5' DNA exonuclease TREX1 cause Aicardi-Goutières syndrome at the AGS1 locus.* Nat Genet. 2006 Aug;38(8):917-20. doi: 10.1038/ng1845.
48. **Mazur DJ, Perrino FW.** *Structure and expression of the TREX1 and TREX2 3' --> 5' exonuclease genes.* J Biol Chem. 2001 May 4;276(18):14718-27. doi: 10.1074/jbc.M010051200.
49. **Yang YG, Lindahl T, Barnes DE.** *Trex1 exonuclease degrades ssDNA to prevent chronic checkpoint activation and autoimmune disease.* Cell. 2007 Nov 30;131(5):873-86. doi: 10.1016/j.cell.2007.10.017.
50. **Yuan F, Dutta T, Wang L, et al.** *Human DNA Exonuclease TREX1 Is Also an Exoribonuclease That Acts on Single-stranded RNA.* J Biol Chem. 2015 May 22;290(21):13344-53. doi: 10.1074/jbc.M115.653915.
51. **Lee-Kirsch MA, Gong M, Chowdhury D, et al.** *Mutations in the gene encoding the 3'-5' DNA exonuclease TREX1 are associated with systemic lupus erythematosus.* Nat Genet. 2007 Sep;39(9):1065-7. doi: 10.1038/ng2091.
52. **Rice G, Newman WG, Dean J, et al.** *Heterozygous mutations in TREX1 cause familial chilblain lupus and dominant Aicardi-Goutieres syndrome.* Am J Hum Genet. 2007 Apr;80(4):811-5. doi: 10.1086/513443.
53. **Richards A, van den Maagdenberg AM, Jen JC, et al.** *C-terminal truncations in human 3'-5' DNA exonuclease TREX1 cause autosomal dominant retinal vasculopathy with cerebral leukodystrophy.* Nat Genet. 2007 Sep;39(9):1068-70. doi: 10.1038/ng2082.
54. **Ali M, Highet LJ, Lacombe D, et al.** *A second locus for Aicardi-Goutieres syndrome at chromosome 13q14-21.* J Med Genet. 2006 May;43(5):444-50. doi: 10.1136/jmg.2005.031880.
55. **Crow YJ, Leitch A, Hayward BE, et al.** *Mutations in genes encoding ribonuclease H2 subunits cause Aicardi-Goutières syndrome and mimic congenital viral brain infection.* Nat Genet. 2006 Aug;38(8):910-6. doi: 10.1038/ng1842.

56. **Hiller B, Achleitner M, Glage S, Naumann R, Behrendt R, Roers A.** *Mammalian RNase H2 removes ribonucleotides from DNA to maintain genome integrity.* J Exp Med. 2012 Jul 30;209(8):1419-26. doi: 10.1084/jem.20120876.
57. **Rice GI, Bond J, Asipu A, et al.** *Mutations involved in Aicardi-Goutières syndrome implicate SAMHD1 as regulator of the innate immune response.* Nat Genet. 2009 Jul;41(7):829-32. doi: 10.1038/ng.373.
58. **Ahn J.** *Functional organization of human SAMHD1 and mechanisms of HIV-1 restriction.* Biol Chem. 2016 Apr;397(4):373-9. doi: 10.1515/hsz-2015-0260.
59. **Laguette N, Sobhian B, Casartelli N, et al.** *SAMHD1 is the dendritic- and myeloid-cell-specific HIV-1 restriction factor counteracted by Vpx.* Nature. 2011 May 25;474(7353):654-7. doi: 10.1038/nature10117.
60. **Zhao K, Du J, Han X, et al.** *Modulation of LINE-1 and Alu/SVA retrotransposition by Aicardi-Goutières syndrome-related SAMHD1.* Cell Rep. 2013 Sep 26;4(6):1108-15. doi: 10.1016/j.celrep.2013.08.019.
61. **Yan J, Kaur S, DeLucia M, et al.** *Tetramerization of SAMHD1 is required for biological activity and inhibition of HIV infection.* J Biol Chem. 2013 Apr 12;288(15):10406-17. doi: 10.1074/jbc.M112.443796.
62. **Hansen EC, Seamon KJ, Cravens SL, Stivers JT.** *GTP activator and dNTP substrates of HIV-1 restriction factor SAMHD1 generate a long-lived activated state.* Proc Natl Acad Sci U S A. 2014 May 6;111(18):E1843-51. doi: 10.1073/pnas.1401706111.
63. **Lahouassa H, Daddacha W, Hofmann H, et al.** *SAMHD1 restricts the replication of human immunodeficiency virus type 1 by depleting the intracellular pool of deoxynucleoside triphosphates.* s.l. : Nat Immunol. 2012 Feb 12;13(3):223-228. doi: 10.1038/ni.2236.
64. **Li M, Zhang D, Zhu M, et al.** *Roles of SAMHD1 in antiviral defense, autoimmunity and cancer.* Rev Med Virol. 2017 Jul;27(4). doi: 10.1002/rmv.1931.
65. **Rice GI, Kasher PR, Forte GM, et al.** *Mutations in ADAR1 cause Aicardi-Goutières syndrome associated with a type I interferon signature.* Nat Genet. 2012 Nov;44(11):1243-8. doi: 10.1038/ng.2414.
66. **Hogg M, Paro S, Keegan LP, O'Connell MA.** *RNA editing by mammalian ADARs.* Adv Genet. 2011;73:87-120. doi: 10.1016/B978-0-12-380860-8.00003-3.
67. **George CX, Samuel CE.** *Human RNA-specific adenosine deaminase ADAR1 transcripts possess alternative exon 1 structures that initiate from different promoters, one constitutively active and the other interferon inducible.* Proc Natl Acad Sci U S A. 1999 Apr 13;96(8):4621-6. doi: 10.1073/pnas.96.8.4621.
68. **Herbert A, Alfken J, Kim YG, Mian IS, Nishikura K, Rich A.** *A Z-DNA binding domain present in the human editing enzyme, double-stranded RNA adenosine deaminase.* Proc Natl Acad Sci U S A. 1997 Aug 5;94(16):8421-6. doi: 10.1073/pnas.94.16.8421.
69. **Bahn JH, Ahn J, Lin X, Zhang Q, Lee JH, Civelek M, Xiao X.** *Genomic analysis of ADAR1 binding and its involvement in multiple RNA processing pathways.* Nat Commun. 2015 Mar 9;6:6355. doi: 10.1038/ncomms7355.
70. **Mannion NM, Greenwood SM, Young R, et al.** *The RNA-editing enzyme ADAR1 controls innate immune responses to RNA.* Cell Rep. 2014 Nov 20;9(4):1482-94. doi: 10.1016/j.celrep.2014.10.041.
71. **Bazak L, Haviv A, Barak M, et al.** *A-to-I RNA editing occurs at over a hundred million genomic sites, located in a majority of human genes.* Genome Res. 2014 Mar;24(3):365-76. doi: 10.1101/gr.164749.113.
72. **Vitali P, Scadden AD.** *Double-stranded RNAs containing multiple IU pairs are sufficient to suppress interferon induction and apoptosis.* Nat Struct Mol Biol. 2010 Sep;17(9):1043-50. doi: 10.1038/nsmb.1864.
73. **Rice GI, Del Toro Duany Y, Jenkinson EM, et al.** *Gain-of-function mutations in IFIH1 cause a spectrum of human disease phenotypes associated with upregulated type I interferon signaling.* Nat Genet. 2014 May;46(5):503-509. doi: 10.1038/ng.2933.
74. **Goubau D, Deddouche S, Reis e Sousa C.** *Cytosolic sensing of viruses.* Immunity. 2013 May 23;38(5):855-69. doi: 10.1016/j.immuni.2013.05.007.

75. **Barrat FJ, Elkon KB, Fitzgerald KA.** *Importance of Nucleic Acid Recognition in Inflammation and Autoimmunity.* Annu Rev Med. 2016;67:323-36. doi: 10.1146/annurev-med-052814-023338.
76. **Dias Junior AG, Sampaio NG, Rehwinkel J.** *A Balancing Act: MDA5 in Antiviral Immunity and Autoinflammation.* Trends Microbiol. 2019 Jan;27(1):75-85. doi: 10.1016/j.tim.2018.08.007.
77. **Oda H, Nakagawa K, Abe J, et al.** *Aicardi-Goutières Syndrome Is Caused by IFIH1 Mutations.* Am J Hum Genet. 2014 Jul 3;95(1):121-5. doi: 10.1016/j.ajhg.2014.06.007.
78. **Rutsch F, MacDougall M, Lu C, et al.** *A Specific IFIH1 Gain-of-Function Mutation Causes Singleton-Merten Syndrome.* Am J Hum Genet. 2015 Feb 5;96(2):275-82. doi: 10.1016/j.ajhg.2014.12.014.
79. **Al Mutairi F, Alfadhel M, Nashabat M, et al.** *Phenotypic and Molecular Spectrum of Aicardi-Goutières Syndrome: A Study of 24 Patients.* Pediatr Neurol. 2018 Jan;78:35-40. doi: 10.1016/j.pediatrneurol.2017.09.002.
80. **Livingston JH, Lin JP, Dale RC, et al.** *A type I interferon signature identifies bilateral striatal necrosis due to mutations in ADAR1.* J Med Genet. 2014 Feb;51(2):76-82. doi: 10.1136/jmedgenet-2013-102038.
81. **Stark GR, Kerr IM, Williams BR, Silverman RH, Schreiber RD.** *How cells respond to interferons.* Annu Rev Biochem. 1998;67:227-64. doi: 10.1146/annurev.biochem.67.1.227.
82. **Stetson DB, Medzhitov R.** *Type I interferons in host defense.* Immunity. 2006 Sep;25(3):373-81. doi: 10.1016/j.immuni.2006.08.007.
83. **Kawasaki T, Kawai T.** *Toll-like receptor signaling pathways.* Front Immunol. 2014 Sep 25;5:461. doi: 10.3389/fimmu.2014.00461.
84. **Pichlmair A, Reis e Sousa C.** *Innate recognition of viruses.* Immunity. 2007 Sep;27(3):370-83. doi: 10.1016/j.immuni.2007.08.012.
85. **Stetson DB, Ko JS, Heidmann T, Medzhitov R.** *Trex1 prevents cell-intrinsic initiation of autoimmunity.* Cell. 2008 Aug 22;134(4):587-98. doi: 10.1016/j.cell.2008.06.032.
86. **Rigby RE, Webb LM, Mackenzie KJ, et al.** *RNA:DNA hybrids are a novel molecular pattern sensed by TLR9.* EMBO J. 2014 Mar 18;33(6):542-58. doi: 10.1002/embj.201386117.
87. **Mankan AK, Schmidt T, Chauhan D, et al.** *Cytosolic RNA:DNA hybrids activate the cGAS-STING axis.* EMBO J. 2014 Dec 17;33(24):2937-46. doi: 10.15252/embj.201488726.
88. **Stein H, Hausen P.** *Enzyme from calf thymus degrading the RNA moiety of DNA-RNA Hybrids: effect on DNA-dependent RNA polymerase.* Science. 1969 Oct 17;166(3903):393-5. doi: 10.1126/science.166.3903.393.
89. **Krug MS, Berger SL.** *Ribonuclease H activities associated with viral reverse transcriptases are endonucleases.* Proc Natl Acad Sci U S A. 1989 May;86(10):3539-43. doi: 10.1073/pnas.86.10.3539.
90. **Nowotny M.** *Retroviral integrase superfamily: the structural perspective.* EMBO Rep. 2009 Feb;10(2):144-51. doi: 10.1038/embor.2008.256.
91. **Hyjek M, Figiel M, Nowotny M.** *RNases H: Structure and mechanism.* DNA Repair (Amst). 2019 Dec;84:102672. doi: 10.1016/j.dnarep.2019.102672.
92. **Ohtani N, Haruki M, Morikawa M, Kanaya S.** *Molecular diversities of RNases H.* J Biosci Bioeng. 1999;88(1):12-9. doi: 10.1016/s1389-1723(99)80168-6.
93. **Cerritelli SM, Crouch RJ.** *Ribonuclease H: the enzymes in eukaryotes.* FEBS J. 2009 Mar;276(6):1494-505. doi: 10.1111/j.1742-4658.2009.06908.x.
94. **Nowotny M, Cerritelli SM, Ghirlando R, Gaidamakov SA, Crouch RJ, Yang W.** *Specific recognition of RNA/DNA hybrid and enhancement of human RNase H1 activity by HBD.* EMBO J. 2008 Apr 9;27(7):1172-81. doi: 10.1038/emboj.2008.44.
95. **Cerritelli SM, Frolova EG, Feng C, Grinberg A, Love PE, Crouch RJ.** *Failure to produce mitochondrial DNA results in embryonic lethality in Rnaseh1 null mice.* Mol Cell. 2003 Mar;11(3):807-15. doi: 10.1016/s1097-2765(03)00088-1.

96. **Lima WF, Murray HM, Damle SS, et al.** *Viable RNaseH1 knockout mice show RNaseH1 is essential for R loop processing, mitochondrial and liver function.* Nucleic Acids Res. 2016 Jun 20;44(11):5299-312. doi: 10.1093/nar/gkw350.
97. **Posse V, Al-Behadili A, Uhler JP, et al.** *RNase H1 directs origin-specific initiation of DNA replication in human mitochondria.* PLoS Genet. 2019 Jan 3;15(1):e1007781. doi: 10.1371/journal.pgen.1007781.
98. **Rydberg B, Game J.** *Excision of misincorporated ribonucleotides in DNA by RNase H (type 2) and FEN-1 in cell-free extracts.* Proc Natl Acad Sci U S A. 2002 Dec 24;99(26):16654-9. doi: 10.1073/pnas.262591699.
99. **Eder PS, Walder RY, Walder JA.** *Substrate specificity of human RNase H1 and its role in excision repair of ribose residues misincorporated in DNA.* s.l. : Biochimie. 1993;75(1-2):123-6. doi: 10.1016/0300-9084(93)90033-o.
100. **Sparks JL, Chon H, Cerritelli SM, Kunkel TA, Johansson E, Crouch RJ, Burgers PM.** *RNase H2-initiated ribonucleotide excision repair.* Mol Cell. 2012 Sep 28;47(6):980-6. doi: 10.1016/j.molcel.2012.06.035.
101. **Jeong HS, Backlund PS, Chen HC, Karavanov AA, Crouch RJ.** *RNase H2 of Saccharomyces cerevisiae is a complex of three proteins.* Nucleic Acids Res. 2004 Jan 20;32(2):407-14. doi: 10.1093/nar/gkh209.
102. **Shaban NM, Harvey S, Perrino FW, Hollis T.** *The structure of the mammalian RNase H2 complex provides insight into RNA:DNA hybrid processing to prevent immune dysfunction.* J Biol Chem. 2010 Feb 5;285(6):3617-24. doi: 10.1074/jbc.M109.059048.
103. **Reijns MA, Bubeck D, Gibson LC, Graham SC, Baillie GS, Jones EY, Jackson AP.** *The structure of the human RNase H2 complex defines key interaction interfaces relevant to enzyme function and human disease.* J Biol Chem. 2011 Mar 25;286(12):10530-9. doi: 10.1074/jbc.M110.177394.
104. **El Hage A, French SL, Beyer AL, Tollervey D.** *Loss of Topoisomerase I leads to R-loop-mediated transcriptional blocks during ribosomal RNA synthesis.* Genes Dev. 2010 Jul 15;24(14):1546-58. doi: 10.1101/gad.573310.
105. **Maga G, Hubscher U.** *Proliferating cell nuclear antigen (PCNA): a dancer with many partners.* J Cell Sci. 2003 Aug 1;116(Pt 15):3051-60. doi: 10.1242/jcs.00653.
106. **Reijns MA, Rabe B, Rigby RE, et al.** *Enzymatic removal of ribonucleotides from DNA is essential for mammalian genome integrity and development.* Cell. 2012 May 25;149(5):1008-22. doi: 10.1016/j.cell.2012.04.011. Epub 2012 May 10.
107. **Figiel M, Chon H, Cerritelli SM, Cybulska M, Crouch RJ, Nowotny M.** *The structural and biochemical characterization of human RNase H2 complex reveals the molecular basis for substrate recognition and Aicardi-Goutières syndrome defects.* J Biol Chem. 2011 Mar 25;286(12):10540-50. doi: 10.1074/jbc.M110.181974.
108. **Rabe B.** *Aicardi-Goutières syndrome: clues from the RNase H2 knock-out mouse.* J Mol Med (Berl). 2013 Nov;91(11):1235-40. doi: 10.1007/s00109-013-1061-x.
109. **Nick McElhinny SA, Watts BE, Kumar D, et al.** *Abundant ribonucleotide incorporation into DNA by yeast replicative polymerases.* Proc Natl Acad Sci U S A. 2010 Mar 16;107(11):4949-54. doi: 10.1073/pnas.0914857107.
110. **Härtlova A, Erttmann SF, Raffi FA, et al.** *DNA damage primes the type I interferon system via the cytosolic DNA sensor STING to promote anti-microbial innate immunity.* Immunity. 2015 Feb 17;42(2):332-343. doi: 10.1016/j.immuni.2015.01.012.
111. **Lan YY, Londoño D, Bouley R, Rooney MS, Hacohen N.** *Dnase2a deficiency uncovers lysosomal clearance of damaged nuclear DNA via autophagy.* Cell Rep. 2014 Oct 9;9(1):180-192. doi: 10.1016/j.celrep.2014.08.074.
112. **Menendez D, Shatz M, Azzam K, Garantziotis S, Fessler MB, Resnick MA.** *The Toll-like receptor gene family is integrated into human DNA damage and p53 networks.* PLoS Genet. 2011 Mar;7(3):e1001360. doi: 10.1371/journal.pgen.1001360.

113. **Pizzi S, Sertic S, Orcesi S, et al.** *Reduction of hRNase H2 activity in Aicardi-Goutières syndrome cells leads to replication stress and genome instability.* Hum Mol Genet. 2015 Feb 1;24(3):649-58. doi: 10.1093/hmg/ddu485.
114. **Kind B, Muster B, Staroske W, et al.** *Altered spatio-temporal dynamics of RNase H2 complex assembly at replication and repair sites in Aicardi-Goutières syndrome.* Hum Mol Genet. 2014 Nov 15;23(22):5950-60. doi: 10.1093/hmg/ddu319.
115. **Günther C, Kind B, Reijns MA, et al.** *Defective removal of ribonucleotides from DNA promotes systemic autoimmunity.* J Clin Invest. 2015 Jan;125(1):413-24. doi: 10.1172/JCI78001.
116. **Thomas M, White RL, Davis RW.** *Hybridization of RNA to double-stranded DNA: formation of R-loops.* Proc Natl Acad Sci U S A. 1976 Jul;73(7):2294-8. doi: 10.1073/pnas.73.7.2294.
117. **Kojima K, Baba M, Tsukiashi M, Nishimura T, Yasukawa K.** *RNA/DNA structures recognized by RNase H2.* Brief Funct Genomics. 2018 Jun 20;18(3):169-173. doi: 10.1093/bfgp/ely024.
118. **Roy D, Lieber MR.** *G clustering is important for the initiation of transcription-induced R-loops in vitro, whereas high G density without clustering is sufficient thereafter.* Mol Cell Biol. 2009 Jun;29(11):3124-33. doi: 10.1128/MCB.00139-09.
119. **Roy D, Zhang Z, Lu Z, Hsieh CL, Lieber MR.** *Competition between the RNA transcript and the nontemplate DNA strand during R-loop formation in vitro: a nick can serve as a strong R-loop initiation site.* Mol Cell Biol. 2010 Jan;30(1):146-59. doi: 10.1128/MCB.00897-09.
120. **Roberts RW, Crothers DM.** *Stability and properties of double and triple helices: dramatic effects of RNA or DNA backbone composition.* Science. 1992 Nov 27;258(5087):1463-6. doi: 10.1126/science.1279808.
121. **Burgers PM.** *Solution to the 50-year-old Okazaki-fragment problem.* Proc Natl Acad Sci U S A. 2019 Feb 26;116(9):3358-3360. doi: 10.1073/pnas.1900372116.
122. **Sugino A, Hirose S, Okazaki R.** *RNA-linked nascent DNA fragments in Escherichia coli.* Proc Natl Acad Sci U S A. 1972 Jul;69(7):1863-7. doi: 10.1073/pnas.69.7.1863.
123. **Xu B, Clayton DA.** *RNA-DNA hybrid formation at the human mitochondrial heavy-strand origin ceases at replication start sites: an implication for RNA-DNA hybrids serving as primers.* EMBO J. 1996 Jun 17;15(12):3135-43.
124. **Yu K, Chedin F, Hsieh CL, Wilson TE, Lieber MR.** *R-loops at immunoglobulin class switch regions in the chromosomes of stimulated B cells.* Nat Immunol. 2003 May;4(5):442-51. doi: 10.1038/ni919.
125. **Greider CW, Blackburn EH.** *A telomeric sequence in the RNA of Tetrahymena telomerase required for telomere repeat synthesis.* Nature. 1989 Jan 26;337(6205):331-7. doi: 10.1038/337331a0.
126. **Groh M, Gromak N.** *Out of balance: R-loops in human disease.* PLoS Genet. 2014 Sep 18;10(9):e1004630. doi: 10.1371/journal.pgen.1004630.
127. **Lujan SA, Williams JS, Clausen AR, Clark AB, Kunkel TA.** *Ribonucleotides are signals for mismatch repair of leading-strand replication errors.* Mol Cell. 2013 May 9;50(3):437-43. doi: 10.1016/j.molcel.2013.03.017.
128. **Ghodgaonkar MM, Lazzaro F, Olivera-Pimentel M, et al.** *Ribonucleotides misincorporated into DNA act as strand-discrimination signals in eukaryotic mismatch repair.* Mol Cell. 2013 May 9;50(3):323-32. doi: 10.1016/j.molcel.2013.03.019.
129. **Pryor JM, Conlin MP, Carvajal-Garcia J, Luedeman ME, Luthman AJ, Small GW, Ramsden DA.** *Ribonucleotide incorporation enables repair of chromosome breaks by nonhomologous end joining.* Science. 2018 Sep 14;361(6407):1126-1129. doi: 10.1126/science.aat2477.
130. **Niehrs C, Luke B.** *Regulatory R-loops as facilitators of gene expression and genome stability.* Nat Rev Mol Cell Biol. 2020 Mar;21(3):167-178. doi: 10.1038/s41580-019-0206-3.
131. **Ginno PA, Lott PL, Christensen HC, Korf I, Chédin F.** *R-loop formation is a distinctive characteristic of unmethylated human CpG island promoters.* Mol Cell. 2012 Mar 30;45(6):814-25. doi: 10.1016/j.molcel.2012.01.017.

132. **Boque-Sastre R, Soler M, Oliveira-Mateos C, et al.** *Head-to-head antisense transcription and R-loop formation promotes transcriptional activation.* Proc Natl Acad Sci U S A. 2015 May 5;112(18):5785-90. doi: 10.1073/pnas.1421197112.
133. **Skourti-Stathaki K, Kamieniarz-Gdula K, Proudfoot NJ.** *R-loops induce repressive chromatin marks over mammalian gene terminators.* Nature. 2014 Dec 18;516(7531):436-9. doi: 10.1038/nature13787.
134. **Ribeiro de Almeida C, Dhir S, Dhir A, Moghaddam AE, Sattentau Q, Meinhart A, Proudfoot NJ.** *RNA Helicase DDX1 Converts RNA G-Quadruplex Structures into R-Loops to Promote IgH Class Switch Recombination.* Mol Cell. 2018 May 17;70(4):650-662.e8. doi: 10.1016/j.molcel.2018.04.001.
135. **Chakraborty P, Huang JTJ, Hiom K.** *DHX9 helicase promotes R-loop formation in cells with impaired RNA splicing.* Nat Commun. 2018 Oct 19;9(1):4346. doi: 10.1038/s41467-018-06677-1.
136. **Skourti-Stathaki K, Proudfoot NJ.** *A double-edged sword: R loops as threats to genome integrity and powerful regulators of gene expression.* Genes Dev. 2014 Jul 1;28(13):1384-96. doi: 10.1101/gad.242990.114.
137. **Polak P, Arndt PF.** *Transcription induces strand-specific mutations at the 5' end of human genes.* Genome Res. 2008 Aug;18(8):1216-23. doi: 10.1101/gr.076570.108.
138. **Domínguez-Sánchez MS, Barroso S, Gómez-González B, Luna R, Aguilera A.** *Genome instability and transcription elongation impairment in human cells depleted of THO/TREX.* PLoS Genet. 2011 Dec;7(12):e1002386. doi: 10.1371/journal.pgen.1002386.
139. **Huertas P, Aguilera A.** *Cotranscriptionally formed DNA:RNA hybrids mediate transcription elongation impairment and transcription-associated recombination.* Mol Cell. 2003 Sep;12(3):711-21. doi: 10.1016/j.molcel.2003.08.010.
140. **Hamperl S, Bocek MJ, Saldivar JC, Swigut T, Cimprich KA.** *Transcription-Replication Conflict Orientation Modulates R-Loop Levels and Activates Distinct DNA Damage Responses.* Cell. 2017 Aug 10;170(4):774-786.e19. doi: 10.1016/j.cell.2017.07.043.
141. **Allison DF, Wang GG.** *R-loops: formation, function, and relevance to cell stress.* Cell Stress. 2019 Jan 21;3(2):38-46. doi: 10.15698/cst2019.02.175.
142. **Tuduri S, Crabbé L, Conti C, et al.** *Topoisomerase I suppresses genomic instability by preventing interference between replication and transcription.* Nat Cell Biol. 2009 Nov;11(11):1315-24. doi: 10.1038/ncb1984.
143. **Richard P, Manley JL.** *R Loops and Links to Human Disease.* Mol Biol. 2017 Oct 27;429(21):3168-3180. doi: 10.1016/j.jmb.2016.08.031.
144. **Hatchi E, Skourti-Stathaki K, Ventz S, et al.** *BRCA1 recruitment to transcriptional pause sites is required for R-loop-driven DNA damage repair.* Mol Cell. 2015 Feb 19;57(4):636-647. doi: 10.1016/j.molcel.2015.01.011.
145. **Bhatia V, Barroso SI, García-Rubio ML, Tumini E, Herrera-Moyano E, Aguilera A.** *BRCA2 prevents R-loop accumulation and associates with TREX-2 mRNA export factor PCID2.* Nature. 2014 Jul 17;511(7509):362-5. doi: 10.1038/nature13374.
146. **Schlacher K, Christ N, Siaud N, Egashira A, Wu H, Jasin M.** *Double-strand break repair-independent role for BRCA2 in blocking stalled replication fork degradation by MRE11.* Cell. 2011 May 13;145(4):529-42. doi: 10.1016/j.cell.2011.03.041.
147. **Reddy K, Tam M, Bowater RP, et al.** *Determinants of R-loop formation at convergent bidirectionally transcribed trinucleotide repeats.* Nucleic Acids Res. 2011 Mar;39(5):1749-62. doi: 10.1093/nar/gkq935.
148. **Loomis EW, Sanz LA, Chédin F, Hagerman PJ.** *Transcriptionassociated R-loop formation across the human FMR1 CGG-repeat.* PLoS Genet. 2014 Apr 17;10(4):e1004294. doi: 10.1371/journal.pgen.1004294.
149. **Groh M, Lufino MM, Wade-Martins R, Gromak N.** *R-loops associated with triplet repeat expansions promote gene silencing in Friedreich ataxia and fragile X syndrome.* PLoS Genet. 2014 May 1;10(5):e1004318. doi: 10.1371/journal.pgen.1004318.

150. **Colak D, Zaninovic N, Cohen MS, et al.** *Promoter-bound trinucleotide repeat mRNA drives epigenetic silencing in fragile X syndrome.* Science. 2014 Feb 28;343(6174):1002-5. doi: 10.1126/science.1245831.
151. **Renton AE, Majounie E, Waite A, et al.** *A hexanucleotide repeat expansion in C9ORF72 is the cause of chromosome 9p21-linked ALS-FTD.* Neuron. 2011 Oct 20;72(2):257-68. doi: 10.1016/j.neuron.2011.09.010.
152. **Majounie E, Renton AE, Mok K, et al.** *Frequency of the C9orf72 hexanucleotide repeat expansion in patients with amyotrophic lateral sclerosis and frontotemporal dementia: a cross-sectional study.* Lancet Neurol. 2012 Apr;11(4):323-30. doi: 10.1016/S1474-4422(12)70043-1.
153. **Haeusler AR, Donnelly CJ, Periz G, et al.** *C9orf72 nucleotide repeat structures initiate molecular cascades of disease.* Nature. 2014 Mar 13;507(7491):195-200. doi: 10.1038/nature13124.
154. **Waite AJ, Bäumer D, East S, Neal J, Morris HR, Ansorge O, Blake DJ.** *Reduced C9orf72 protein levels in frontal cortex of amyotrophic lateral sclerosis and frontotemporal degeneration brain with the C9ORF72 hexanucleotide repeat expansion.* Neurobiol Aging. 2014 Jul;35(7):1779.e5-1779.e13. doi: 10.1016/j.neurobiolaging.2014.01.016.
155. **Lim YW, Sanz LA, Xu X, Hartono SR, Chédin F.** *Genome-wide DNA hypomethylation and RNA:DNA hybrid accumulation in Aicardi-Goutières syndrome.* Elife. 2015 Jul 16;4:e08007. doi: 10.7554/eLife.08007.
156. **Lee-Kirsch MA, Wolf C, Günther C.** *Aicardi-Goutières syndrome: a model disease for systemic autoimmunity.* Clin Exp Immunol. 2014 Jan;175(1):17-24. doi: 10.1111/cei.12160.
157. **Chon H, Sparks JL, Rychlik M, Nowotny M, Burgers PM, Crouch RJ, Cerritelli SM.** *RNase H2 roles in genome integrity revealed by unlinking its activities.* Nucleic Acids Res. 2013 Mar 1;41(5):3130-43. doi: 10.1093/nar/gkt027.
158. **Bubeck D, Reijns MA, Graham SC, Astell KR, Jones EY, Jackson AP.** *PCNA directs type 2 RNase H activity on DNA replication and repair substrates.* Nucleic Acids Res. 2011 May;39(9):3652-66. doi: 10.1093/nar/gkq980.
159. **Chan YA, Aristizabal MJ, Lu PY, Luo Z, Hamza A, Kobor MS, Stirling PC, Hieter P.** *Genome-wide profiling of yeast DNA:RNA hybrid prone sites with DRIP-chip.* PLoS Genet. 2014 Apr 17;10(4):e1004288. doi: 10.1371/journal.pgen.1004288.
160. **Bhoj VG, Chen ZJ.** *Linking retroelements to autoimmunity.* Cell. 2008 Aug 22;134(4):569-71. doi: 10.1016/j.cell.2008.08.010.
161. **Janeway CA Jr, Medzhitov R.** *Innate immune recognition.* Annu Rev Immunol. 2002;20:197-216. doi: 10.1146/annurev.immunol.20.083001.084359.
162. **Medzhitov R.** *Recognition of microorganisms and activation of the immune response.* Nature. 2007 Oct 18;449(7164):819-26. doi: 10.1038/nature06246.
163. **Chow J, Franz KM, Kagan JC.** *PRRs are watching you: Localization of innate sensing and signaling regulators.* Virology. 2015 May;479-480:104-9. doi: 10.1016/j.virol.2015.02.051.
164. **Samuel CE.** *Antiviral actions of interferons.* Clin Microbiol Rev. 2001 Oct;14(4):778-809, table of contents. doi: 10.1128/CMR.14.4.778-809.2001.
165. **Roers A, Hiller B, Hornung V.** *Recognition of Endogenous Nucleic Acids by the Innate Immune System.* Immunity. 2016 Apr 19;44(4):739-54. doi: 10.1016/j.immuni.2016.04.002.
166. **Santegoets KC, van Bon L, van den Berg WB, Wenink MH, Radstake TR.** *Toll-like receptors in rheumatic diseases: are we paying a high price for our defense against bugs?* FEBS Lett. 2011 Dec 1;585(23):3660-6. doi: 10.1016/j.febslet.2011.04.028.
167. **Chen JQ, Szodoray P, Zeher M.** *Toll-Like Receptor Pathways in Autoimmune Diseases.* Clin Rev Allergy Immunol. 2016 Feb;50(1):1-17. doi: 10.1007/s12016-015-8473-z.
168. **Krieg AM, Yi AK, Matson S, et al.** *CpG motifs in bacterial DNA trigger direct B-cell activation.* Nature. 1995 Apr 6;374(6522):546-9. doi: 10.1038/374546a0.

169. **Kim YM, Brinkmann MM, Paquet ME, Ploegh HL.** *UNC93B1 delivers nucleotide-sensing toll-like receptors to endolysosomes.* Nature. 2008 Mar 13;452(7184):234-8. doi: 10.1038/nature06726.
170. **Ewald SE, Lee BL, Lau L, Wickliffe KE, Shi GP, Chapman HA, Barton GM.** *The ectodomain of Toll-like receptor 9 is cleaved to generate a functional receptor.* Nature. 2008 Dec 4;456(7222):658-62. doi: 10.1038/nature07405.
171. **Honda K, Yanai H, Mizutani T, et al.** *Role of a transductional-transcriptional processor complex involving MyD88 and IRF-7 in Toll-like receptor signaling.* Proc Natl Acad Sci U S A. 2004 Oct 26;101(43):15416-21. doi: 10.1073/pnas.0406933101.
172. **Takaoka A, Yanai H, Kondo S, et al.** *Integral role of IRF-5 in the gene induction programme activated by Toll-like receptors.* Nature. 2005 Mar 10;434(7030):243-9. doi: 10.1038/nature03308.
173. **Negishi H, Fujita Y, Yanai H, et al.** *Evidence for licensing of IFN-gamma-induced IFN regulatory factor 1 transcription factor by MyD88 in Toll-like receptor-dependent gene induction program.* Proc Natl Acad Sci U S A. 2006 Oct 10;103(41):15136-41. doi: 10.1073/pnas.0607181103.
174. **Wu J, Sun L, Chen X, Du F, Shi H, Chen C, Chen ZJ.** *Cyclic GMP-AMP Synthase Is a Cytosolic DNA Sensor That Activates the Type I Interferon Pathway.* Science. 2013 Feb 15;339(6121):826-30. doi: 10.1126/science.1229963.
175. **Sun L, Wu J, Du F, Chen X, Chen ZJ.** *Cyclic GMP-AMP synthase is a cytosolic DNA sensor that activates the type I interferon pathway.* Science. 2013 Feb 15;339(6121):786-91. doi: 10.1126/science.1232458.
176. **Xiao TS, Fitzgerald KA.** *The cGAS-STING pathway for DNA sensing.* Mol Cell. 2013 Jul 25;51(2):135-9. doi: 10.1016/j.molcel.2013.07.004.
177. **Cai X, Chiu YH, Chen ZJ.** *The cGAS-cGAMP-STING pathway of cytosolic DNA sensing and signaling.* Mol Cell. 2014 Apr 24;54(2):289-96. doi: 10.1016/j.molcel.2014.03.040.
178. **Ablasser A, Goldeck M, Cavlar T, et al.** *cGAS produces a 2'-5'-linked cyclic dinucleotide second messenger that activates STING.* Nature. 2013 Jun 20;498(7454):380-4. doi: 10.1038/nature12306.
179. **Diner EJ, Burdette DL, Wilson SC, et al.** *The innate immune DNA sensor cGAS produces a noncanonical cyclic dinucleotide that activates human STING.* Cell Rep. 2013 May 30;3(5):1355-61. doi: 10.1016/j.celrep.2013.05.009.
180. **Gao P, Ascano M, Wu Y, et al.** *Cyclic [G(2',5')pA(3',5')p] is the metazoan second messenger produced by DNA-activated cyclic GMP-AMP synthase.* Cell. 2013 May 23;153(5):1094-107. doi: 10.1016/j.cell.2013.04.046.
181. **Zhang X, Shi H, Wu J, Zhang X, Sun L, Chen C, Chen ZJ.** *Cyclic GMP-AMP containing mixed phosphodiester linkages is an endogenous high-affinity ligand for STING.* Mol Cell. 2013 Jul 25;51(2):226-35. doi: 10.1016/j.molcel.2013.05.022.
182. **Ishikawa H, Barber GN.** *STING is an endoplasmic reticulum adaptor that facilitates innate immune signalling.* Nature. 2008 Oct 2;455(7213):674-8. doi: 10.1038/nature07317.
183. **Gao D, Li T, Li XD, Chen X, Li QZ, Wight-Carter M, Chen ZJ.** *Activation of cyclic GMP-AMP synthase by self-DNA causes autoimmune diseases.* Proc Natl Acad Sci U S A. 2015 Oct 20;112(42):E5699-705. doi: 10.1073/pnas.1516465112.
184. **Ablasser A, Hemmerling I, Schmid-Burgk JL, Behrendt R, Roers A, Hornung V.** *TREX1 deficiency triggers cell-autonomous immunity in a cGAS-dependent manner.* J Immunol. 2014 Jun 15;192(12):5993-7. doi: 10.4049/jimmunol.1400737.
185. **Gray EE, Treuting PM, Woodward JJ, Stetson DB.** *Cutting Edge: cGAS Is Required for Lethal Autoimmune Disease in the Trex1-Deficient Mouse Model of Aicardi-Goutières Syndrome.* J Immunol. 2015 Sep 1;195(5):1939-43. doi: 10.4049/jimmunol.1500969.
186. **Ahn J, Ruiz P, Barber GN.** *Intrinsic self-DNA triggers inflammatory disease dependent on STING.* J Immunol. 2014 Nov 1;193(9):4634-42. doi: 10.4049/jimmunol.1401337.

187. **Mackenzie KJ, Carroll P, Lettice L, et al.** *Ribonuclease H2 mutations induce a cGAS/STING-dependent innate immune response.* EMBO J. 2016 Apr 15;35(8):831-44. doi: 10.15252/embj.201593339.
188. **Gentili M, Manel N.** *cGAS-STING do it again: pivotal role in RNase H2 genetic disease.* EMBO J. 2016 Apr 15;35(8):796-7. doi: 10.15252/embj.201694226.
189. **Hu WS, Hughes SH.** *HIV-1 reverse transcription.* Cold Spring Harb Perspect Med. 2012 Oct 1;2(10):a006882. doi: 10.1101/cshperspect.a006882.
190. **Lee HK, Lund JM, Ramanathan B, Mizushima N, Iwasaki A.** *Autophagy-dependent viral recognition by plasmacytoid dendritic cells.* Science. 2007 Mar 9;315(5817):1398-401. doi: 10.1126/science.1136880.
191. **Fujiwara Y, Wada K, Kabuta T.** *Lysosomal degradation of intracellular nucleic acids-multiple autophagic pathways.* J Biochem. 2017 Feb 1;161(2):145-154. doi: 10.1093/jb/mvw085.
192. **Fujiwara Y, Furuta A, Kikuchi H, et al.** *Discovery of a novel type of autophagy targeting RNA.* Autophagy. 2013 Mar;9(3):403-9. doi: 10.4161/auto.23002.
193. **Fujiwara Y, Kikuchi H, Aizawa S, et al.** *Direct uptake and degradation of DNA by lysosomes.* Autophagy. 2013 Aug;9(8):1167-71. doi: 10.4161/auto.24880.
194. **Eskelinen EL, Cuervo AM, Taylor MR, et al.** *Unifying nomenclature for the isoforms of the lysosomal membrane protein LAMP-2.* Traffic. 2005 Nov;6(11):1058-61. doi: 10.1111/j.1600-0854.2005.00337.x.
195. **Aizawa S, Fujiwara Y, Contu VR, et al.** *Lysosomal putative RNA transporter SIDT2 mediates direct uptake of RNA by lysosomes.* Autophagy. 2016;12(3):565-78. doi: 10.1080/15548627.2016.1145325.
196. **Aizawa S, Contu VR, Fujiwara Y, et al.** *Lysosomal membrane protein SIDT2 mediates the direct uptake of DNA by lysosomes.* Autophagy. 2017 Jan 2;13(1):218-222. doi: 10.1080/15548627.2016.1248019.
197. **Jialin G, Xuefan G, Huiwen Z.** *SID1 transmembrane family, member 2 (Sidt2): a novel lysosomal membrane protein.* Biochem Biophys Res Commun. 2010 Nov 26;402(4):588-94. doi: 10.1016/j.bbrc.2010.09.133.
198. **Deshpande RA, Shankar V.** *Ribonucleases from T2 family.* Crit Rev Microbiol. 2002;28(2):79-122. doi: 10.1080/1040-840291046704.
199. **Evans CJ, Aguilera RJ.** *DNase II: genes, enzymes and function.* Gene. 2003 Dec 11;322:1-15. doi: 10.1016/j.gene.2003.08.022.
200. **Deter RL, De Duve C.** *Influence of glucagon, an inducer of cellular autophagy, on some physical properties of rat liver lysosomes.* J Cell Biol. 1967 May;33(2):437-49. doi: 10.1083/jcb.33.2.437.
201. **Siqueira MDS, Ribeiro RM, Travassos LH.** *Autophagy and Its Interaction With Intracellular Bacterial Pathogens.* Front Immunol. 2018 May 23;9:935. doi: 10.3389/fimmu.2018.00935.
202. **Yang Z, Klionsky DJ.** *Mammalian autophagy: core molecular machinery and signaling regulation.* Curr Opin Cell Biol. 2010 Apr;22(2):124-31. doi: 10.1016/j.ceb.2009.11.014.
203. **Parzych KR, Klionsky DJ.** *An overview of autophagy: morphology, mechanism, and regulation.* Antioxid Redox Signal. 2014 Jan 20;20(3):460-73. doi: 10.1089/ars.2013.5371.
204. **van der Vaart A, Reggiori F.** *The Golgi complex as a source for yeast autophagosomal membranes.* Autophagy. 2010 Aug;6(6):800-1. doi: 10.1091/mbc.E09-04-0345.
205. **Hayashi-Nishino M, Fujita N, Noda T, Yamaguchi A, Yoshimori T, Yamamoto A.** *A subdomain of the endoplasmic reticulum forms a cradle for autophagosome formation.* Nat Cell Biol. 2009 Dec;11(12):1433-7. doi: 10.1038/ncb1991.
206. **Hailey DW, Rambold AS, Satpute-Krishnan P, Mitra K, Sougrat R, Kim PK, Lippincott-Schwartz J.** *Mitochondria supply membranes for autophagosome biogenesis during starvation.* Cell. 2010 May 14;141(4):656-67. doi: 10.1016/j.cell.2010.04.009.
207. **Ravikumar B, Moreau K, Jahreiss L, Puri C, Rubinsztein DC.** *Plasma membrane contributes to the formation of pre-autophagosomal structures.* Nat Cell Biol. 2010 Aug;12(8):747-57. doi: 10.1038/ncb2078.

208. **Weidberg H, Shvets E, Elazar Z.** *Biogenesis and cargo selectivity of autophagosomes.* Annu Rev Biochem. 2011;80:125-56. doi: 10.1146/annurev-biochem-052709-094552.
209. **Ichimura Y, Kirisako T, Takao T, et al.** *A ubiquitin-like system mediates protein lipidation.* Nature. 2000 Nov 23;408(6811):488-92. doi: 10.1038/35044114.
210. **Hanada T, Noda NN, Satomi Y, et al.** *The Atg12-Atg5 conjugate has a novel E3-like activity for protein lipidation in autophagy.* J Biol Chem. 2007 Dec 28;282(52):37298-302. doi: 10.1074/jbc.C700195200.
211. **Fujita N, Itoh T, Omori H, Fukuda M, Noda T, Yoshimori T.** *The Atg16L complex specifies the site of LC3 lipidation for membrane biogenesis in autophagy.* Mol Biol Cell. 2008 May;19(5):2092-100. doi: 10.1091/mbc.e07-12-1257.
212. **Kirisako T, Ichimura Y, Okada H, et al.** *The reversible modification regulates the membrane-binding state of Apg8/Aut7 essential for autophagy and the cytoplasm to vacuole targeting pathway.* J Cell Biol. 2000 Oct 16;151(2):263-76. doi: 10.1083/jcb.151.2.263.
213. **Eskelinen, EL.** *Maturation of autophagic vacuoles in Mammalian cells.* Autophagy. 2005 Apr;1(1):1-10. doi: 10.4161/auto.1.1.1270.
214. **Noda T, Fujita N, Yoshimori T.** *The late stages of autophagy: how does the end begin?* Cell Death Differ. 2009 Jul;16(7):984-90. doi: 10.1038/cdd.2009.54.
215. **Jäger S, Bucci C, Tanida I, Ueno T, Kominami E, Saftig P, Eskelinen EL.** *Role for Rab7 in maturation of late autophagic vacuoles.* J Cell Sci. 2004 Sep 15;117(Pt 20):4837-48. doi: 10.1242/jcs.01370.
216. **Li WW, Li J, Bao JK.** *Microautophagy: lesser-known self-eating.* Cell Mol Life Sci. 2012 Apr;69(7):1125-36. doi: 10.1007/s00018-011-0865-5.
217. **Kaushik S, Cuervo AM.** *The coming of age of chaperone-mediated autophagy.* Nat Rev Mol Cell Biol. 2018 Jun;19(6):365-381. doi: 10.1038/s41580-018-0001-6.
218. **Dice JF.** *Altered degradation of proteins microinjected into senescent human fibroblasts.* J Biol Chem. 1982 Dec 25;257(24):14624-7.
219. **Crow YJ, Shetty J, Livingston JH.** *Treatments in Aicardi–Goutières syndrome.* Dev Med Child Neurol. 2020 Jan;62(1):42-47. doi: 10.1111/dmcn.14268.
220. **Rice GI, Meyzer C, Bouazza N, et al.** *Reverse-Transcriptase Inhibitors in the Aicardi–Goutières Syndrome.* N Engl J Med. 2018 Dec 6;379(23):2275-7. doi: 10.1056/NEJMc1810983.
221. **Tonduti D, Fazzi E, Badolato R, Orcesi S.** *Novel and emerging treatments for Aicardi-Goutières syndrome.* Expert Rev Clin Immunol. 2020 Feb;16(2):189-198. doi: 10.1080/1744666X.2019.1707663.
222. **Zimmermann N, Wolf C, Schwenke R, et al.** *Assessment of Clinical Response to Janus Kinase Inhibition in Patients With Familial Chilblain Lupus and TREX1 Mutation.* JAMA Dermatol. 2019 Mar 1;155(3):342-346. doi: 10.1001/jamadermatol.2018.5077.
223. **Briand C, Frémond ML, Bessis D, et al.** *Efficacy of JAK1/2 inhibition in the treatment of chilblain lupus due to TREX1 deficiency.* Ann Rheum Dis. 2019 Mar;78(3):431-433. doi: 10.1136/annrheumdis-2018-214037.
224. **Boyadzhiev M, Marinov L, Boyadzhiev V, Iotova V, Aksentijevich I, Hambleton S.** *Disease course and treatment effects of a JAK inhibitor in a patient with CANDLE syndrome.* Pediatr Rheumatol Online J. 2019 May 2;17(1):19. doi: 10.1186/s12969-019-0322-9.
225. **Frémond ML, Rodero MP, Jeremiah N, et al.** *Efficacy of the Janus kinase 1/2 inhibitor ruxolitinib in the treatment of vasculopathy associated with TMEM173-activating mutations in 3 children.* J Allergy Clin Immunol. 2016 Dec;138(6):1752-1755. doi: 10.1016/j.jaci.2016.07.015.
226. **Rodero MP, Frémond ML, Rice GI, Neven B, Crow YJ.** *JAK inhibition in STING-associated interferonopathy.* Ann Rheum Dis. 2016 Dec;75(12):e75. doi: 10.1136/annrheumdis-2016-210504.
227. **Tüngler V, König N, Günther C, et al.** *Response to: 'JAK inhibition in STING-associated interferonopathy' by Crow et al.* Ann Rheum Dis. 2016 Dec;75(12):e76. doi: 10.1136/annrheumdis-2016-210565.

228. **Meesilpavikkai K, Dik WA, Schrijver B, et al.** *Efficacy of Baricitinib in the Treatment of Chilblains Associated With Aicardi-Goutières Syndrome, a Type I Interferonopathy.* Arthritis Rheumatol. 2019 May;71(5):829-831. doi: 10.1002/art.40805.
229. **McLellan KE, Martin N, Davidson JE, et al.** *JAK 1/2 Blockade in MDA5 Gain-of-Function.* J Clin Immunol. 2018 Nov;38(8):844-846. doi: 10.1007/s10875-018-0563-2.
230. **Yao Y, Higgs BW, Morehouse C, et al.** *Development of Potential Pharmacodynamic and Diagnostic Markers for Anti-IFN-α Monoclonal Antibody Trials in Systemic Lupus Erythematosus.* Hum Genomics Proteomics. 2009 Nov 17;2009:374312. doi: 10.4061/2009/374312.
231. **Baccala R, Gonzalez-Quintial R, Schreiber RD, Lawson BR, Kono DH, Theofilopoulos AN.** *Anti-IFN-α/β receptor antibody treatment ameliorates disease in lupus-predisposed mice.* J Immunol. 2012 Dec 15;189(12):5976-84. doi: 10.4049/jimmunol.1201477.
232. **An J, Woodward JJ, Sasaki T, Minie M, Elkon KB.** *Cutting edge: Antimalarial drugs inhibit IFN-β production through blockade of cyclic GMP-AMP synthase-DNA interaction.* J Immunol. 2015 May 1;194(9):4089-93. doi: 10.4049/jimmunol.1402793.
233. **Rainsford KD, Parke AL, Clifford-Rashotte M, Kean WF.** *Therapy and pharmacological properties of hydroxychloroquine and chloroquine in treatment of systemic lupus erythematosus, rheumatoid arthritis and related diseases.* Inflammopharmacology. 2015 Oct;23(5):231-69. doi: 10.1007/s10787-015-0239-y.
234. **Schrezenmeier E, Dörner T.** *Mechanisms of action of hydroxychloroquine and chloroquine: implications for rheumatology.* Nat Rev Rheumatol. 2020 Mar;16(3):155-166. doi: 10.1038/s41584-020-0372-x.
235. **Chandler LC, Yusuf IH, McClements ME, Barnard AR, MacLaren RE, Xue K.** *Immunomodulatory Effects of Hydroxychloroquine and Chloroquine in Viral Infections and Their Potential Application in Retinal Gene Therapy.* Int J Mol Sci. 2020 Jul 14;21(14):4972. doi: 10.3390/ijms21144972.
236. **Kuznik A, Bencina M, Svajger U, Jeras M, Rozman B, Jerala R.** *Mechanism of endosomal TLR inhibition by antimalarial drugs and imidazoquinolines.* J Immunol. 2011 Apr 15;186(8):4794-804. doi: 10.4049/jimmunol.1000702.
237. **van den Borne BE, Dijkmans BA, de Rooij HH, le Cessie S, Verweij CL.** *Chloroquine and hydroxychloroquine equally affect tumor necrosis factor-alpha, interleukin 6, and interferon-gamma production by peripheral blood mononuclear cells.* J Rheumatol. 1997 Jan;24(1):55-60.
238. **Jang CH, Choi JH, Byun MS, Jue DM.** *Chloroquine inhibits production of TNF-alpha, IL-1beta and IL-6 from lipopolysaccharide-stimulated human monocytes/macrophages by different modes.* Rheumatology (Oxford). 2006 Jun;45(6):703-10. doi: 10.1093/rheumatology/kei282.
239. **Vodicka P, Lim J, Williams DT, et al.** *Assessment of chloroquine treatment for modulating autophagy flux in brain of WT and HD mice.* J Huntingtons Dis. 2014;3(2):159-74. doi: 10.3233/JHD-130081.
240. **Livingston JH, Stivaros S, van der Knaap MS, Crow YJ.** *Recognizable phenotypes associated with intracranial calcification.* Dev Med Child Neurol. 2013 Jan;55(1):46-57. doi: 10.1111/j.1469-8749.2012.04437.x.
241. **Zucca S, Villaraggia M, Gagliardi S, Grieco GS, Valente M, Cereda C, Magni P.** *Analysis of amplicon-based NGS data from neurological disease gene panels: a new method for allele drop-out management.* BMC Bioinformatics. 2016 Nov 8;17(Suppl 12):339. doi: 10.1186/s12859-016-1189-0.
242. **Rice GI, Melki I, Frémond ML, et al.** *Assessment of Type I Interferon Signaling in Pediatric Inflammatory Disease.* J Clin Immunol. 2017 Feb;37(2):123-132. doi: 10.1007/s10875-016-0359-1.
243. **Pfaffl MW.** *A new mathematical model for relative quantification in real-time RT-PCR.* Nucleic Acids Res. 2001 May 1;29(9):e45. doi: 10.1093/nar/29.9.e45.
244. **Li B, Dewey CN.** *RSEM: accurate transcript quantification from RNA-Seq data with or without a reference genome.* BMC Bioinformatics. 2011 Aug 4;12:323. doi: 10.1186/1471-2105-12-323.

245. **Leng N, Dawson JA, Thomson JA, et al.** *EBSeq: an empirical Bayes hierarchical model for inference in RNA-seq experiments.* Bioinformatics. 2013 Apr 15;29(8):1035-43. doi: 10.1093/bioinformatics/btt087.
246. **Carrara M, Lum J, Cordero F, et al.** *Alternative splicing detection workflow needs a careful combination of sample prep and bioinformatics analysis.* BMC Bioinformatics. 2015;16 Suppl 9(Suppl 9):S2. doi: 10.1186/1471-2105-16-S9-S2.
247. **Aryee MJ, Jaffe AE, Corrada-Bravo H, Ladd-Acosta C, Feinberg AP, Hansen KD, Irizarry RA.** *Minfi: a flexible and comprehensive Bioconductor package for the analysis of Infinium DNA methylation microarrays.* Bioinformatics. 2014 May 15;30(10):1363-9. doi: 10.1093/bioinformatics/btu049.
248. **Tian Y, Morris TJ, Webster AP, Yang Z, Beck S, Feber A, Teschendorff AE.** *ChAMP: updated methylation analysis pipeline for Illumina BeadChips.* Bioinformatics. 2017 Dec 15;33(24):3982-3984. doi: 10.1093/bioinformatics/btx513.
249. **Yu G, Wang LG, Han Y, He QY.** *clusterProfiler: an R package for comparing biological themes among gene clusters.* OMICS. 2012 May;16(5):284-7. doi: 10.1089/omi.2011.0118.
250. **Houseman EA, Accomando WP, Koestler DC, et al.** *DNA methylation arrays as surrogate measures of cell mixture distribution.* BMC Bioinformatics. (2012) 13:86.
251. **Necchi V, Sommi P, Ricci V, Solcia E.** *In vivo accumulation of Helicobacter pylori products, NOD1, ubiquitinated proteins and proteasome in a novel cytoplasmic structure.* PLoS One. 2010 Mar 16;5(3):e9716. doi: 10.1371/journal.pone.0009716.
252. **Tao W, Xu W, Valdivia MM, Hao S, Zhai ZH.** *Distribution and transcription activity of nucleolar DNA in higher plant cells.* Cell Biol Int. 2001;25(11):1167-71. doi: 10.1006/cbir.2001.0791.
253. **Garau J, Cavallera V, Valente M, et al.** *Molecular Genetics and Interferon Signature in the Italian Aicardi Goutières Syndrome Cohort: Report of 12 New Cases and Literature Review.* J Clin Med. 2019 May 26;8(5):750. doi: 10.3390/jcm8050750.
254. **Kato H, Takeuchi O, Mikamo-Satoh E, et al.** *Length-dependent recognition of double-stranded ribonucleic acids by retinoic acid-inducible gene-I and melanoma differentiation-associated gene 5.* J Exp Med. 2008;205(7):1601-1610.
255. **Visse R, Nagase H.** *Matrix metalloproteinases and tissue inhibitors of metalloproteinases: structure, function, and biochemistry.* Circ Res. 2003 May 2;92(8):827-39. doi: 10.1161/01.RES.0000070112.80711.3D.
256. **Hotta K, Kitamoto A, Kitamoto T, et al.** *Identification of differentially methylated region (DMR) networks associated with progression of nonalcoholic fatty liver disease.* Sci Rep. 2018 Sep 11;8(1):13567. doi: 10.1038/s41598-018-31886-5.
257. . **Bailey CC, Zhong G, Huang IC, Farzan M.** *IFITM-Family Proteins: The Cell's First Line of Antiviral Defense*. Annu Rev Virol. 2014 Nov 1;1:261-283. doi: 10.1146/annurev-virology-031413-085537.
258. **Pope JH, Horne MK, Scott W.** *Transformation of Foetal Human Keukocytes in Vitro by Filtrates of a Human Leukaemic Cell Line Containing Herpes-Like Virus.* Int J Cancer, 1968, Int J Cancer. 1968 Nov 15;3(6):857-66.
259. **Phillips DD, Garboczi DN, Singh K, Hu Z, Leppla SH, Leysath CE.** *The sub-nanomolar binding of DNA-RNA hybrids by the single-chain Fv fragment of antibody S9.6.* J Mol Recognit. 2013 Aug;26(8):376-81. doi: 10.1002/jmr.2284.
260. **Vanoosthuyse V.** *Strengths and Weaknesses of the Current Strategies to Map and Characterize R-Loops.* Noncoding RNA. 2018 Mar 27;4(2):9. doi: 10.3390/ncrna4020009.
261. **Halász L, Karányi Z, Boros-Oláh B, et al.** *RNA-DNA hybrid (R-loop) immunoprecipitation mapping: an analytical workflow to evaluate inherent biases.* s.l. : Genome Res. 2017 Jun;27(6):1063-1073. doi: 10.1101/gr.219394.116.
262. **Bao W, Xia H, Liang Y, et al.** *Toll-like Receptor 9 Can Be Activated by Endogenous Mitochondrial DNA to Induce Podocyte Apoptosis.* Sci Rep. 2016 Mar 3;6:22579. doi: 10.1038/srep22579.

263. **Kang I, Chu CT, Kaufman BA.** *The mitochondrial transcription factor TFAM in neurodegeneration: emerging evidence and mechanisms.* FEBS, Letters Mar;592(5):793-811. doi: 10.1002/1873-3468.12989.
264. **Caielli S, Athale S, Domic B, et al.** *Oxidized Mitochondrial Nucleoids Released by Neutrophils Drive Type I Interferon Production in Human Lupus.* J Exp Med. 2016 May 2;213(5):697-713. doi: 10.1084/jem.20151876.
265. **West AP, Khoury-Hanold W, Staron M, et al.** *Mitochondrial DNA stress primes the antiviral innate immune response.* Nature 2015 Apr 23;520(7548):553-7. doi: 10.1038/nature14156.
266. **Julian MW, Shao G, Bao S, et al.** *Mitochondrial Transcription Factor A, an Endogenous Danger Signal, Promotes TNFα Release via RAGE- and TLR9-Responsive Plasmacytoid Dendritic Cells.* PLoS One. 2013 Aug 12;8(8):e72354. doi: 10.1371/journal.pone.0072354.
267. **Rynes RI.** *Antimalarial drugs in the treatment of rheumatological diseases.* Br J Rheumatol. 1997, 36(7), 799-805; doi: 10.1093/rheumatology/36.7.799.
268. **Schrezenmeier E, Dörner T.** *Mechanisms of action of hydroxychloroquine and chloroquine: implications for rheumatology.* Nat Rev Rheumatol. 2020, 16(3), 155-166; doi: 10.1038/s41584-020-0372-x.
269**. Ponticelli C, Moroni G.** *Hydroxychloroquine in systemic lupus erythematosus (SLE).* Exp. Op. Drug Saf. 2017, 16(3), 411-419; doi: 10.1080/14740338.2017.1269168.
270. **Al-Bari MA.** *Chloroquine analogues in drug discovery: new directions of uses, mechanisms of actions and toxic manifestations from malaria to multifarious diseases.* J Antimicrob Chemother. 2015, 70(6), 1608-21; doi: 10.1093/jac/dkv018.
271. **Hu C, Lu L, Wan J, Wen C.** *The pharmacological mechanisms and therapeutic activities of hydroxychloroquine in rheumatic and related diseases.* Curr. Med. Chem. 2017, 24, 2241-2249; doi: 10.2174/0929867324666170316115938.
272. **Karim MR, Kanazawa T, Daigaku Y, Fujimura S, Miotto G, Kadowaki M.** *Cytosolic LC3 ratio as a sensitive index of macroautophagy in isolated rat hepatocytes and H4-II-E cells.* Autophagy. 2007 Nov-Dec;3(6):553-60. doi: 10.4161/auto.4615.
273. **Haud N, Kara F, Diekmann S, et al.** *rnaset2 mutant zebrafish model familial cystic leukoencephalopathy and reveal a role for RNase T2 in degrading ribosomal RNA*s. Proc Natl Acad Sci U S A. 2011 Jan 18;108(3):1099-103. doi: 10.1073/pnas.1009811107.
274. **Baranzini N, Pedrini E, Girardello R, et al.** *Human recombinant RNASET2-induced inflammatory response and connective tissue remodeling in the medicinal leech.* Cell Tissue Res. 2017 May;368(2):337-351. doi: 10.1007/s00441-016-2557-9.
275. **Wang R, Li Y, Chen Y, et al.** *Inhibition of RAD54B suppresses proliferation and promotes apoptosis in hepatoma cells.* Oncol Rep. 2018 Sep;40(3):1233-1242. doi: 10.3892/or.2018.6522.
276. **McManus KJ, Barrett IJ, Nouhi Y, Hieter P.** *Specific synthetic lethal killing of RAD54B-deficient human colorectal cancer cells by FEN1 silencing.* Proc Natl Acad Sci U S A. 2009 Mar 3;106(9):3276-81. doi: 10.1073/pnas.0813414106.
277. **Gupta S, Kaplan MJ.** *The role of neutrophils and NETosis in autoimmune and renal diseases.* Nat Rev Nephrol. 2016 Jul;12(7):402-13. doi: 10.1038/nrneph.2016.71.
278. **Tilgner K, Neganova I, Moreno-Gimeno I, et al.** *A human iPSC model of Ligase IV deficiency reveals an important role for NHEJ-mediated-DSB repair in the survival and genomic stability of induced pluripotent stem cells and emerging haematopoietic progenitors.* Cell Death Differ. 2013 Aug;20(8):1089-100. doi: 10.1038/cdd.2013.44.
279. **Coffin SR, Hollis T, Perrino FW**. *Functional consequences of the RNase H2A subunit mutations that cause Aicardi-Goutieres syndrome*. J Biol Chem. 2011 May 13;286(19):16984-91. doi:10.1074/jbc.M111.228833.
280. **Hase K, Fujiwara Y, Kikuchi H, et al.** *RNautophagy/DNautophagy possesses selectivity for RNA/DNA substrates.* Nucleic Acids Res. 2015 Jul 27;43(13):6439-49. doi: 10.1093/nar/gkv579.

281. **El Kebir D, József L, Pan W, Wang L, Filep JG.** *Bacterial DNA activates endothelial cells and promotes neutrophil adherence through TLR9 signaling.* J Immunol. 2009 Apr 1;182(7):4386-94. doi: 10.4049/jimmunol.0803044.
282. **Zhang Q, Raoof M, Chen Y, et al.** *Circulating mitochondrial DAMPs cause inflammatory responses to injury.* Nature. 2010 Mar 4;464(7285):104-7. doi: 10.1038/nature08780.
283. **de Moura MB, dos Santos LS, Van Houten B.** *Mitochondrial dysfunction in neurodegenerative diseases and cancer.* Environ Mol Mutagen. 2010 Jun;51(5):391-405. doi: 10.1002/em.20575.
284. **Fang C, Wei X, Wei Y.** *Mitochondrial DNA in the regulation of innate immune responses.* Protein Cell. 2016 Jan;7(1):11-6. doi: 10.1007/s13238-015-0222-9.
285. **Ojha CR, Lapierre J, Rodriguez M, et al.** *Interplay between Autophagy, Exosomes and HIV-1 Associated Neurological Disorders: New Insights for Diagnosis and Therapeutic Applications.* Viruses. 2017 Jul 6;9(7):176. doi: 10.3390/v9070176.